Behaviour of Reduced-Scale Fully-Grouted Concrete Block Shear Walls

By

Joseph Curtis Wierzbicki

B. Eng.

A Thesis

Submitted to the School of Graduate Studies

In Partial Fulfillment of the Requirements

For the Degree of

Master of Applied Science

McMaster University

MASTER OF APPLIED SCIENCE (2010) McMaster University

(CIVIL ENGINEERING) Hamilton Ontario

Title: Behaviour of Reduced-Scale Fully-Grouted Concrete Block Shear Walls

Author: Joe Wierzbicki, B. Eng (McMaster University)

Advisors: Dr. R. Drysdale and Dr. W. El-Dakhakhni

Number of Pages: xiii, 196

Abstract

A majority of the experimental research on masonry shear wall behaviour has been done on single storey walls and on piers in many cases due to physical and equipment limitations in laboratories or time and cost constraints. Although full scale testing of multi-storey masonry shear walls has been carried out at McMaster University where the laboratory could accommodate walls up to about 8 m high, such testing is indeed very time consuming, costly, and even somewhat dangerous as the result of working at significant heights above the laboratory floor. Therefore, a decision was made to make use of scaled concrete blocks and proportionately scaled walls to conduct shear wall research over a range of wall sizes representative of walls in buildings. Half scale units have been used at McMaster University for the past 6 years and the research presented in this thesis represents the initiation of shear wall research using one-third scale concrete blocks. Therefore, one of the important and unavoidable focuses of this research is to provide a solid basis for future research on scaled shear walls.

In terms of shear wall behaviour, the focus of this study is the flexural response of ductile reinforced masonry shear walls of various sizes and configurations. In addition to this documentation of basic shear wall response, an added objective is to initiate study of the interaction of various sizes and configurations of shear walls on the seismic performance of representative shear wall buildings as the next logical step beyond response of individual walls. To

this end, an objective is to assess the results of using combinations of the tested walls contained within a conceptual structure.

In terms of practical output, the experimental testing of shear walls will concentrate on inducing large displacements and examining the responses as they pertain to seismic parameters. The primary objective is to augment existing research focused on the displacement ductility of reinforced masonry shear walls and the force modification factor, R_d, as well as to provide a comparison between observed performance and the current design practices within the National Building Code of Canada (2005) and the masonry design standard, CSA S304.1 (2004).

Overall, the results obtained from this study provide positive feedback for the use of fully grouted reinforced one third scale concrete block shear wall testing. The observed ductility was below the expected level, however, these results are an indicator that the current R_d value is a lower bound value. Although the relatively brittle steel presented complications and prevented full value from being achieved from the tests, when considered as lower bound results, they provide a positive indication of the resistance of ductile reinforced masonry shear walls subjected to seismic forces.

Acknowledgements

I wish to thank Dr. Drysdale and Dr. El-Dakhakhni for their continued encouragement, insight, and funding during my research. I have learned invaluable knowledge from both of them during my time at McMaster. Thanks go out to Marwan Shedid for all of his help during the initial phases of experimental testing. I would also like to extend my sincere thanks to the technicians at the ADL, Kent Wheeler and David Perrett. Their knowledge and expertise was a tremendous asset. Lastly, I would like to thank Kevin Hughes and Bennett Banting for their continued help and support.

I would like to express my thanks and appreciation for the provision of mason (Tim Maxson) time made by the Ontario Masonry Contractor's Association and the Canada Masonry Design Centre. A big thank you goes to the Canadian Concrete Masonry Producers Association, Niagara Block Inc, and the Grimo family for producing the much needed concrete blocks under such short notice.

Table of Contents

List of Figures

List of Tables

Chapter 1
Introduction

1.1 Background

Masonry has been the most widely used building material for the majority of non-single family housing types of low rise construction due to ease of construction, ability to sustain compression loading, and durability. With the evidence of earthquake caused masonry collapses occurring even in modern construction in developed countries, it has been clear for several decades that design codes and practices needed to be improved. While unacceptable very large losses of life have been witnessed in recent times in places like China and Haiti, much of this is attributable to either very old construction or very poor modern design and construction. Alternatively, while improvements in safety are still required in developed countries such as Canada, a parallel concern is to develop design methods and construction details that combine safety with economically feasible construction. Otherwise, continuation of current methods will continue to create a competitive disadvantage for masonry construction which is resulting in decreasing use of masonry in zones where design is governed by earthquake forces.

The weaknesses of unreinforced hollow masonry construction to seismic excitation have been documented as many such low rise structures have failed during seismic events. While improved design techniques can be used to increase the redundancy and toughness of such structures, the current emphasis in Canada is to optimize the use of reinforced masonry. Due to its capacity and ductile capabilities, reinforced concrete became the popular building material choice in regions of moderate to high seismic activity, whereas masonry continued to be the choice building material for low rise construction in regions of low seismic activity. In order to increase the use of masonry in medium to high-rise structures and in regions of moderate to high seismic activity, it is necessary to improve the seismic performance of reinforced masonry construction However, despite significant progress in this direction, the limited seismic performance of unreinforced masonry has led to conservative design code provisions for reinforced masonry. This is in spite of research that has shown that properly designed reinforced masonry can, in fact, provide adequate safety against seismic forces (Sucuoglu, McNiven (1991)).

The development of reinforced masonry led to the use of reinforced masonry shear walls. With hollow construction, the typically large walls provided the primary gravity load resistance of the structure. The addition of reinforcing steel allowed these elements to take on the role of the primary lateral load resisting system which, due to its physical and material properties, possessed the required large stiffness and high lateral load capacity to provide lateral resistance and displacement control. With the increasing use of shear wall structures as an efficient system, there has been an accompanying increase in experimental testing and analysis, the majority of which focused on the in-plane behaviour of masonry shear walls subjected to seismic loading.

Examining the in-plane behaviour of masonry led to observations regarding the failure modes of reinforced masonry. The two modes of failure can be simplistically categorized as flexural failure and shear failure modes. During seismic events, flexural failure is favoured as it is accompanied by large inelastic deformations that create energy absorption and dissipation capacities. Shear failure, however, is more brittle, with limited ductility (Sucuoglu, McNiven (1991)).

When designing for seismic forces, it is not economically practical to design a section or system that will remain within the elastic range of loading. In order to design a system which is economically feasible, and also provides adequate strength and safety, it must be allowed to exhibit large inelastic deformation (ductility) and plastic hinging (damage) in order to absorb and dissipate energy and alter the natural frequency of the structure.

1.2 Objectives and Research Significance

A majority of the experimental research on masonry shear wall behaviour has been done on single storey walls and on piers in many cases due to physical and equipment limitations in laboratories or time and cost constraints. Although testing of full scale multi-storey masonry shear walls has been carried out at McMaster University where the laboratory could accommodate walls up to about 8 m high, such testing is indeed very time consuming, costly, and even somewhat dangerous as the result of working at significant heights above the test floor. Therefore, a decision was made to make use of scaled concrete blocks and proportionately scaled shear walls over a range of wall sizes more representative of walls in buildings. Half scale units have been used for the past 6 years and the research presented in this thesis represents the initiation of shear wall research using one-third scale concrete blocks. Therefore, one of the important and unavoidable focuses of this research is to provide a solid basis for future research on scaled shear walls.

In terms of shear wall behaviour, the focus of this study is the flexural response of ductile reinforced masonry shear walls of various sizes and configurations. In addition to this documentation of basic shear wall response, an added objective is to initiate study of the interaction of various sizes and configurations of shear walls on the seismic performance of representative shear wall buildings as the next logical step beyond response of individual walls. To this end, an objective is to assess the results of using combinations of the tested walls contained within a conceptual structure.

In terms of practical output, the experimental testing of shear walls will concentrate on inducing large displacements and examining the responses as they pertain to seismic parameters. The primary objective is to augment existing research focused on the displacement ductility of reinforced masonry shear walls and the force modification factor R_d as well as to provide a comparison between observed performance and the current design practices within the National

Building Code of Canada (2005) and the masonry design standard, CSA S304.1 (2004).

1.3 Scope

In order to accomplish the objectives of this research, a test matrix consisting of 4 concrete block shear walls was chosen. The walls (See Figure 1.1) correspond to shear walls designed to be part of a conceptual shear wall building. As such the walls were designed to have a wide range of relative stiffness and strength. The parameters of study included varying aspect ratio, a flanged section, and flexural coupling. All specimens were designed such that they would be expected to exhibit ductile flexural behaviour.

It was decided that all walls should be instrumented such that the lateral load, vertical and horizontal displacements, and reinforcing bar strain could be measured and recorded. The resulting data would then be used to examine aspects such as equivalent plastic hinge length, extent of plasticity, curvatures, displacements, and ductility.

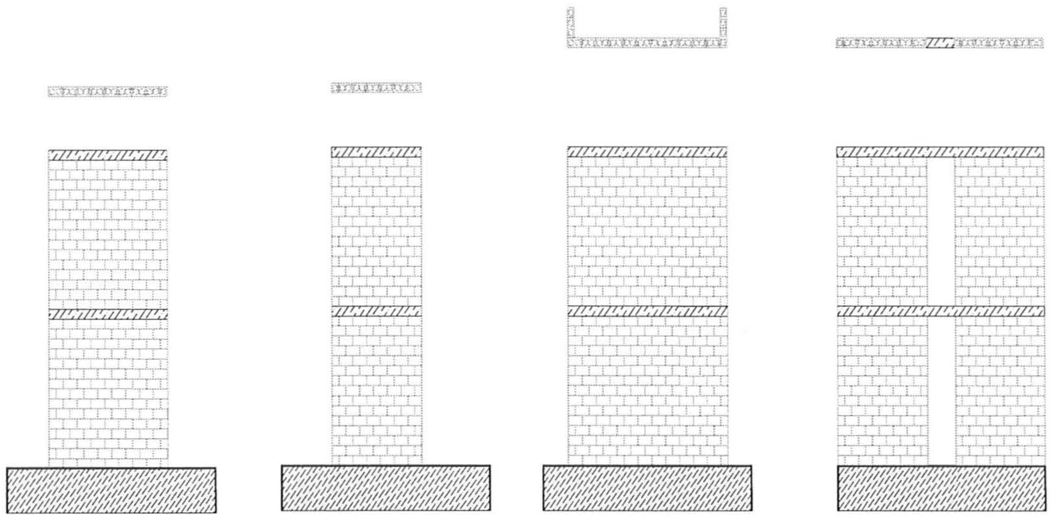

Figure 1.1: RM Shear Wall Specimens

1.4 Literature Review

1.4.1 Flexural and Shear Behaviour

Flexural behaviour involves the formation of longitudinal cracks, typically coinciding with the bed joints, within the tension area of the wall and the formation of vertical compression cracks in the area of the wall under highest compression. At later stages of inelastic deformations, the bars located in the compression zone may buckle if a sufficient amount of the grout core has been damaged and tension reinforcement may fracture due to the large amount of inelastic strain (Shedid, 2006). According to Shing et al. (1989) analysis using simple beam theory was shown to represent experimental results accurately in terms of yield and ultimate load conditions but, due to the significant effects of shear deformation, displacements based on flexure alone would not be expected to be accurate.

Due to the slenderness of masonry walls, stability has been considered to be a potentially limiting factor in assessing ductility. Paulay and Priestley (1993) showed that out-of-plane instability was not caused by compressive strains but rather it was caused by the inelastic tensile strains in the reinforcement. During load reversal, tensile stresses would be reversed to zero and on into compression yet a vertical tensile displacement would still exist. At this point, the centrally located reinforcing bar(s) supply all of the compressive resistance as tensile cracks in the masonry would still be open. It is at this stage that the cracks can close on one side of the wall and open further on the opposite side leading to an out-of plane curvature and out-of-plane deflection. It has been suggested that the wall is susceptible to buckling at this point but observations by Shedid (2006) indicate that this is not a limiting feature at least in cases when the compression zone is a small part of the wall length. After the masonry in the compression zone has become severely damaged local buckling of the reinforcing bars has been observed but not until after very large displacements have been reached.

Thomsen and Wallace (2004) conducted experimental research using six quarter-scale wall specimens with rectangular and T-shape cross-sections. Experimental results showed that the inelastic shear response occurred primarily within the bottom third of the wall, measurements over the middle third were essentially elastic, and almost constant over the top third of the wall. A similar experiment conducted by Massone and Wallace (2004) also indicated that the shear deformation contribution in the first storey was relatively large compared to the other storeys. This indicates that shear resistance is critical within the same region as the equivalent plastic hinge occurs.

1.4.2 Plastic Behaviour

Plastic behaviour is an important aspect of the overall seismic performance of shear walls; more specifically the plastic behaviour at the base of the wall and within the equivalent plastic hinge zone is of particular importance. Plastic behaviour at the base of the wall including penetration of plastic deformations into the base of the wall (Paulay and Priestley (1992)) allows for large curvatures to be developed which in turn contributes to ductility. The extent of plastic behaviour is the area where large inelastic curvatures and yielding of flexural reinforcement occur.

Within the elastic range of loading, the moment variation along the height of the wall is linear, as is the curvature profile and, while this moment variation remains linear in the inelastic stages of loading, the curvature profile does not. To account for this in calculations, Paulay and Priestley (1992) suggested that the curvature profile consists of an elastic region and a plastic region of length l_p. Plastic rotation of the wall was then said to occur about the centre of this plastic region which implicitly means that uniform plastic curvature is assumed. Using this assumption and the subsequent curvature profile, the plastic as well as ultimate behaviour can be predicted. Various methods for determining the length of the assumed equivalent plastic hinge and extent of plasticity have been presented by previous researchers (Priestley and Park (1987), Paulay and Priestley (1992), Paulay and Priestley (1993), Hart and Jaw (1993)). Some of these were used in this study and are discussed in subsequent sections as they are presented.

1.4.3 Displacement Ductility and Ductility Related Force Modification Factor, R_d

Many researchers ((Park and Paulay (1975), Shing et al. (1989), Paulay and Priestley (1992), Priestley et al. (1996), Tomazevic (1998), Vasconcelos, G. and Lourenço, P. B. (2009)) have proposed methods of evaluating ductility. However, to date, there is no agreement on which method is most suitable but there is agreement in the fact that assessment of ductility requires that experimental backbone or pushover curves must be idealized into an elasto-plastic behaviour.

The difficulty of using experimental curves to quantify ductility lies in the fact that the yield point often is not clearly defined and may be open to the interpretation of the researcher. The importance of quantifying the yield point is due to the fact that displacement ductility and the force modification factor are the ratio of ultimate displacement to displacement at first yield (Drysdale and Hamid (2005)). In terms of design, the force modification factor directly affects the seismic design force. Greater values of displacement ductility result in greater R_d values which equates to lesser seismic design forces when designing according to CSA S304.1-04.

Priestley (1986) reported that there is a reduction in displacement ductility as the ratio of length to height increases. Therefore, with increasing aspect ratio (height to length), it can be expected that displacement ductility will also increase.

According to CSA S304.1 (2004), shear walls designed for seismic regions fall into 2 categories; Limited ductility shear walls and moderately ductile shear walls. Limited ductility shear walls are allowed a force modification value, R_d, of 1.5 provided that they meet the requirements set forth by the standard. Similarly, a force modification factor of 2.0 is allowed for moderately ductile shear walls, provided that they satisfy the CSA S304.1-04 requirements. Squat shear walls are designated as walls with a height-to-length ratio less than one (Drysdale, R.G, Hamid, A (2005)). While these walls may qualify for the R_d value of 2.0, they must meet stricter requirements than for a non squat wall. With a maximum R_d value of 2.0, it has been suggested that this value underestimates the ductile capabilities of properly designed reinforced masonry shear walls (El-Sokkary, H., Galal, K. (2009)).

Shedid (2008) reported displacement ductility values, at 1% drift, of 2.1, 2.3, 2.4, 3.3, 3.3, and 5.1, suggesting that the R_d value of 2.0 may be reasonable for specific situations. However, it underestimates the ductile behaviour of 50% of the specimens tested. Further research conducted by Shedid (2009) reports values bracketed by 3.5 and 11.6 with an average value of 7.0, obtained from 14 measurements of ductility across 7 experimentally tested shear walls. Of the 7 specimens tested, Walls 1, 2 and 3 consisted of three storey walls with rectangular, flanged, and end confined cross sections, respectively. Walls 4 through 7 consisted of two storey construction with linear, flanged, and end confined cross sections.

1.4.4 Experimental Procedures

Fully reversed cyclic loading has been the testing method preferred by many researchers including, but not limited to, Priestley (1986), Paulay and Priestley (1993), Pilakoutas and Elnashai (1995), Moon (2004), Thomsen and Wallace (2004), Massone and Wallace (2004), and Shedid (2006). This method is preferred due to the similarities it shares with seismic loading (reversed cyclic loading) as well as its ability to produce hysterisis loops. Monotonic pushover style testing is not capable of generating hysterisis loops and therefore properties such as equivalent viscous damping and energy dissipation cannot be examined.

Pseudo dynamic as well as full dynamic testing are preferred testing methods as well. However laboratory restrictions often prevent these types of testing from being used.

1.4.5 Scaled Research

The appeal of using small scale versions of full scale construction lies in the simple fact that it is much easier to possess the resources needed to test scaled specimens particularly when the full scale equivalents become rather large or complex. Typically, scaled research has been performed with reinforced concrete due to its relative ease of construction, but due to the lack of commercially made, and properly scaled masonry units much less scaled research has been carried out on masonry. The appeal of scaled research is enhanced by its accurate representation of its full scale counterpart. As seen with Hamid and Abboud (1985, 1986) Long (2006), Shedid (2006, 2009) and Hughes (2010), small scale masonry can accurately represent full scale construction.

1.4.6 Component versus System Behaviour

There is some debate on whether testing at the component level is representative of the system behaviour of the structure. However, the reality is that component testing still remains economically superior. While it may be more accurate, in terms of system behaviour, to test at the system level "the response of the complete structure [depends] on the response and interaction of each of the building components." (Seible et al. (1994)). Testing at the system level leads to behavioural differences, compared to component level testing, such as coupling, load redistribution, diaphragm action, and flange effect (a phenomena coined by Yi et al. (2006)) as seen with Seible et al. (1994), Moon (2004), and Tomazevic (1998), to name a few. Such behaviour is not easily quantifiable and, due to the effort involved in constructing a test specimen, some parameters cannot be modified in order to investigate the impact or significance on behaviour.

It should be noted that the flange effect coined by Yi et al. (2006) refers to the coupling of intersecting, or closely spaced, perpendicular, in-plane and out-of-plane walls, an effect that will not be seen within the scope of this study.

1.4.7 Seismic Provisions for Reinforced Shear Walls: CSA A23.3 Versus CSA S304.1

Given the obvious similarities, it is logical to compare design provisions related to reinforced concrete and reinforced masonry shear walls. In this regard, clauses pertaining to seismic design reveal that the standards have similarities; however the advantage is given to reinforced concrete in CSA A23.3 due to the freedom that it has in terms of detailing of the reinforcement. The use of hoops and stirrups at virtually any spacing or diameter allows reinforced concrete to provide additional confinement to the vertical reinforcement and the concrete contained within the hoops or stirrups. While masonry walls can be constructed to exhibit a similar behavior through the use or boundary elements, as seen with Shedid (2009), or the use of "Priestley plates", as seen with Priestley (1982), both the spacing of confining reinforcement and the diameter of the confining reinforcement present a limitation when compared to reinforced concrete.

In terms of plastic hinge length, both CSA A23.3 and CSA S304.1 are in agreement with a plastic hinge length being the greater of l_w (the length of the wall) or $h_w/6$.

The maximum ductility related force reduction factor allowed for RC is 4.0 for ductile coupled walls whereas the masonry limit is 2.0, which gives a sizable advantage to reinforced concrete when used in regions where seismic forces control the design.

1.5 Closure

The historical performance of low rise masonry structures during seismic events has warranted further investigation into the behaviour of masonry. Past research has shown that masonry construction can perform with adequate strength and safety during seismic excitation and can also maintain an adequate post event level of strength and safety. The study of plastic behaviour, energy dissipation, viscous damping, and ductility are used in order to evaluate the performance of masonry construction.

While reinforced concrete and reinforced masonry shear walls possess similar attributes, currently there is a distinct advantage to designing with reinforced concrete due to the flexibility in reinforcement detailing as well as the allowable force reduction modification factor. While current Canadian standards allow a maximum force reduction factor of 2.0, past and present research suggests that this value is overly conservative and may cause masonry construction to be economically uncompetitive.

From the literature reviewed, it is clear that additional research needs to be conducted in this field. In particular there is a lack of research conducted in the area of tall walls and the area of structural systems. The research use of third scale masonry units and third scale shear walls and shear wall buildings offers a practical option to rectify this lack of research.

Chapter 2
Experimental Program

2.1 Introduction

The purpose of this chapter is to provide details of an experimental program designed to evaluate the seismic characteristics and behaviour of fully grouted reinforced one third scale concrete block shear walls. In order to include a range of behaviours, 4 walls with unique properties were tested. These properties consisted of various aspect ratios (height/length), a flanged element, and flexural coupling as design parameters that are expected to exist in practice. The data to be collected includes wall deflections, vertical and diagonal displacements within the wall, and strains on reinforcement. From these, properties such as masonry strain, drift, wall stiffness, strength, post-peak performance, plastic hinge length, curvature profile, and ductility can be calculated.

Details of the experimental program, design and construction of each wall specimen, the experimental set-up, and instrumentation are presented and discussed in the following sections. The properties of the constituent materials are also documented. Since this is the first masonry research at McMaster University that involves testing of one third scale construction, extra details will be provided to assist future researchers.

2.2 Details of Test Materials

As was discussed in Chapter 1, this thesis contains the results of experimental research using one third scale reinforced concrete shear walls as a new part of the McMaster University seismic research program on behaviour of masonry under earthquake loading. The materials used to construct the shear wall specimens are described in this section.

2.2.1 One Third Scale Concrete Blocks

Dimensions: Molds were designed at McMaster University to produce scaled replicas of standard hollow 20cm concrete masonry units using the mold configuration shown in Figure 2.1. This mold was designed to be used in a Columbia block making machine and provided 4 standard stretcher units, 2 half block units, and 1 flat ended full sized unit during each cycle of block production. For the third scale block models, overall block dimensions and web and face shell thicknesses are shown in Figure 2.1.

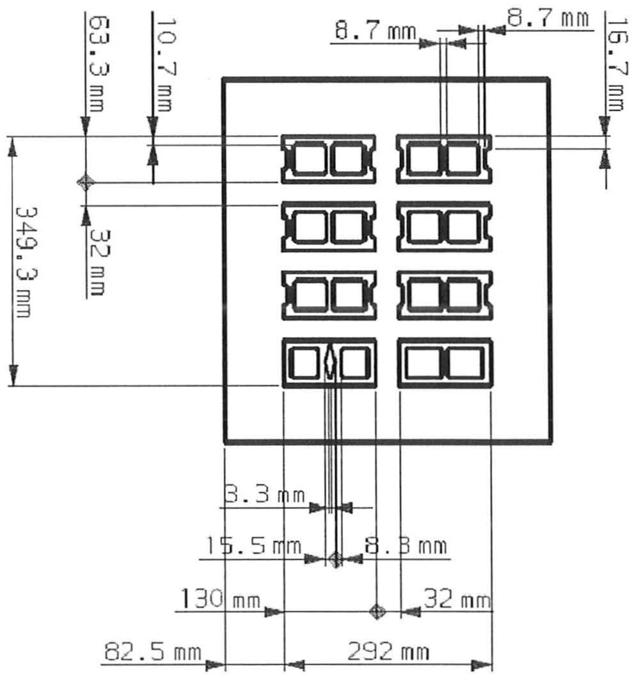

Figure 2.1: Mold Configuration and Product Dimensions

Manufacture of Model Blocks: Although a Columbia block making machine had been generously donated by the Canadian Concrete Masonry Producers Association, it was not operational in time for this research. Therefore, the first series of block were produced at the Niagara Block facilities where Columbia machines were available. Since their regular block production was interrupted during manufacture of approximately 8 thousand model block, experimentation with mix designs was limited. The result was that, although the final choice of mix produced model block with good dimensional control and good appearance, higher strength than normally encountered in practice with full scale units was achieved. However, for the planned research on ductility, yielding of reinforcement was the controlling strength mechanism such that having adequate compressive strength was the main concern and was satisfied with the produced block.

Physical Properties of Block: Table 2.1 contains data on physical properties of the concrete block. It can be seen that the properties of the 3 specimens are consistent, indicating the very good quality of the mixing and production.

Table 2.2 contains the compression test results of five stretcher types blocks where, as mentioned above, the 54.8 MPa strength is much higher than normal but very consistent results were found as indicated by the small 4.7 % coefficient of variation.

Table 2.1: Physical Properties of Block

Block	Wi (g)	Ws (g)	Wd (g)	Height (mm)	Absorption (kg/m^3) (%)	Density (kg/m^3)	Net Volume (mm^3)	Average Net Area (mm^2)
1	0.357	0.633	0.593	64.20	144.93 (6.75)	2148.6	276000	4299
2	0.353	0.627	0.587	64.00	145.99 (6.81)	2142.3	273999	4281
3	0.368	0.641	0.605	63.97	131.87 (5.95)	2216.1	273000	4268
Avg	0.359	0.634	0.595	64.06	140.93 (6.50)	2169.0	274333	4282.7
COV %	2.16	1.11	1.54	0.20	5.58 (7.38)	1.89	0.56	0.36

Table 2.2: Compressive Strength of Block

Specimen	Compressive Strength (MPa)
Specimen 1	56.5
Specimen 2	53.4
Specimen 3	57.6
Specimen 4	55.2
Specimen 5	51.1
Average (COV %)	54.8 (4.7%)

2.2.2 Mortar

Mortar used in construction of the shear wall specimens had proportions by weight of 1:0.2:3.53 of type 10 Portland cement: lime: sand where weight was used as a means of achieving more uniform properties between mortar batches. These proportions correspond approximately with proportions by volume of 1.0:0.5:4.0. Sand was air dried and sieved to achieve the model gradation desired

(See Figure 2.2). Dried and sieved sand was stockpiled indoors in a dry location and in dry containers to reduce variability in mortar batches. For a 5.6 kg batch, approximately 0.85 kg of water was used in the mix to produce a target flow of 125 percent. Mortar was mixed by hand, with a rake and hoe, and in a damp wheelbarrow to prevent moisture loss. Water was slowly and gradually added, and the materials were thoroughly mixed before adding additional water. Typical mixing times were approximately 10 minutes with an additional standing time of approximately 5 minutes for transporting the mortar into the laboratory, making any adjustments requested by the mason, and transferring fresh mortar to the mason's mortar tray. Mortar flow was tested using a flow table set-up. A flow test was performed for each batch of mortar produced. The mortar flow was bracketed by values of 122% and 132% with an average of 128%. The mason constructing the specimens favoured a mortar flow around 132%. The average compressive strength of the mortar cubes was 29.5 MPa with a C.O.V. of 9.1%. Appendix A contains a listing of the mortar strengths obtained from tests on 51 mm cubes.

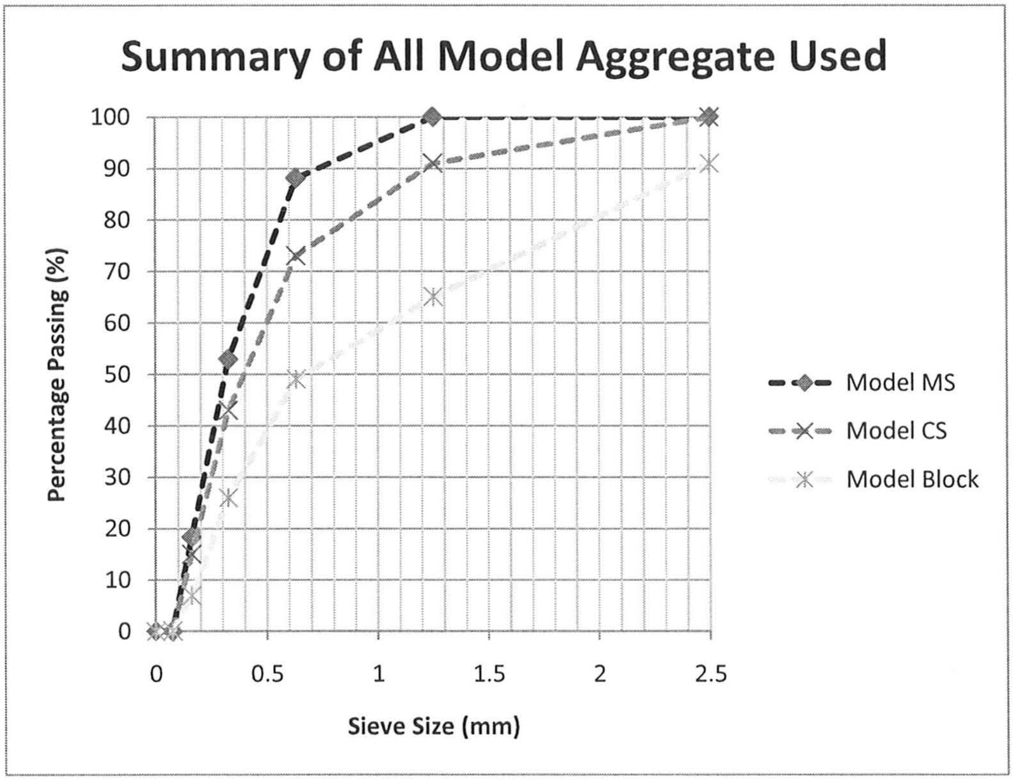

Figure 2.2: Model Aggregate Gradation Curve for Masonry Sand (MS), Grout Sand (CS) and Model Block Used in Specimen Construction

2.2.3 Grout

Grout used in construction of the shear wall specimens had proportions by weight of 1:0.04:3.90 of type 10 Portland cement: lime: sand where weight was used as a means of achieving more uniform properties between grout batches. Concrete sand was air dried and sieved to achieve the model gradation desired (See Figure 2.2). Dried and sieved sand was stockpiled indoors in a dry location and in dry containers to reduce variability in grout batches. For a 5.79 kg batch, approximately 0.85 kg of water was used in the mix to produce a target slump of 250 mm. Grout was mixed by the laboratory horizontal drum mixer. Water was slowly and gradually added while mixing the materials thoroughly before adding additional water.

Typical mixing times were approximately 15-20 minutes with an additional standing time of approximately 5 minutes to transport the grout into the laboratory and begin to grout. Table 2.3 contains a listing of the grout strengths obtained from 100 mm diameter cylinder tests. The overall average strength of 18.9 MPa (C.O.V. = 15.4%) is typical of full scale construction and also represents high quality control between batches.

Table 2.3: Grout Cylinder Test Data

Specimen	Load at Failure(N)	Stress (MPa)	Average
G1-1	177928.0	22.65	21.4
G1-2	156799.0	19.96	
G1-3	169031.6	21.52	
G2-1	128997.8	16.42	16.7
G2-2	131221.9	16.71	
G2-3	133446.0	16.99	
G3-1	136782.1	17.42	16.4
G3-2	122325.5	15.57	
G3-3	127885.8	16.28	
G4-1	187936.4	23.93	18.8
G4-2	131221.9	16.71	
G4-3	124549.6	15.86	
G5-1	152350.8	19.4	21.2
G5-2	164583.4	20.96	
G5-3	182376.2	23.22	

2.2.4 Concrete

Three concrete cylinders were cast for each batch of concrete produced. The concrete mix proportions by weight used were 1:2.73:1.36:0.63 of Type 10 Portland cement: coarse aggregate: sand: water, with a maximum aggregate size of 10 mm. All cast concrete was air cured within the laboratory. Slump tests were not performed however the concrete was made fluid enough to ensure that there were no voids and that there was complete contact around the reinforcing bars. The concrete tests represent the compressive strength of the concrete used in the construction of the reinforced concrete floor slabs, denoted as FSX-Y (See Table 2.4). The first storey floor slabs of Walls 1, 2, 3 and 4 correspond to specimens FS1-1, FS1-2 and FS1-3. The second storey floor slabs of Walls 1, 2, and 3 correspond to specimens FS2-1, FS2-2, and FS2-3. The second storey floor slab of Wall 4 was not poured at the same time as Walls 1, 2, and 3 and corresponds to specimens FSC-1, FSC-2 and FSC-3.

Table 2.4: Concrete Cylinder Compressive Strengths

Specimen	Load at Failure (N)	Compressive Strength (MPa)	Average Strength (MPa)
FS1-1	355856.0	45.3	41.5
FS1-2	315822.2	40.2	
FS1-3	306925.8	39.1	
FS2-1	415906.7	53.0	52.7
FS2-2	413682.6	52.7	
FS2-3	411458.5	52.4	
FSC-1	351407.8	44.7	42.9
FSC-2	320270.4	40.8	
FSC-3	338063.2	43.0	

2.2.5 Reinforcement

Reinforcement consisted of smooth and deformed wire provided by Laurel-LEC Steel. The main vertical reinforcement consisted of D7 deformed wire with a nominal diameter of 7.6 mm and a nominal area of 45 mm^2. The horizontal shear reinforcement consisted of W1.7 smooth wire with a nominal diameter of 3.8 mm and a nominal area of 11 mm^2. Aside from differences in diameter, the D7 and W1.7 wires also differed in surface texture. W1.7 wire had a smooth surface whereas the D7 wire had a ribbed surface, similar to that of standard deformed reinforcing bars.

Tensile testing was performed in order to determine the yield strength of each type of reinforcement. Each type of steel was tested 3 times in a Tinius Olsen machine. The specimen was clamped in a pair of self-tightening steel jaws located within the upper and lower heads of the machine. The lower head of the machine was lowered slowly in order to tighten the jaws and secure the specimen. Once the specimen was secured, the head continued to lower which applied a tensile force on the specimen. A 100 mm long extensometer was used to measure the displacement which was recorded, along with load, on a data acquisition computer. This data was then converted to units of stress and strain and plotted in excel (See Figure 2.3). The 0.2% offset method was used to define the yield strength of the steel listed in Table 2.5. This process was necessary because, as is evident in Figure 2.3, there is no well defined yield point. Using the yield strength from the 0.2% offset method and the experimentally determined modulus of elasticity, the yield strain of the D7 bars was calculated as 0.0027. As seen in Figure 2.4 and Figure 2.5, the W1.7 wire and D4 deformed wire do not have a defined yield either. Using the 0.2% offset method the yield strengths were determined. Using the experimentally determined modulus of elasticity, the yield strain of the D4 bar was calculated as 0.0030. The yield strain of the W1.7 bar was not calculated as it was not used in any calculation.

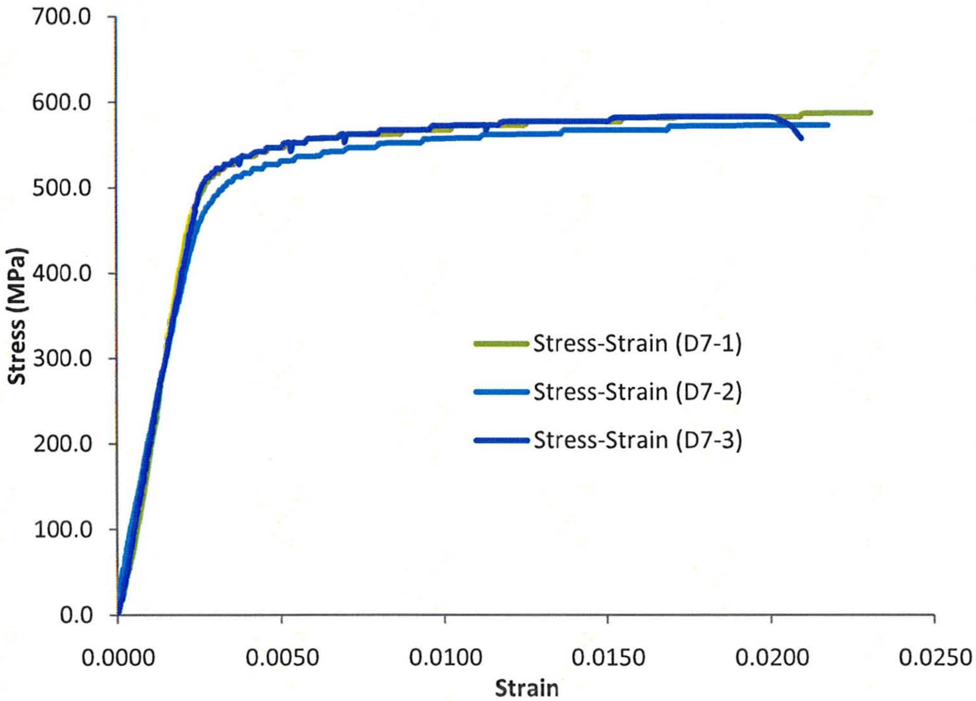

Figure 2.3: Tensile Stress Strain Curves for D7 Deformed Wire

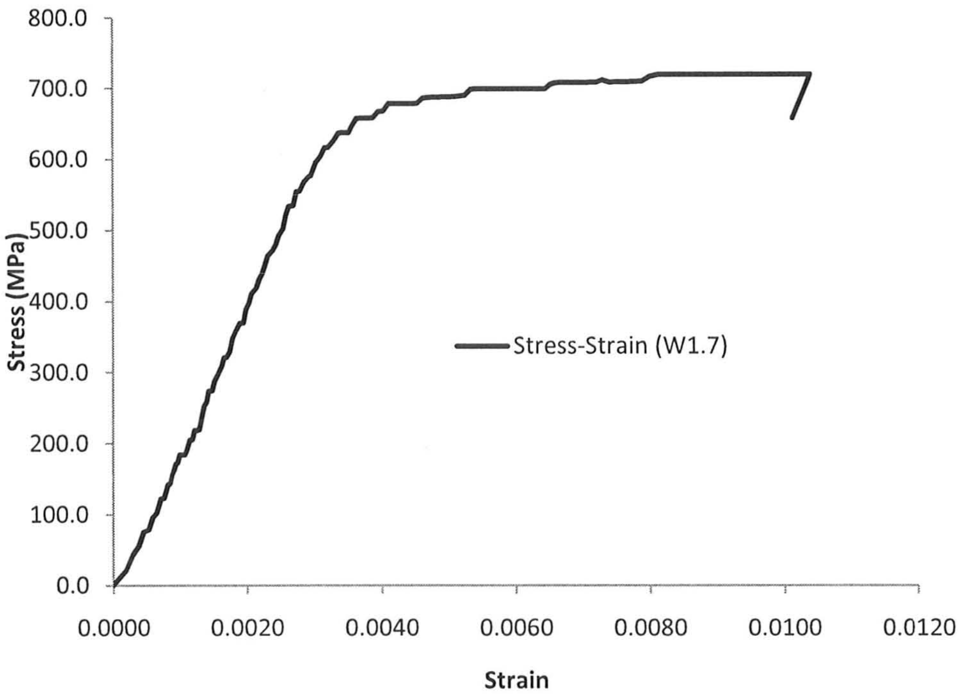

Figure 2.4: Tensile Stress Strain Curve for W1.7 Wire

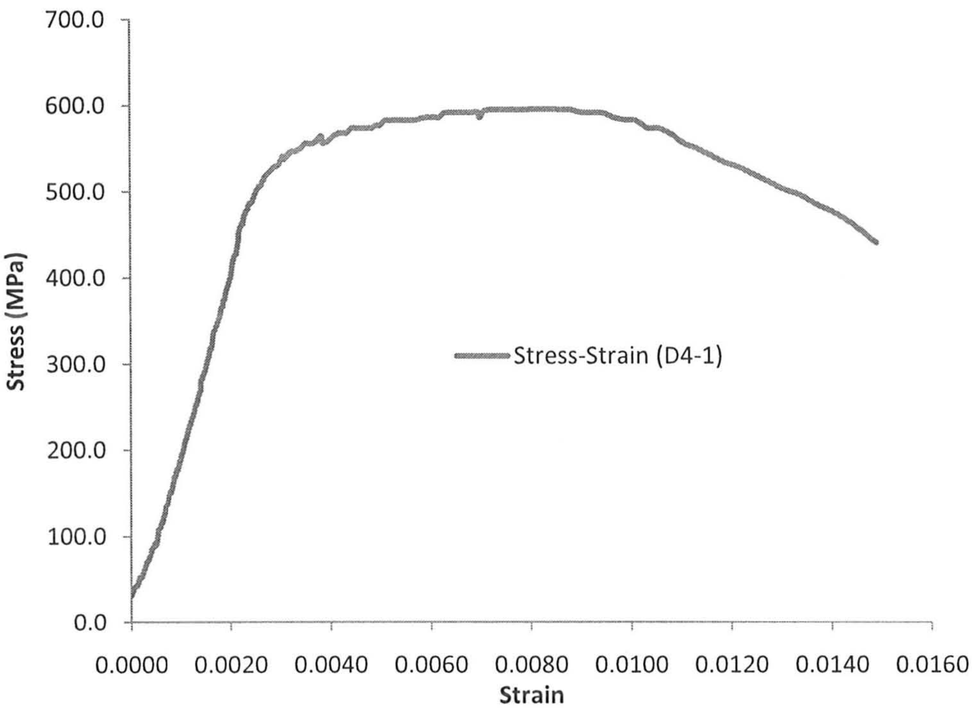

Figure 2.5: Tensile Stress Strain Curve for D4 Deformed Wire

Table 2.5: Reinforcing Steel Tensile Yield Strength

	Tensile Yield Strength of Steel (MPa)		
Specimen	D7	D4	W1.7
Test 1	542.3	573.3	689.0
Test 2	530.8	590.8	670.0
Test 3	546.8	610.0	680.5
Average	540.0	591.4	679.8
C.O.V. (%)	1.53	3.10	1.40

2.3 Properties of Masonry Assemblages

Masonry assemblages are used to document the properties of the masonry as a combination of the individual materials. Therefore, specimens are constructed using the model blocks, mortar and, where applicable, the grout so that strengths and stress-strain relationships can be determined. Availability of such information is essential for meaningful interpretation of the tests on the wall specimens.

2.3.1 Construction of Prisms

For each day of construction, 3 prisms were constructed by the mason. Each prism was a single block in length, 4 blocks in height, and fully grouted. Using a running bond pattern, this resulted in 4 courses consisting of a full stretcher, 2 halves of a stretcher unit, a full stretcher, and another 2 halves of a stretcher unit. It was decided that the most accurate representation of the shear walls would be obtained from cutting stretcher units rather than using half units produced within the mold.

2.3.2 Results of Prism Tests

Prior to testing, gypsum cement capping was placed on the top and bottom surfaces of the prism to ensure even load bearing during testing. When ready to be tested, prisms were placed underneath the centre of the head of Tinius Olsen machine. To determine the stress-strain properties, the prisms were instrumented with 2 linear voltage displacement transducers to measure the displacement while the machine's built in load cell was used to record the load. The test configuration can be seen in Figure 2.6.

Figure 2.6: Prism Test Configuration

Test results are displayed in Table 2.6, 2.7, 2.8, and 2.9. It can be seen that, while the average block strength was 54.8 MPa, the presence of mortar and grout significantly impacted the strength of the assemblages by lowering the compressive strength to an average 22.84 MPa. The stress-strain behaviour for day 1 construction can be seen in Figure 2.7.

The maximum strain was calculated using measured displacements at the measured maximum stress. The maximum strain was below the 0.003 strain value of CSA S304.1-04, but this was because tests were performed under load control conditions. Therefore, no descending branch on the stress-strain curve was recorded. Had the testing been performed under displacement controlled conditions, the ultimate strain would have more closely agreed with the value of 0.003 set forth in CSA S304.1-04. The measured E_m was taken as the slope of the line between the stress and strain at $0.1f'_m$ and $0.5f'_m$. The ratio $(E_{mcode}-E_{mmeasured})/E_{mcode}$ was used to determine the percentage difference of E_m. In all cases, the percentage difference indicated that the predicted modulus from CSA S304.1-04 overestimated the experimentally obtained modulus. For all specimens, failure appeared in the form of vertical cracks accompanied by crushing of the base of the prism.

The values for day one construction were used for theoretical calculations due to the fact that the first day of construction consisted of laying and grouting the first storey of each wall, which is the location of maximum moment.

Table 2.6: Prism Properties- Day 1 Construction

Prism	Comp. Strength f'_m (MPa)	Max Strain	Measured E_m (MPa)	CSA S304.1 E_m (MPa)	% Difference E_m
PC1-1	25.72	0.00209	15640.00	21862.00	+28.46%
PC1-2	23.10	0.00232	17313.00	19635.00	+11.83%
PC1-3	22.51	0.00188	17884.00	19133.50	+6.53%
Average	23.78	0.00210	16945.67	20210.17	+15.61%
C.O.V. (%)	7.19%	10.48%	6.88%	7.19%	73.33%

Table 2.7: Prism Properties- Day 2 Construction

Prism	Comp Strength f'_m (MPa)	Max Strain	Measured E_m (MPa)	CSA S304.1 E_m (MPa)	% Difference E_m (MPa)
PC2-1	19.90	0.00207	14474.00	16915.00	+14.43%
PC2-2	20.18	0.00219	13609.00	17153.00	+20.66%
PC2-3	21.97	0.00241	15258.00	18674.50	+18.30%
average	20.68	0.00222	14447.00	17580.83	+17.80%
C.O.V. (%)	5.43%	7.77%	5.71%	5.43%	17.68%

Table 2.8: Prism Properties- Day 3 Construction

Prism	Comp Strength f'_m (MPa)	Max Strain	Measured E_m (MPa)	CSA S304.1 E_m (MPa)	% Difference E_m (MPa)
PC3-1	23.34	0.00220	18027.00	19839.00	+9.13%
PC3-2	18.54	0.00161	16505.00	15759.00	+4.73%
PC3-3	26.05	0.00249	18168.00	22142.50	+17.95%
average	22.64	0.00210	17566.67	19246.83	+10.61%
C.O.V. (%)	16.80%	21.35%	5.25%	16.80%	63.49%

Table 2.9: Prism Properties- Day 4 Construction

Prism	Comp Strength f'$_m$ (MPa)	Max Strain	Measured E_m (MPa)	CSA S304.1 E_m (MPa)	% Difference E_m (MPa)
PC4-1	24.93	0.00249	16354.00	21190.50	+22.82%
PC4-2	24.51	0.00250	17549.00	20833.50	+15.77%
PC4-3	23.30	0.00186	18876.00	19805.00	+4.69%
average	24.25	0.00228	17593.00	20609.67	+14.43%
C.O.V. (%)	3.49%	16.08%	7.17%	3.49%	63.35%

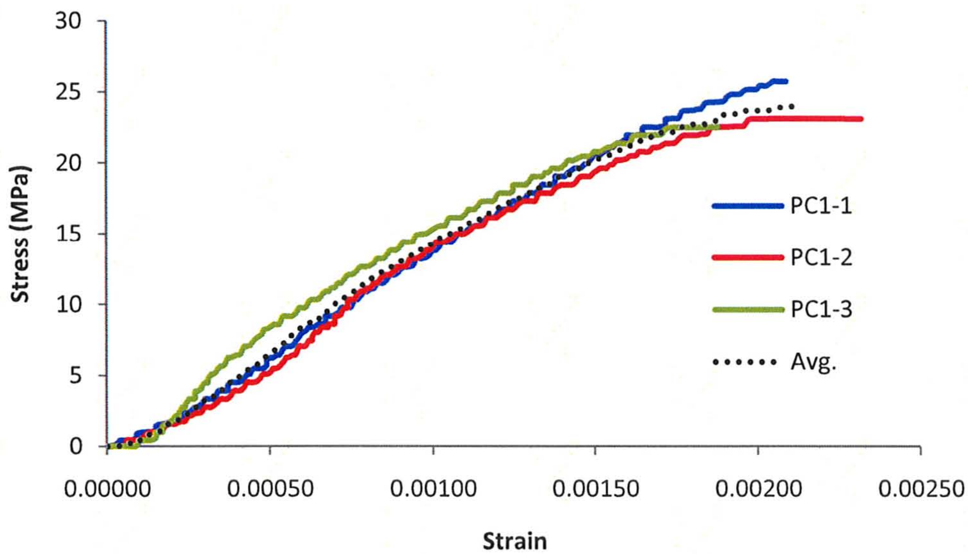

Figure 2.7: Stress-Strain Curve for Prisms Constructed on Day 1

2.4 Description of Shear Wall Test Specimens

The two storey test specimens consisted of 4 fully grouted reinforced one third scale concrete block shear walls. These walls were designed to have the same height and different lengths to produce a range of aspect ratios. As such, the wall test results directly provide information on effect of aspect ratio on ductility and overall behaviour. Also, the load versus displacement histories of the walls are intended to serve as the basis for evaluation of the performance of a two storey test building constructed using combinations of these walls as part of a future research program. Table 2.10 contains a listing of the dimensions and reinforcing used in each of these walls described below.

Table 2.10: Wall Specimen Properties

Specimen	Total Length (l) (mm)	Height (h) (mm)	Aspect Ratio (h/l)	Vertical Reinforcing Ratio (%)	Desired Failure Mode
Wall 1	1132	2200	1.94	0.565	Flexure
Wall 2	865	2208	2.55	0.575	Flexure
Wall 3	1532	2240	1.46	0.662	Flexure
Wall 4	1980	2230	1.11	0.575	Flexure

All wall specimens were reinforced vertically using D7 deformed wires. These scaled reinforcing bars were anchored in a reinforced concrete base and spaced at 133.3 mm to provide reinforcing in every other cell beginning at the centre of the outmost cell. The reinforcement ratio of the test specimens ranged from 0.575% to 0.662% and is classified as a moderately reinforced range as they fell between the range of 1.00%, representing heavily reinforced, and 0.2%, which represents lightly reinforced (Drysdale, R.G, Hamid, A (2005)).

Since flexural behaviour is the focus of this research, each specimen was reinforced horizontally to prevent shear failure and also to limit shear deformations. In order to accomplish this, a conservative amount of shear reinforcement was used. Shear reinforcement was placed at the top of every course throughout the 1st and 2nd storeys. To facilitate the placement of the W1.7 wires, the top of each web was notched, similar to a depressed web used in molding some full scale block. The notches were approximately 15-20 mm in depth and extended for the full width of the web (See Figure 2.8). They were created so that the wire could be placed easily and to allow grout to flow through adjacent webs, creating bond beams. Since the wire surface was smooth, the ends were bent into 180^0 hooks with approximately a 10-15 mm diameter bend to provide anchorage. The rounded bend of each hook was placed snugly around the outermost reinforcing bar and, in conjunction with the embedded length beyond the bend, provided excellent mechanical anchorage to ensure full length effectiveness of this reinforcement (See Figure 2.9).

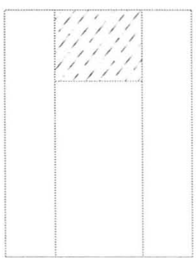

Figure 2.8: Notched Masonry Unit

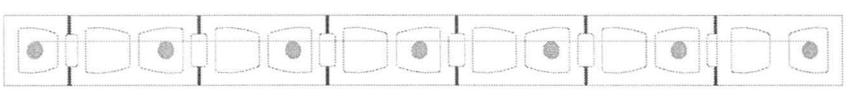

Figure 2.9: Detail of Anchorage of Shear Reinforcement

2.4.1 Wall 1

Wall 1 was a linear wall having a total length of 1132 mm, made up of 8 and a half 1/3rd scale concrete masonry units and 8 head joints each measuring 3.3 mm thick on average. As indicated in Table 2.10 and shown in

Figure 2.10, this wall was reinforced with a D7 deformed wire placed vertically in every other cell for a total of 9 vertical reinforcing bars. This resulted in a reinforcing ratio (A_s/tl_w) of 0.565% which is in the moderate reinforcing range. The total height of the wall was 2200 mm representing two-storey construction and included two 100 mm thick floor slabs, creating a total height to length aspect ratio of 1.94. Theoretical flexural yield capacity was calculated as 71.3 kN-m with a theoretical ultimate flexural capacity of 110.8 kN-m, corresponding to laterally applied loads of 32.4 kN and 50.4 kN, respectively. The effect of compression reinforcing was included in calculation as was the nominal yield strength documented in Section 2.2.5.

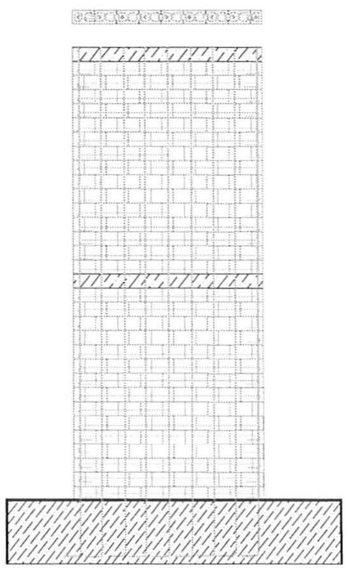

Figure 2.10: Detailed Drawing of Wall 1

2.4.2 Wall 2

Wall 2 was a linear wall which had a total length of 865 mm made up of six and a half 1/3rd scale concrete masonry units and 6 head joints measuring 3.3 mm each. As shown in Figure 2.11, this wall was reinforced with a D7 deformed bar placed in every other cell, for a total of 7 vertical reinforcing bars. This resulted in a reinforcing ratio of 0.575% which is in the moderate reinforcing range. The total height of the wall was 2208 mm, including the two 100 mm floor slabs, creating a total height to length aspect ratio of 2.55. Theoretical flexural yield capacity was calculated as 43.3 kN-m with a theoretical ultimate flexural capacity of 64.5 kN-m, corresponding to laterally applied loads (using an assumed height of 2200 mm) of 19.7 kN and 29.9 kN, respectively. The effect of compression reinforcing was included in calculation as was the nominal yield strength documented in Section 2.2.5.

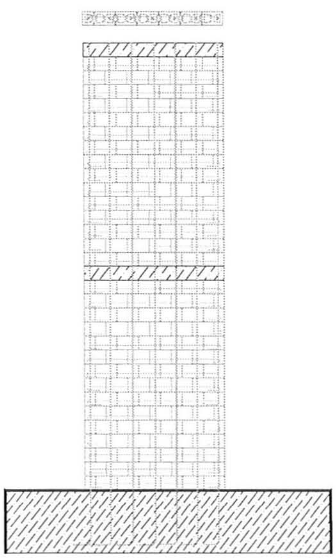

Figure 2.11: Detail Drawing of Wall 2

2.4.3 Wall 3

Wall 3 was a flanged wall, resembling the shape of a 'C'. The total length of the wall was 1532 mm with the web length being 1398.5 mm. Flanges were oriented at 90° to the web at each end with a length of 200 mm and thickness of 63.3 mm as shown in Figure 2.12. The joints at the intersection of the web and flanges were interlocked at every second course. The linear web portion contained 10.5 units while the flanges each contained 2 units (See Figure 2.13).

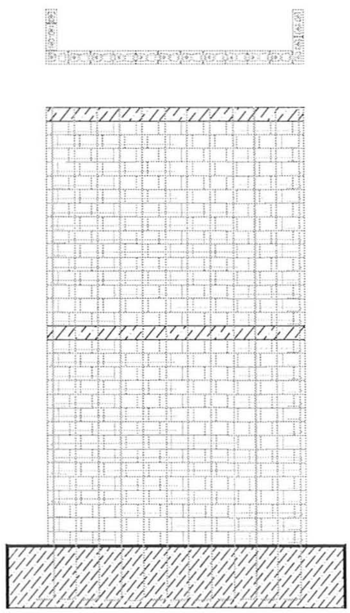

Figure 2.12: Detailed Drawing of Wall 3

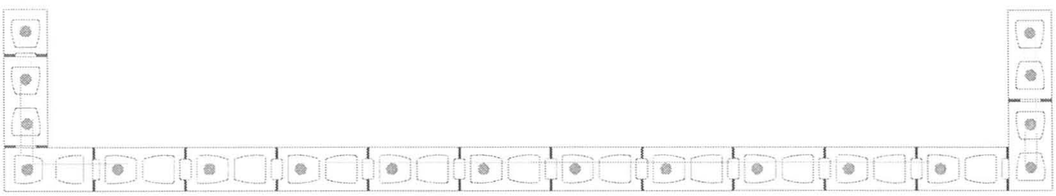

Figure 2.13: Cross-Section of Wall 3

Vertical reinforcement was similar to the other wall specimens with D7 deformed bars placed at 133.3 mm spacing corresponding to every other cell beginning at the 2nd outermost cell, for a total of 10 vertical reinforcing bars within the linear web segment. The flanges, however, were reinforced with a D7 deformed bar placed in every cell, for a total of 4 vertical reinforcing bars in each flange section. Shear reinforcement was placed similarly to other specimens with the addition of a short shear reinforcing bar placed at every course within the flanged section. Shear reinforcement within the flange was oriented in the plane of the flange, perpendicular to the linear section (web), and anchored within the interface between the flanged and linear sections to provide mechanical anchorage (See Figure 2.13)

Theoretical flexural yield capacity was calculated as 238.4 kN-m with a theoretical ultimate flexural capacity of 320.4 kN-m, corresponding to laterally applied loads (using an assumed height of 2200 mm) of 108.4 kN and 146.9 kN, respectively. The effect of compression reinforcing was included in calculation as was the nominal yield strength documented in Section 2.2.5.

2.4.4 Wall 4

Wall 4, shown in Figure 2.14, was designed to investigate coupling of shear walls. It consisted of 2 shear walls measuring 865 mm (6.5 units) in length with each similar to Wall 2. The two walls were spaced 250 mm apart and connected by continuous 1/3rd scale reinforced concrete floor slabs at the top of the first and second storeys, which acted as the source of coupling. These coupling beams were minimally reinforced in order to simulate a typical minimally reinforced concrete floor slab. The scaled floor slab was reinforced with 2 D4 ($As = 26\ mm^2$) deformed wires placed at a depth of 30 mm from the top of the 100 mm floor slab and another 2 D4 deformed wires placed at a depth of 70 mm. The details of each wall corresponded with Wall 2.

Due to the unknown effect of coupling, no theoretical calculations for yield load were determined. However, at ultimate conditions, assuming that the full ultimate capacity of the coupling beams (1.9 kN.m) was attained, the axial forces introduced into the walls were 38.2 kN tension in Wall A and compression in Wall B. Under the action of these two forces, the individual flexural capacities of these two walls were calculated to be 53.4 kN-m and 77.8 kN-m for Walls A and B, respectively. Then, combined with the coupling effect, the coupled shear wall capacity was determined to be 189.5 kN-m corresponding to a lateral load at the top of the test specimen of 86.1 kN. In the case of zero coupling, the capacities of Wall 4 would be, theoretically, double that of Wall 2. It was anticipated that the capacity would more closely agree with fully coupled behaviour.

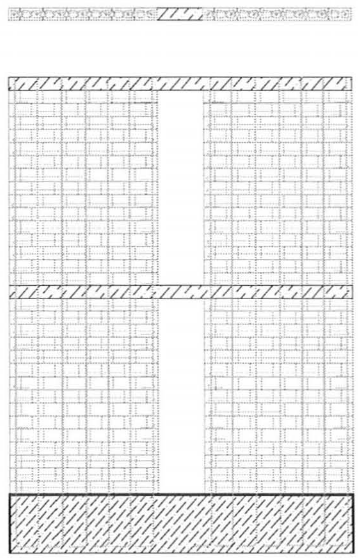

Figure 2.14: Detail Drawing of Wall 4

2.5 Construction of the Test Walls

The specimens were constructed using accepted construction techniques employed in full scale construction except that 3.3 mm thick mortar joints were used. The mason, who is a qualified instructor at the Canada Masonry Centre, quickly adjusted to these different conditions and was able to adhere closely to the specified dimensions.

Each specimen was constructed on a level surface consisting of the concrete base beam (to be described later) which had the required vertical reinforcement positioned and anchored into it; each course of construction was checked to ensure it was both level and plumb. Due to the relatively small amount of mortar and the relatively small size of the masonry unit cells, the amount of mortar droppings was very minor. In most cases, the excess mortar was simply removed by hand in order to allow for ease of grouting. Mortar joints were tooled in a concave pattern using a joint tool which was fabricated specifically for these specimens. Although construction of each specimen had its' own unique features, there are a number of aspects that are typical of all specimens. These are described in the following sections.

2.5.1 Reinforced Concrete Base Beams

Separate 300 mm high x 300 mm wide x 2000 mm long RC Base Beams were used to develop full strength of the flexural reinforcement and also to attach the specimen to the test set-up. These were constructed prior to construction of the wall specimen itself and were reinforced with 3 No. 10 reinforcing bars placed in the top and bottom as shown in Figure 2.15 and included No. 10 stirrups at a spacing of 300 mm.

The bottom of the vertical reinforcement for each wall specimen was bent 90^0 and tied with wire to the RC base reinforcement at the correct spacing and position. The full height of the wall reinforcing was anchored in this way to avoid the complexities associated with requiring splicing of the reinforcement. Due to the extreme slenderness of the vertical reinforcing bars additional support was needed to stabilize them during construction. This support came in the form of drilled wooden blocks, as seen in Figure 2.16. Each bar was inserted through a hole in the wood board and it was then secured using nylon rope which was pulled taut and tied to laboratory columns and/or stacks of full scale concrete block units.

ABS plastic tubes were placed and secured within the form for the Base Beam. This produced holes in the base that were later used to attach the RC base to the test set-up.

Figure 2.15: Construction of Bases for Shear Wall Specimens

Figure 2.16: Support of Vertical Reinforcement during Construction

2.5.2 Grouting

During construction of the 1st storey, lifts of 5 courses were laid and, after a few hours time to allow the mortar to harden, grouted using the scaled grout described in Section 2.2.3. During the grouting of each lift, the top course in that lift (i.e., the 5th and 10th courses) were not grouted level to the top of the course but rather they were grouted to the mid-height. This created a shear key when the following lift of grout was poured. The purpose of the shear key was to prevent slip failure at the point at which the grout column lost continuity when it coincided with the weak plane along the bed joints of blockwork. The point of reduced strength occurs at the interface between the point at which the previous day's pour ended and the next day's pour begun. The construction time for the first storey was 3 days. For the second storey, 7 courses were laid and grouted (to mid-height of the 7th course). Then the remaining 8 courses were laid the following work day and grouted. Total construction time for the 2nd storey was 2 days.

2.5.3 Reinforced Concrete Floor Slabs in the Shear Wall Specimen

Each specimen's floor slabs were constructed using the concrete described in Section 2.2.4. The purpose was to simulate the interaction between the block masonry, grout, and concrete slab. In addition to scaled aggregates in the concrete mix, the dimensions of the floor slabs were also scaled in order to represent realistic dimensions of a full scale floor slab. To facilitate the pouring of the 1st and 2nd storey floor slabs, forms were built which provided the shape of the slab. To provide support for the form, lengths of 25 mm square lumber were used (as seen in Figure 2.17). For the 1st storey slab these posts were supported on the reinforced concrete base beam. Shims were used at the top to provide a means of levelling the form. Duct tape was applied to underside of the form in locations where there was a possibility that the concrete paste could escape. Slab reinforcement was supported by small pieces of 1/3rd scale block faceshell. This was needed to lift the reinforcement from the bottom of the form and allow the concrete to fully encase the steel.

Figure 2.17: Support Work for 2nd Storey Formwork

The reinforced concrete slabs were 100 mm thick and 190 mm wide. In terms of full scale construction, this represents a 300 mm thick floor slab and, although this is a rather thick floor slab, it is a dimension which has been used in the design of reinforced concrete floors. Although a full width of floor slab representing the typical distance between parallel walls in a building was not used, it was decided that the chosen dimensions were sufficient to produce the desired effects. These effects relate to modification of the spread of cracking from the first storey units to the second storey and causing the previously mentioned coupling of the shear walls. Use of a wider slab section would have complicated the evaluation of coupling by introducing complicated load transfer mechanisms between the slab and the wall and by introducing the possibility that the strain profile through the thickness of the slab would not be similar across the entire width.

With the exception of Wall 4, the scaled floor slabs were reinforced using 2 No.10 reinforcing bars at midheight of the slab. The reinforcement was included to control cracks running through the slab cross-section and in general to prevent slab failure.

2.6 Experimental Set-up for Reversed Cyclic Loading of Shear Walls

2.6.1 Loading Frame

The experimental test set-up consisted of: a steel base beam, 6 WF steel columns, 2 fabricated HSS sections, 4 adjustable arms complete with 300 mm bench mount style bearing rollers, and a 650 kN (500 mm stroke) MTS actuator. Figure 2.18 is a labelled drawing of this test set-up.

2.6.2 Specimen Installation

To ensure even bearing between the base of the specimen and the base of the test set-up, the specimens were placed on an approximately 15 mm thick layer of very fluid mortar, spread on the top of the steel base beam. The base of the set-up consisted of a stiffened large steel I-beam which was bolted to the strong floor of the laboratory. After 24 hours, the base of the wall was prestressed onto the steel base using 8 threaded rods. Each threaded rod was ¾inch in diameter and prestressed to a force of 35 kN.

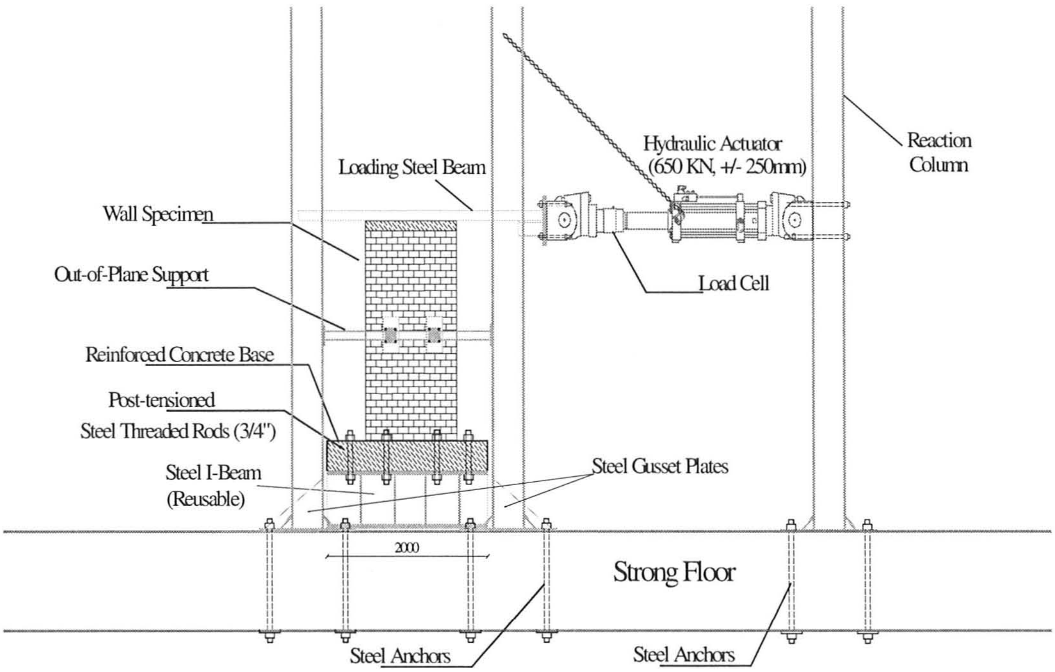

Figure 2.18: Detailed Drawing of Experimental Test Set-up

Fabricated steel HSS sections spanned between each set of columns in order to create an out-of-plane bracing system. Once the HSS sections were bolted to the columns and the specimen was in place, the Adjustable Arms were then attached to the fabricated HSS sections in order to prevent out-of-plane movement. The rollers on the arms were in close proximity to the first storey floor slab and in the event of contact, between slab and roller, the roller provided the required out-of-plane support while still maintaining the ability of the wall to deflect in plane. Figure 2.19 is a detailed drawing of the roller system used to prevent out-of-plane deflection of the wall at the first and second storey floor slabs.

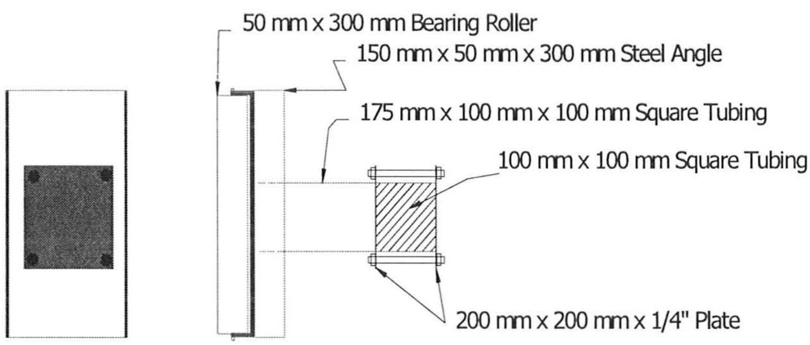

Figure 2.19: Detail Drawing of Out-Of-Plane Rollers

2.6.3 Loading Beam

The main portion of the loading beams was constructed using two 102 x 102 mm steel L-sections with 6.3 mm thickness, which were separated by a 10 mm gap in order to allow vertical reinforcement to pass through. The L-sections were welded to a 15 mm thick 305 x 356 mm steel plate which served as the attachment point for the actuator head. Each L-Section was oriented such that one leg lay horizontal along the top of the wall and the other leg extended vertically upward. For the end of the loading beam opposite the actuator head, the L-Sections were welded together with a short piece of similar angle oriented perpendicular to the L-Sections. A stiffener in the form of a small I-Section was welded to the mounting piece and to the underside of the L-Sections to ensure that local buckling of the L-Section between the actuator and the wall would not occur.

Prior to installation of the loading beam, an approximately 10 mm thick layer of mortar was placed between the top floor slab and underside of the steel L-Sections in order to ensure that the loading beam was level. Walls 1, 2, and 3 were loaded using a loading beam which was welded to the main vertical wall reinforcement which extended through the floor slab. Also, in order to distribute the lateral load across a greater number of bars, during pouring of the 2nd storey floor slab, additional D7 bars, which had been bent with 90^{o} hooks approximately 100 mm long, were placed upright in the fresh concrete. A bar was placed equidistant between each vertical reinforcing bar in order to create a dowel action and facilitate welding them to the loading beam.

To attach the loading beam to the reinforcement, 6.3 mm thick by 51 mm square steel plates were drilled and slid over top of the reinforcement. At a minimum of 24 hours after seating the loading beam in its bed of mortar, each plate was welded to each L-Section and then each reinforcing bar was welded to the plate. Figure 2.20 below is a photograph of a typical loading beam which had been installed onto the wall specimen and attached to the head of the actuator.

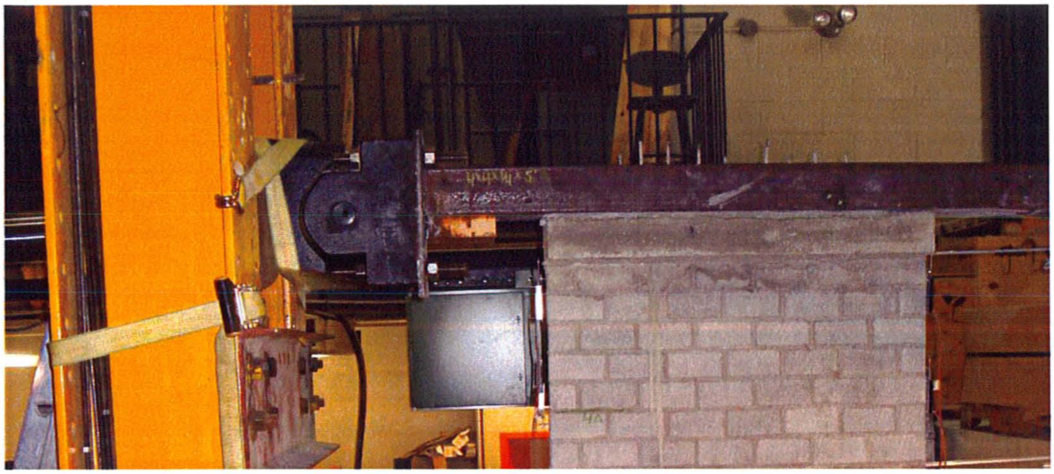

Figure 2.20: Photograph of a Typical Steel Loading Beam Installed on Wall Specimen

The loading beam used for Wall 4 was designed differently in order to be able to observe the coupling effect of the floor slabs joining the two walls. To achieve this, the loading beam must not be allowed to aid in the coupling of the walls. For this reason, the typical method of welding the loading beam to the vertical reinforcement could not be used as this would add to the flexural coupling. The solution was that the lateral force was applied to one wall and allowed to transfer through the coupling beam slab to the other wall. As a result, Wall 4 used a loading beam which acted as a steel cap around the second storey floor slab. During the 'pushing' phase of testing, the beam would bear against Wall A and the force would transfer through the coupling beam and into Wall B. During the 'pulling' phase of testing, the beam would bear against Wall B and similarly transfer the force to Wall A via the coupling beam.

2.6.4 Mounting of the Actuator and Horizontal Displacement

A 650 kN actuator was used to supply the lateral force for all 4 wall specimens. The actuator loading was displacement controlled using MTS FlexTest software. The actuator was bolted to a spreader beam which consisted of twin I-beams, welded together along the adjoining flanges. The strong axes of the I-beams were oriented in the direction of the actuator to achieve maximum stiffness. In turn, the I-beams were bolted, at each end, to two WF steel columns which were bolted to the strong floor of the laboratory.

During testing, the reaction load provided by the actuator was transferred through the I-beams into the columns and down to the strong floor. Therefore, minor lateral movement of the columns was expected and for this reason the lateral displacement of the actuator was not used in any calculations of wall deflection. Figure 2.21 shows the actuator bolted to the twin I-beams, which were bolted to the adjoined columns; the chain was used to support the body of the actuator at all times.

In order to measure the lateral displacements of the wall specimen, a wooden column with multiple shelves was built and bolted to a steel channel section that bridged between two columns that were not part of the loading frame. Shelves were placed at predetermined heights in order to attach LVDTs and Temposonic instrumentation onto the wall to record true displacements of the wall.

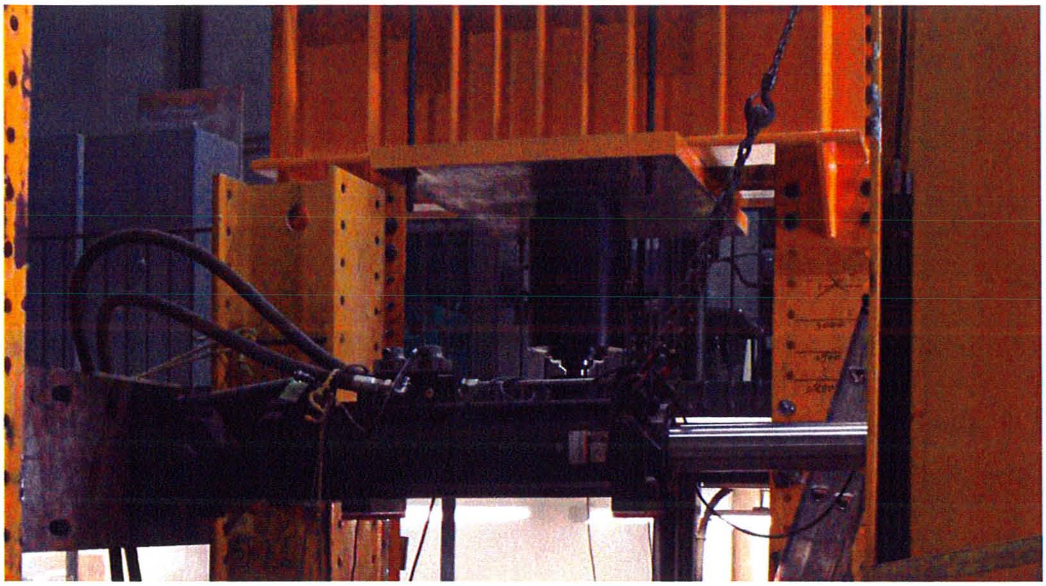

Figure 2.21: Photograph of Actuator Mounted in Test Frame

2.7 Instrumentation

2.7.1 Strain Gauges

Foil strain gauges were installed on specific reinforcing bars and at specific locations (discussed later in the section) in order to determine when the initial yield point was reached as well as the extent of yielding along the height of the first storey. In order to install the strain gauges, the rough surface of the deformed wire had to be removed to create a smooth installation surface. Reinforcing bars were lightly ground using an electric grinder. Care was taken to ensure that the amount of steel removed from the bar was minimal and that grinding was at the correct place along the bar.

After the bars were ground, the strain gauge leads were soldered to a Flag (FG) terminal. Then the bars were cleaned with alcohol to ensure a clean surface and maximize the adhesion of the gauge and terminal to the surface of the bar. Once cleaned, an epoxy was placed on the bar and the gauge was installed onto the bar. The gauge was held in place to allow initial curing of the epoxy and ensure proper adhesion. The next step was to install the FG terminal. Leads on the strain gauges were soldered to one side of the terminal, wires which would be hooked up to a quarter bridge were soldered to the other side. This involved applying epoxy to a second section of the bar and placing the terminal on the epoxy. Again, time was allowed for the epoxy to cure. Following this, a set of wires were soldered to the terminal. These wires would later connect to a quarter bridge to allow the data acquisition system to read an appropriate signal. Once the solder had cooled, the resistance of the gauge was measured to ensure that the gauges had been installed correctly, and a generous layer of epoxy was brushed onto the entire strain gauge in order to protect it electrically. Upon drying a generous layer of household silicon caulking was applied over the area in order to protect it from damage during construction and grouting. This gauging method had proven to be effective and reliable in the work of previous students at McMaster University.

Walls 1 and 2 were instrumented with 14 strain gauges each. Five strain gauges were placed on the outmost bar at each end of the wall (10 total) and the second outmost bar at each end of the wall had 2 strain gauges (4 total) attached. The locations of the strain gauges can be seen in Figure 2.22.

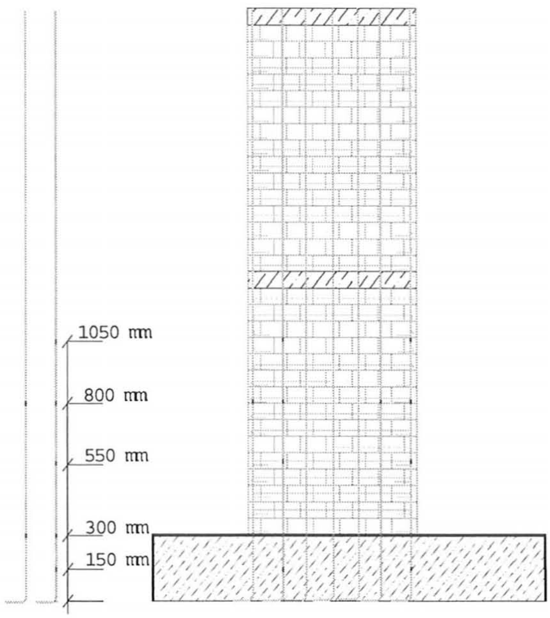

Figure 2.22: Location of Strain Gauge Instrumentation

Wall 3 was instrumented with a similar configuration except that two bars within each flange were instrumented with 5 strain gauges and the outmost bar of the web was instrumented with 2 strain gauges. The strain gauge locations on the reinforcing bar remained consistent with the ones used for Walls 1 and 2. Wall 4 was instrumented with 28 strain gauges, resulting from each of the walls within Wall 4 being instrumented in the same manner as Walls 1 and 2. Locations in the wall and along the reinforcing bar remained unchanged compared to Walls 1 and 2.

Prior to the first wall test, the strain gauges were connected to the data acquisition system and monitored for a period of approximately 4-5 hours. During this time, it was discovered that strain gauges in Wall 1 were faulty. Some gauges displayed inconsistent values and incorrect values (in the order of 10^6 microstrain). Although several explanations were thought of, the fact that the strain gauges were functioning properly prior to the application of the silicone caulking led to the hypothesis that the silicone caulking was responsible for causing the malfunction of the gauges. To verify this, a test was performed on a sample of the caulking. A bead of caulking was placed on top of a thick piece of hard plastic and the electrical resistance of the caulking was measured with a digital multi-meter. According to the digital multi-meter, the caulking had no electrical resistance and therefore would affect the circuit of the strain gauge wherever the epoxy had not entirely coated and insulated the strain gauge. This also explains why some strain gauges functioned properly while others did not.

2.7.2 Vertical and Horizontal Instrumentation

Varying sizes of linear variable displacement transducers as well as 3 temposonic sensors were installed horizontally on the wall specimens. These devices were used to measure the lateral movement at various positions along the height of the wall. The resulting data was then used to calculate the drift, displacement ductility, extent of plasticity and average curvature. Vertical instrumentation was installed along the ends of the specimen to measure vertical displacements required to create curvature profiles. Instruments were installed diagonally across the face of each storey to measure distortion due to shear deformations. Instruments were installed horizontally at the base of the wall as well as the base of the specimen to monitor slipping of the wall with respect to its base and slip of the base with respect to the steel base beam.

Figure 2.23 is a detailed drawing of the typical instrumentation configuration for Walls 1, 2, and 3. Figure 2.24 is a detailed drawing of the corresponding configuration for Wall 4.

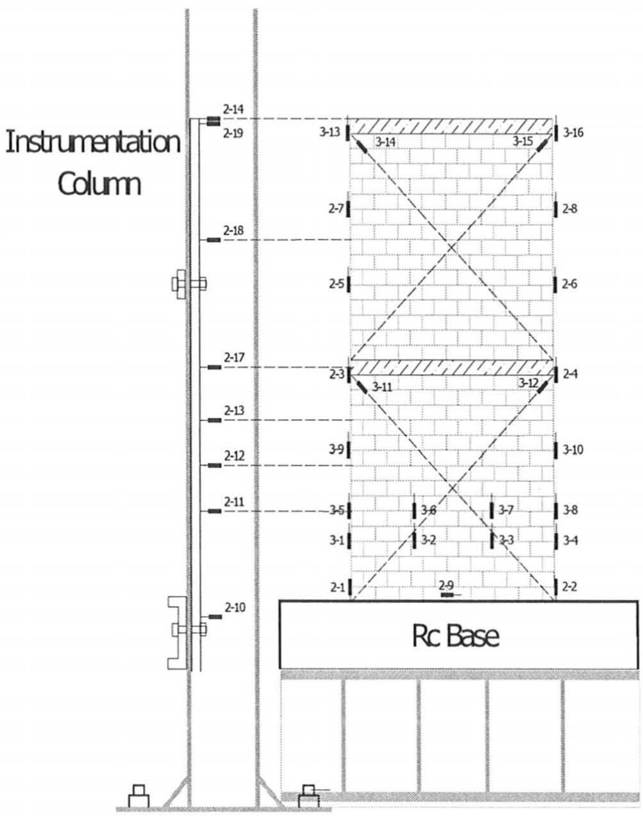

Figure 2.23: Details of Typical LVDT Configuration for Walls 1, 2, and 3

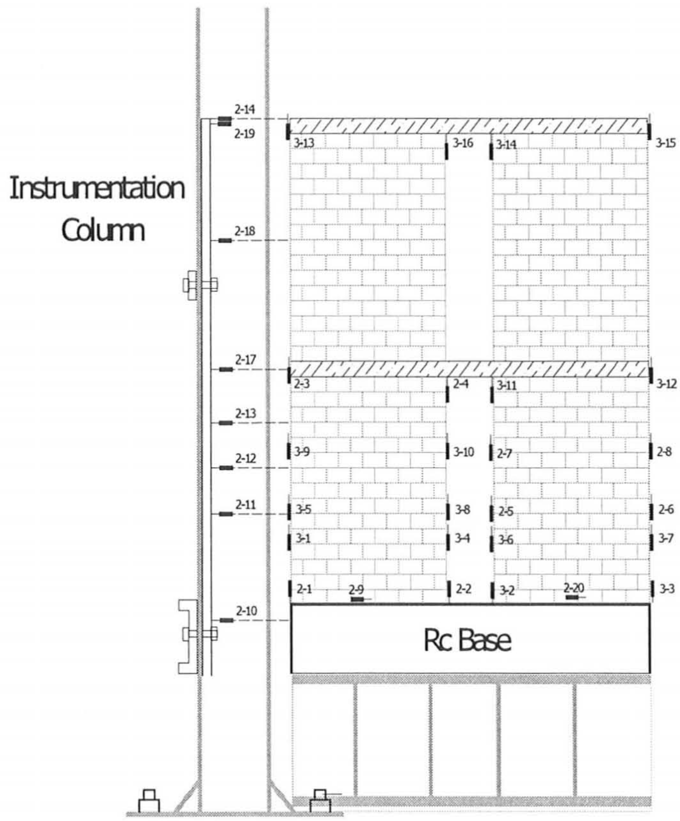

Figure 2.24: Detail of LVDT Configuration for Wall 4

As discussed above, LVDT's were placed horizontally at regular intervals over the height of the wall to capture not only the lateral displacement of the wall but also to aid in determining the curvature and the extent of plasticity. The same purposes can be assigned to the vertical LVDT's which recorded vertical displacements that were then expressed as average strains, based on gauge reading and gauge length, and finally used to calculate curvature and to estimate the extent of plasticity.

According to previous work, "It is common practice to estimate the contribution of flexural deformations to first story lateral displacement by assuming the center of rotation of the inelastic curvature distribution to be 1/3 of the distance from the base of the wall (a-value of 2/3). This assumption is common because sufficient instrumentation is not usually provided to determine the center of rotation directly using experimental measurements. An analytical study was conducted where key terms were varied to assess a reasonable distribution of vertical displacement transducers to determine a directly from experimental measurements. The results indicated that four to six displacement transducers at each wall boundary would be sufficient for the wall tests" (Massone and Wallace, 2004).

Due to the large amount of instrumentation that would have been needed to instrument Wall 4 in a similar manner to Walls 1, 2 and 3, some of the instrumentation points were omitted. Most notably, the vertical instrumentation to be placed at the 5^{th} and 10^{th} courses on the second storey was omitted. Diagonal instrumentation was also omitted as were the 4 vertical instrument points located on the face of the lower half of the first storey. Vertical instrumentation along the ends of the first storey of each wall was unchanged, as was the horizontal instrumentation along the full height of the wall.

2.8 Conclusion

The details of the experimental program were presented in this chapter and focused on the material testing, properties of the shear wall specimens, construction of the specimens, experimental set-up, and instrumentation.

Construction of the walls presented a unique challenge arising from he fact that the dimensions of 1/3rd scale masonry are rather small. Considering that the modular length of a single unit plus head joint is theoretically 133.3 mm, this leads to rather strict construction layout tolerances (i.e., vertical steel placement) as an error of as little as 0.3 mm can become substantial when compounded. Considering that 0.3 mm accuracy is extremely difficult to achieve, it is highly probable that cumulative errors in construction of 1-2 mm can occur. The associated errors in laying the masonry units (i.e., bed joint and head joint thickness, in-plane and out-of-plane alignment of individual units) are very sensitive to the skill of the mason. Fortunately, these wall specimens were built by a mason with experience in scaled masonry construction.

While bed joint thickness is critical to achieving correct wall height, the head joint thickness is critical to proper bar alignment. With the small tolerances present, cumulative errors in head joint thickness can lead to improper bar alignment within the cell of the unit or, in severe cases, may interfere with the web of the unit. Once this occurs there is no choice but to remove the units and lay them again. Additionally, improper bar alignment can lead to a void in the grout column as the bar prevents grout from flowing between it and the web of the unit.

Bars that are bent around a small radius to fit within the cells of the block to allow proper placement of units and not disrupt freshly laid units are forced to yield in order to remain in the desired shape. The bent shape may lead to additional stresses within the wall due to the straightening of the bar when under tension.

The experimental test set-up was created for this experimental program and represented another set of unique challenges including, in particular, the method of prestressing the RC base beam of the wall onto the test base and preventing out-of-plane movement. Details of the experimental test set-up were presented in Section 2.6.

The RC base was prestressed using threaded rods which were tightened to produce sufficient tension to secure the base and prevent it from sliding or lifting up. The threaded rods were tightened with a torque wrench to achieve the desired force. In order to determine the force at a specific torque, tests were done using a threaded rod bolted between the two heads of one of the laboratory test machines. Nuts were threaded on the ends of the rod to secure it and then tightened with a torque wrench. The load cell on the test machine was able to record the compressive force that the tightening exerted on the heads of the machine. Force was recorded for specific levels of torque and repeated with different threaded rods and nuts to ensure repeatability. Once this was finished, the level of torque required to produce a specific level of prestressing force was known and could be used to prestress the RC base of the specimen to the experimental set-up.

The design of the out-of-plane bracing supports presented a challenge due to the fact that there was limited distance (in the out-of-plane direction) between the floor slabs of the wall and the nearest support (i.e., vertical columns). Therefore, using a rotating arm type brace was not feasible due to the fact that the arm would require sufficient length such that it would not resist the in-plane movement of the wall. Due to these space constraints and ease of construction, the roller system presented in this chapter was built. These supports served to prevent out-of-plane movement as well as provide a solution with the least amount of friction or other resistance to in plane movement being introduced.

Instrumentation was used to determine the average curvature profile, lateral displacements, slip displacements, and also to record the strain within the reinforcement. However due to the problem with the caulking (presented in 2.7.1) used to protect the strain gauges, several of strain gauges malfunctioned and become unusable.

Material tests were performed for each material in order to determine their properties. Several results were discussed in this chapter and more complete details of material testing can be found in Appendix A.

Experimental procedure and experimental results are presented in the following chapter.

Chapter 3
Experimental Results

3.1 Introduction

This chapter contains the experimental results of the test walls described in Chapter 2. A description of observations during the test and wall cracking patterns are provided for each specimen, complete with corresponding photographs. Load-displacement details are provided in graphical form. For ease of interpretation, *pushing*, or the *push direction*, refers to the wall being pushed to the West and *pulling*, or the *pull direction*, refers to the wall being pulled to the East. Unless noted, photos are taken of the North face of the wall so that the right side of the photograph is West or the *push direction.*

3.2 Wall 1

3.2.1 Test Documentation and Description of Test

Wall 1 was the only specimen loaded using the originally intended experimental procedure. It was tested using quasi-static fully reversed cyclic loading conditions with each cycle consisting of a push and pull phase. The loading on Wall 1 was cycled twice at lateral loads of 20%, 40%, 60%, 80% and 100% of the theoretical lateral yield load corresponding to loads of approximately 6, 13, 19, 26, and 32 kN, respectively. Upon reaching flexural yield, using displacement control, Wall 1 was cyclically loaded twice at displacement values of 2, 3 and 4 times that of the lateral yield displacement.

Figure 3.1 (a) illustrates the cracking pattern present after two cycles at yield load. This phase of testing corresponded to a lateral load of approximately 32 kN and a top lateral yield displacement, Δ_y, of approximately 6.7 mm (push) and 7.7 mm (pull). For this test, the yield point was set as the point at which the theoretical lateral yield load was reached. Due to malfunctioning strain gauges, electrical strain gauge readings could not be used to identify nor verify the yielding point. For subsequent levels of displacement, the average value of 7.2 mm was taken as the yield displacement. As can be seen in the figure, very little damage to the masonry occurred during the initial loading cycles. Minor bed joint cracking and a single stepped crack were observed.

Increasing the displacement to 14.4 mm, ($2\Delta_y$) with a corresponding lateral load of approximately 47 kN, led to increased stepped cracking patterns. Figure 3.1(b) indicates the cracked state of the wall after one cycle of testing at $2\Delta_y$ displacement. During this phase, several previously formed bed joint cracks increased in length and width. There was a very minor amount of additional bed joint cracking.

The displacement was then increased to 21.6 mm, ($3\Delta_y$) with a corresponding lateral load of approximately 50.7 kN. Figure 3.1(c) is a photograph of the cracking pattern at this level of displacement and shows that the stepped cracking was more significant than after the previous cycles. Bed joint cracking increased slightly as well. At this phase of the test, cracking appeared in the second storey of the wall. As seen in Figure 3.1(d), there was significant bed joint cracking as well as a stepped crack which propagated through the first storey concrete floor slab. During the test, it was believed that a minor twisting of the upper storey was being caused by a slight misalignment of the actuator. At this point the actuator head was restrained perpendicular to the direction of the applied load, using a woven cloth strap such that it forced the actuator head to remain within the plane of the specimen and did not provide resistance to the actuator loading.

As the Wall reached a displacement level of 22 mm in the push direction, a snapping noise was heard and the load decreased suddenly. At this point, the test was stopped and it was concluded that the outermost flexural reinforcing bar at the East end of the wall had fractured. The wall was then pulled to achieve a displacement of $4\Delta_y$ in the East direction, however, the West outmost flexural bar fractured at a displacement of 25.6 mm. When the wall was pushed in the second loading cycle at this displacement, 2 more East end bars fractured before reaching the previous level of displacement. During this phase of testing, there was some additional cracking and damage to the masonry. From Figure 3.1 (e), it can be seen that a few new cracks had formed. However they were no more than 50-100 mm in length. The wall was unloaded to zero lateral load and this concluded the testing of Wall 1.

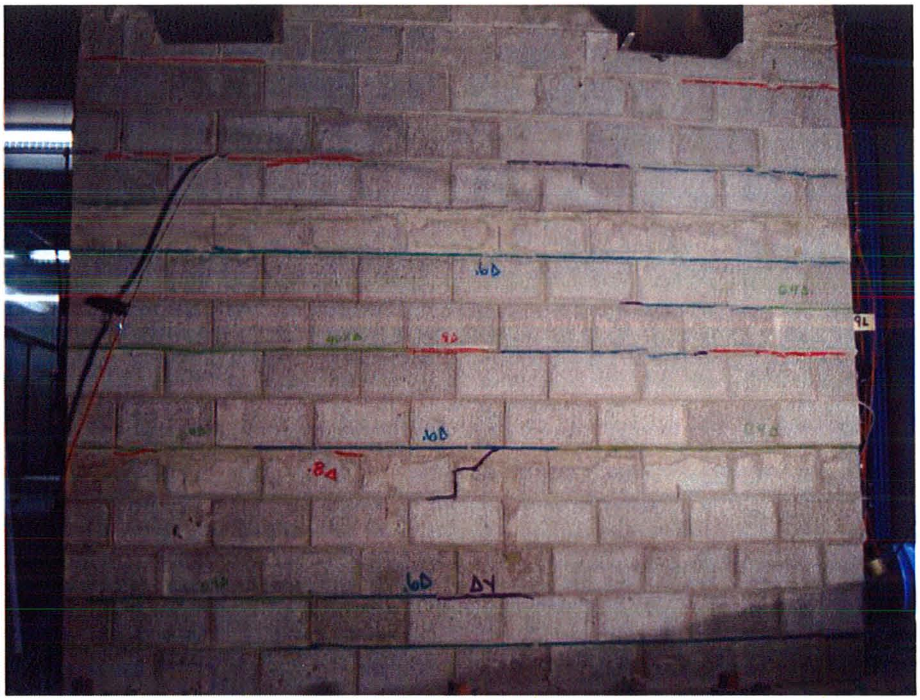

(a) Cracking Pattern of Wall 1 After One Cycle at Δy

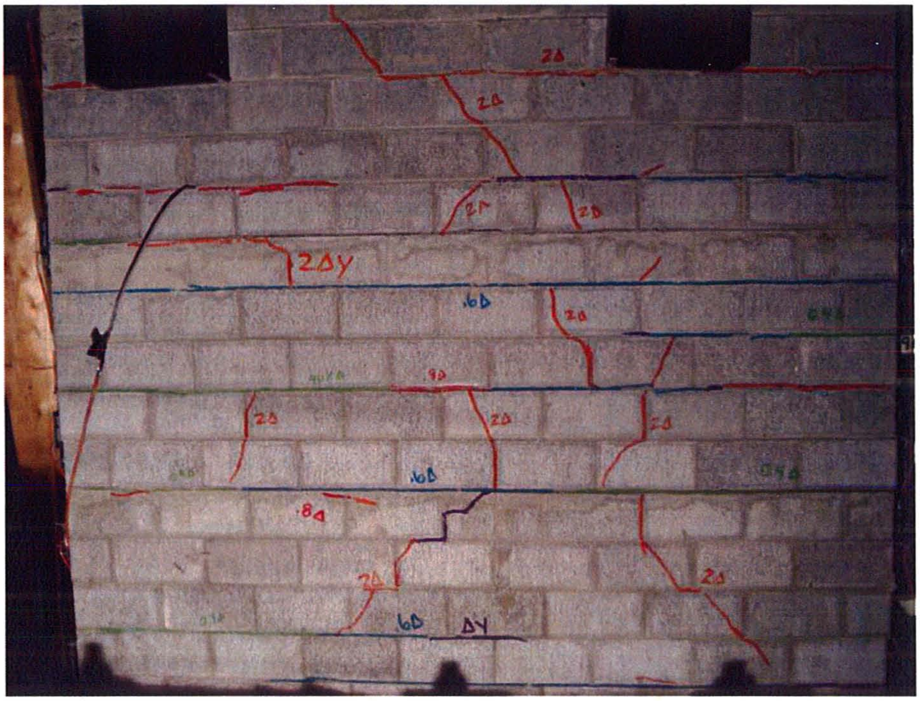

(b) Cracking Pattern of Wall 1 After One Cycle at $2\Delta_y$

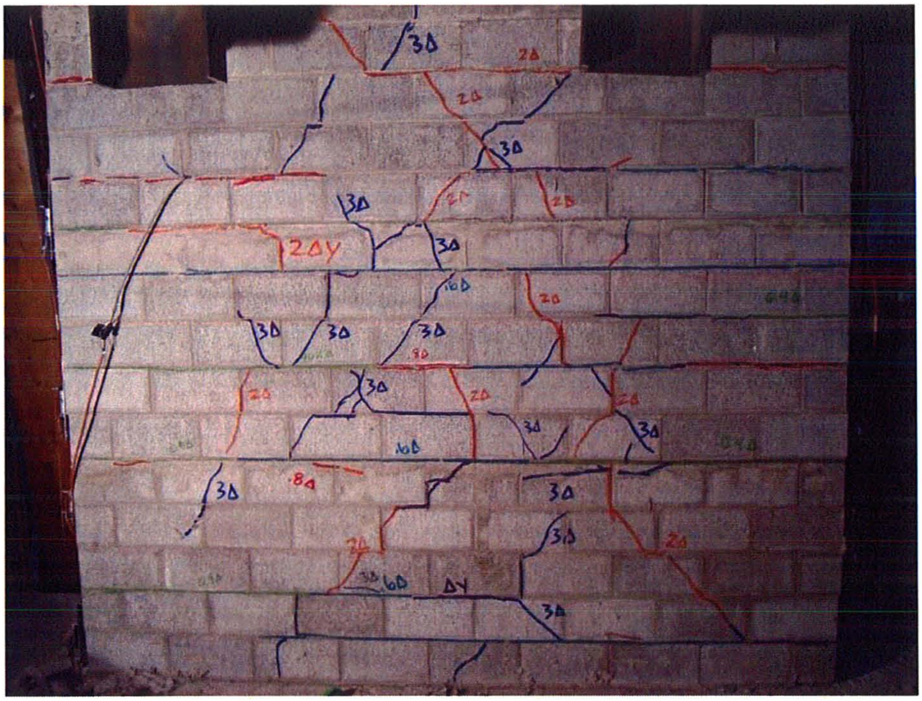

(c) First Storey Cracking Pattern of Wall 1 after One Cycle at 3Δ_y

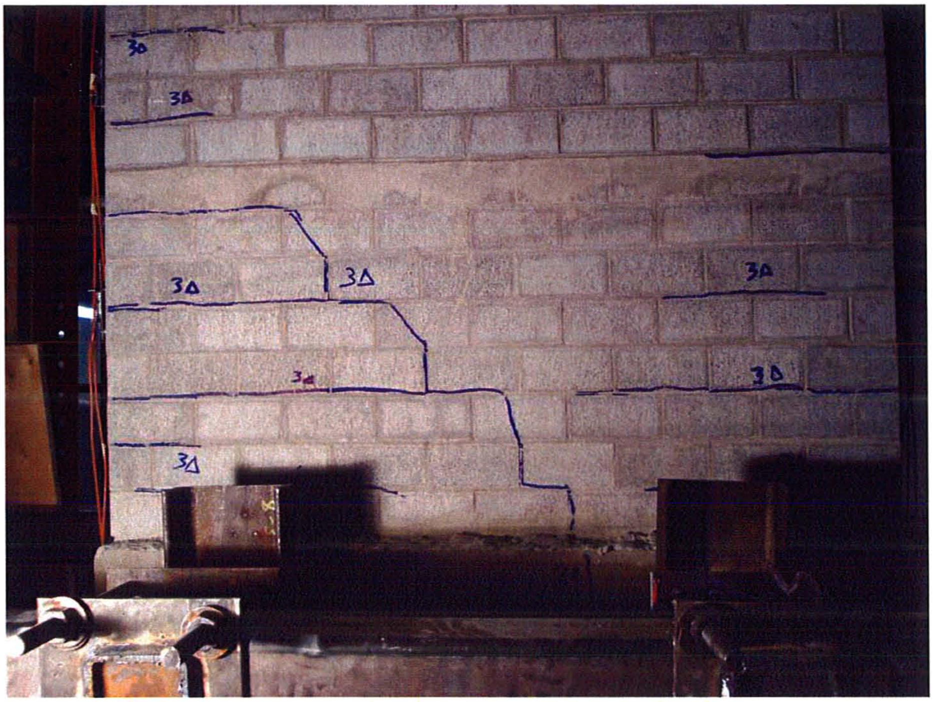

(d) Second Storey Cracking Pattern of Wall 1 After One Cycle at 3Δ_y

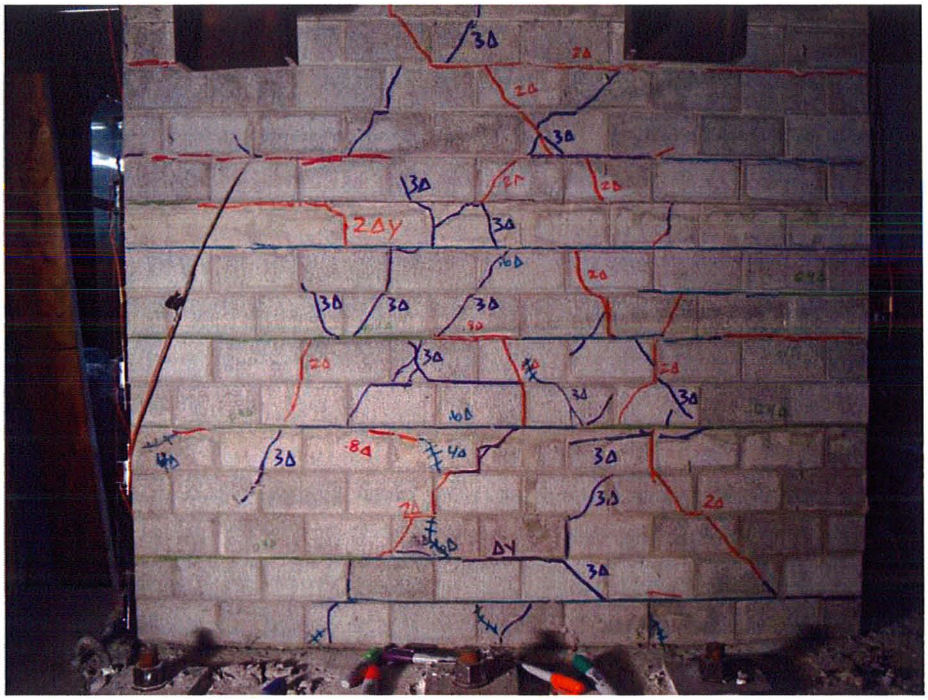

(e) Cracking Pattern of Wall 1 After One Cycle at 4Δy

Figure 3.1: Cracking Patterns for Wall 1

After terminating the test, the wall was examined further and the East end of the wall was found to have retained about 8 mm of permanent uplift as shown in Figure 3.2 (a). The South face of the West toe exhibited evidence of compression cracking as well as crushing (See Figure 3.2 (b)).

(a) Permanent Uplift of the East End of Wall 1

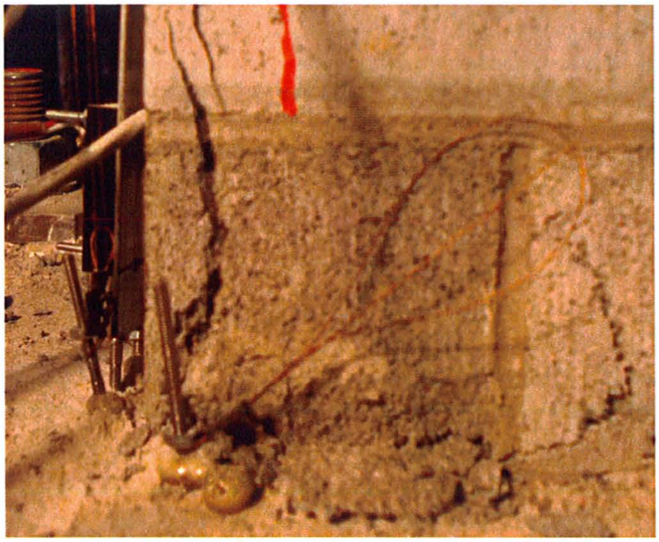

(b) Compression Damage of West Toe of Wall 1 (South Face)

Figure 3.2: Damage to Wall 1 at End of Test

3.2.2 General Observations

The behaviour of Wall 1 was dominated primarily by flexure as is apparent due to the large amount of horizontal bed joint cracking. Many of these cracks had formed by the time yield load was reached and, at subsequent levels of displacement, these cracks merely increased in width and length.

The wall exhibited a relatively symmetric load-displacement response in both directions of loading. As mentioned earlier, the wall initially yielded at a top lateral displacement of 6.7 mm and a lateral load of 32.2 kN. However, in the pull direction, the wall reached flexural yield at a displacement of 7.7 mm and a lateral load of 32.4 kN. Thus, the top lateral yield displacements differed by approximately 13%. Given the lack of a yield plateau for the reinforcing steel and the effect of some permanent set in bars at the nominal yield, this difference is considered to be acceptable.

Wall 1 was designed to fail in flexure with the eventual crushing and spalling of the masonry. This eventual compression failure of the masonry was not achieved due to the unexpected relatively brittle behaviour of the longitudinal reinforcement. As presented in the previous chapter, the steel used for longitudinal reinforcement appeared to have a flat yield plateau as well as sufficient ductility. However, the steel was, in fact, relatively brittle and fractured before the masonry could achieve a significant level of compressive strain. It was hypothesized that the steel behaviour was sensitive to low cycle fatigue and, therefore, the amount of load cycling should be significantly reduced in subsequent tests.

The load-displacement hysteresis loops for Wall 1 were reproduced in Figure 3.3 along with displacement shown as percent drift.

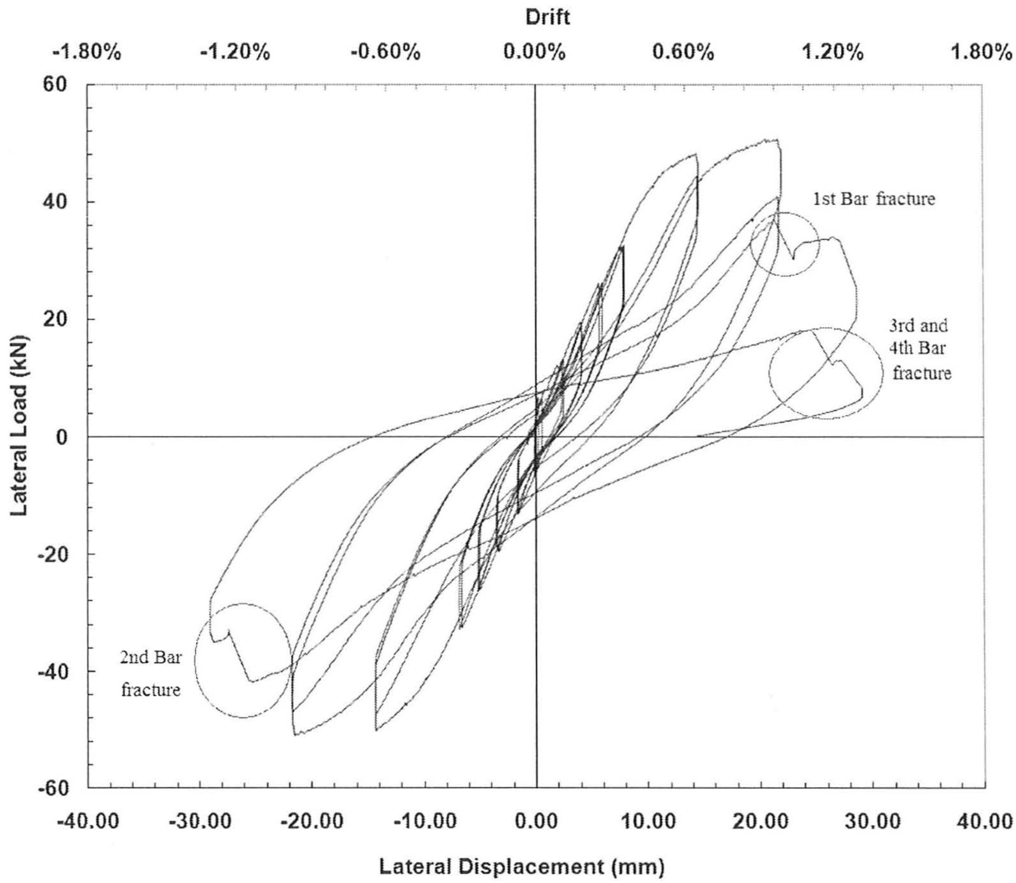

Figure 3.3: Hysteresis Load-Displacement Loops for Wall 1

As previously mentioned, the outmost flexural steel fractured as the wall approached $4\Delta_y$ displacement. From Figure 3.3, it can be seen that the bar fracture was accompanied by a sharp decrease in wall capacity and a reduced stiffness. The wall was then unloaded to zero lateral load and displaced in the pull direction. As the wall approached $4\Delta_y$, the West outmost bar fractured. This was the second bar to fracture and it was also accompanied by a sharp drop in wall capacity as indicated in the left side of Figure 3.3. At this point the wall was brought back to zero lateral load and displaced in the push direction. The wall's stiffness had decreased significantly. As the wall approached $4\Delta_y$ displacement, the second outmost East bar fractured. The wall was displaced further and the third outmost East bar fractured. Due to the dramatically decreased stiffness and the fact that 4 out of the 9 flexural bars (and possibly more) had fractured, the test was terminated. This decision was based on the quality and relevancy of the data that would be collected as well as the safety of test participants and the instrumentation. Analysis and discussion of the analysis will be presented in Chapter 4.

3.3 Wall 2

3.3.1 Test Documentation and Description of Test

As a result of the steel behaviour exhibited in the previous test (Wall 1), it was postulated that the flexural steel was susceptible to low cycle fatigue. In an attempt to avoid premature fracture of the flexural reinforcement prior to masonry crushing, the testing procedure was modified. The number of cycles below yield displacement was reduced from 2 cycles, at 20%, 40%, 60%, 80% and 100% of the theoretical lateral yield load to 1 cycle at 50% of the theoretical lateral yield load. In this regard, Jamison (1997) has suggested that the envelope of the load-displacement hysteresis loops is insensitive to the imposed displacement increments and to the number of cycles. Therefore, this supported the decision that the testing procedure would consist of a single, fully reversed, cycle at 50% flexural yield load followed by pushing to a multiple of Δ_y displacement and then pulling to a matching level of displacement.

During the pushing and pulling phases, the test was paused at each level of displacement (i.e., Δ_y, $2\Delta_y$, etc) at which time cracks were marked and photographs were taken. Following this cyclic testing, it was decided that the wall would be pushed until fracture of the outmost bar(s) occurred. At that point, the additional pulling phase would depend on the outcome of the previous pushing phase.

The theoretical lateral yield load and displacement were 19.7 kN and 6.6 mm, respectively. Therefore, the 50% yield load cycle was performed at a lateral load of 9.8 kN. As in the previous test, this cycle was used to verify the correct operation of the internal and external instrumentation.

After one cycle at 50% lateral yield load, there was minor bed joint cracking. This cracking occurred only on the West side as can be seen on the right hand side of the photograph in Figure 3.4 (a) but no cracking was visible on the East side.

The wall was then pushed until yielding of the outermost flexural reinforcing bar was achieved. Unlike the previous test, the yield point was not set as the point at which the theoretical lateral yield load was reached. The electrical strain gauges installed in this wall were operating properly and therefore were used to identify and verify flexural yielding. Therefore, the yield point for this test was set as the point at which the electrical strain gauge, placed on the outmost bar and located at the interface between the concrete foundation and first course of the wall, recorded a yielding strain of 0.0027. This corresponds to the 540 MPa yield stress and a nominal elastic yield strain as determined in Section 2.2.5.

Flexural yielding of the outermost bar was achieved in the push direction at a lateral load of 15.3 kN and a lateral displacement of 6.6 mm. As shown in the photograph in Figure 3.4 (b), highlighted cracks illustrate the cracking pattern present at flexural yield. Typical bed joint cracking, similar to that which occurred during the 50% yield load cycle was observed, however the cracks were slightly longer.

Following the revised testing method, the wall was then pushed to a displacement of 13.1 mm ($2\Delta_y$) with a measured corresponding lateral load of 26.8 kN. An existing bed joint crack propagated further and new bed joint cracks formed in the upper half of the first storey. In addition, a single stepped crack formed near the mid region of the wall between the fourth and seventh courses as can be seen in Figure 3.4 (c).

At a lateral displacement of 19.7 mm in the push direction, (approximately $3\Delta_y$), and a measured lateral load of 31.4 kN, bed joints cracks became wider but no additional bed joint cracks formed and none of the existing cracks lengthened. Some stepped cracks formed, the majority of which occurred in the mid region of the wall and in the upper half of the first storey as shown in Figure 3.4 (d).

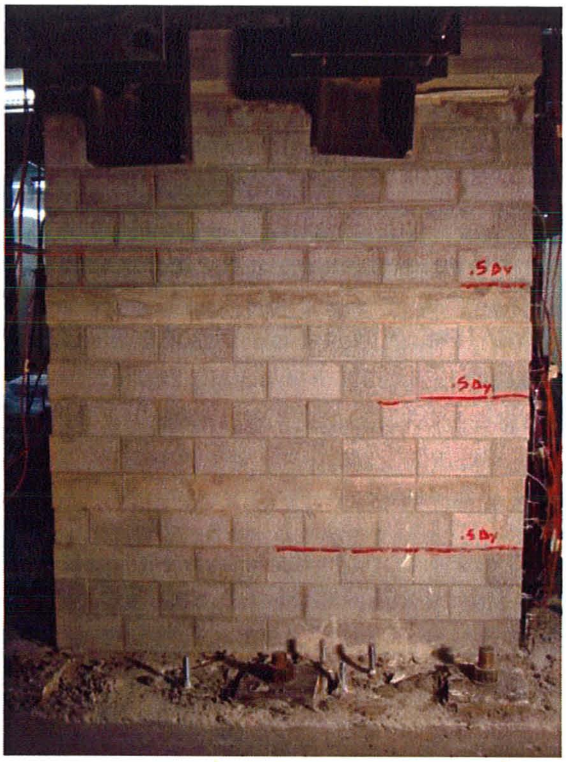

(a) Cracking Pattern of Wall 2 at 0.5 Δ_y (Pull)

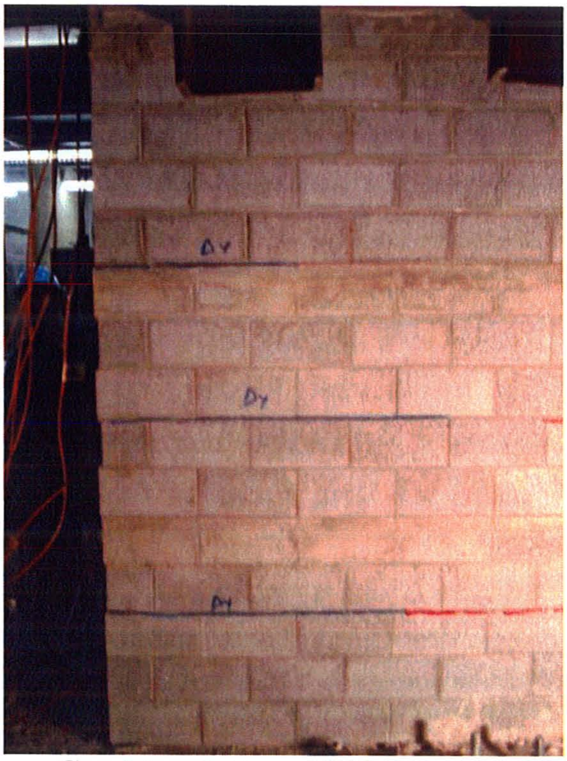

(b) Cracking Pattern of Wall 2 at Δy (Push)

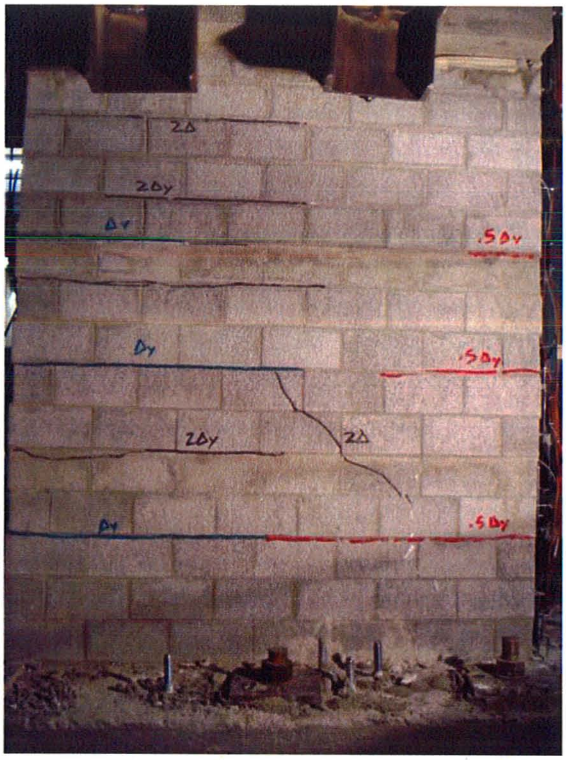

(c) Cracking Pattern of Wall 2 at $2\Delta_y$ (Push)

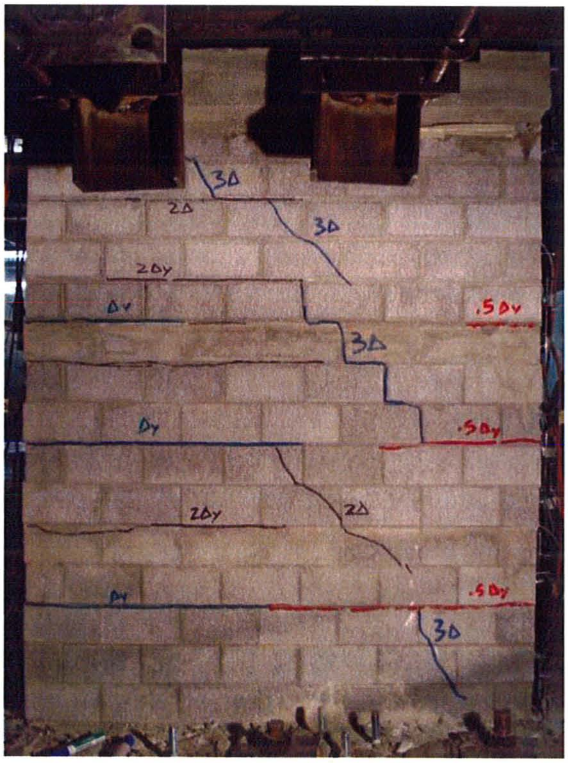

(d) Cracking Pattern of Wall 2 at $3\Delta_y$ (Push)

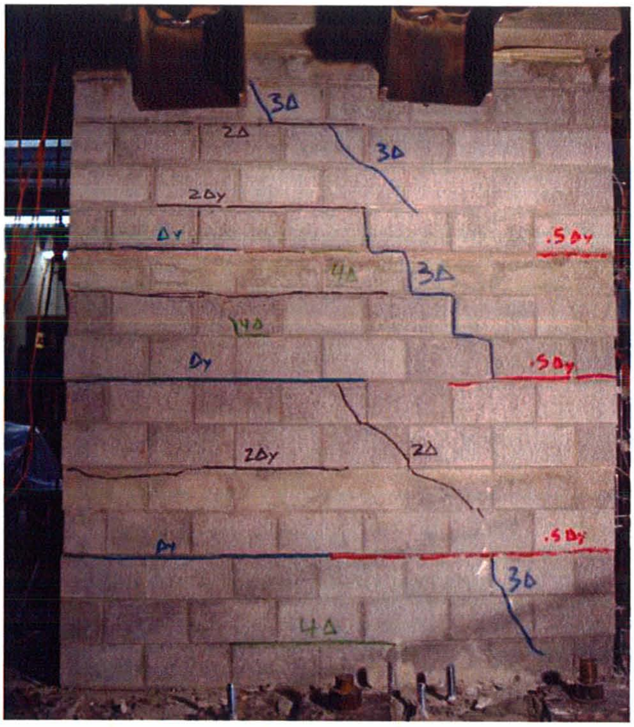

(e) Cracking Pattern of Wall 2 at $4\Delta_y$ (Push)

(f) Second Storey Cracking Pattern of Wall 2 at $4\Delta_y$ (Push)

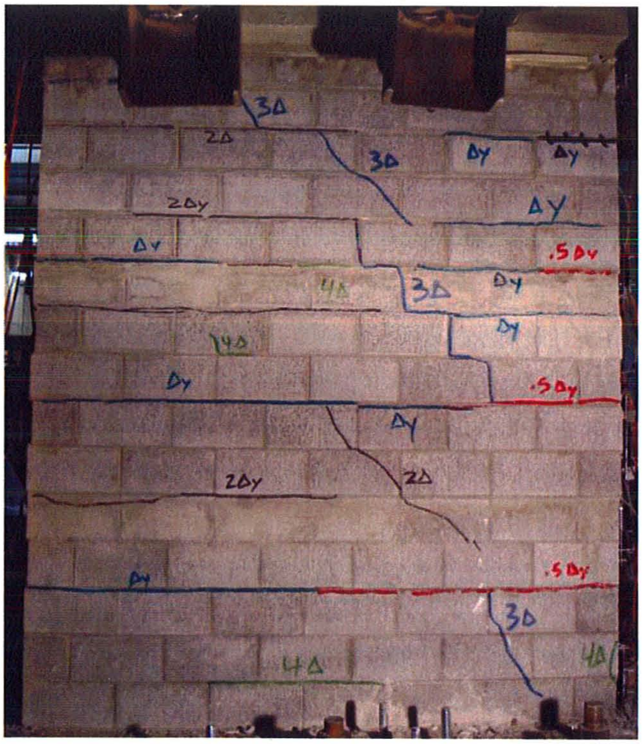

(g) **Cracking Pattern of Wall 2 at Δ_y (Pull)**

(h) **Second Storey Cracking Pattern of Wall 2 at Δ_y (Pull)**

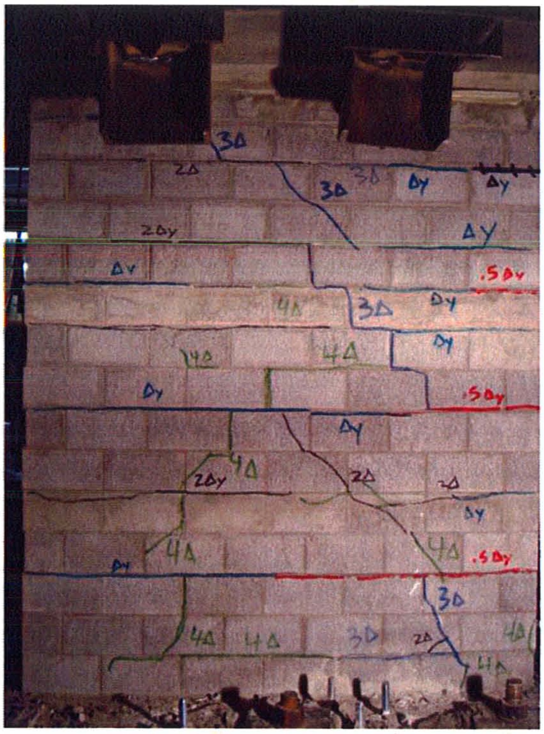

(i) Cracking Pattern of Wall 2 at $4\Delta_y$ (Pull)

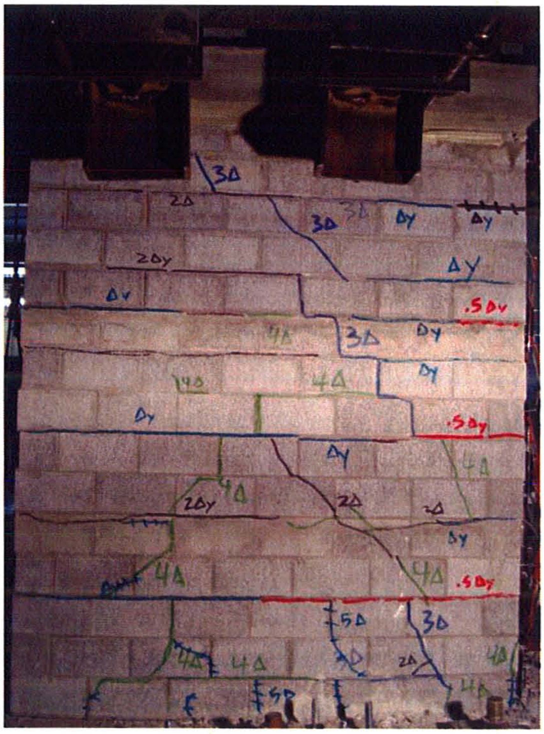

(j) Cracking Pattern of Wall 2 at $5\Delta_y$ (Push)

Figure 3.4: Cracking Patterns for Wall 2

At a displacement of 26.3 mm ($4\Delta_y$) and a measured lateral load of 32.8 kN, there was minor additional cracking. Cracking in the first storey consisted of bed joint cracks at the second, ninth, and tenth courses. The bed joint crack on the ninth course propagated upward to approximately half way through the masonry unit. Some bed joint cracking also occurred in the second storey of the wall. The extent of cracking can be seen in Figure 3.4 (e) and (f). At this point the wall was unloaded to zero lateral load and then displaced in the pull direction.

For the yield displacement level in the pull direction, the yield displacement previously established was used. The wall was pulled to a displacement of 6.5 mm which corresponded to a lateral load of 16.4 kN (approximately 1 kN greater than in the push direction). New bed joint cracks were formed at this displacement, the majority of which occurred in the top half of the wall on the tension side. This can be seen on the upper right hand side of Figure 3.4 (g). Bed joint cracks also formed in the second storey of the wall as shown in Figure 3.4 (h).

At a displacement of 13.2 mm ($2\Delta_y$) in the pull direction, the wall reached a lateral load of 22.7 kN. At this point additional cracking was minimal. One new bed joint crack formed while others simply increased in width.

At a displacement of 19.7 mm ($3\Delta_y$) in the pull direction, the wall reached a lateral load of 27.4 kN and, similarly to the push direction, this was accompanied by the formation of additional minor bed joint cracking. Two bed joint cracks formed, both of which were merely the propagation of previous cracks (See Figure 3.4 (i)). The second storey cracking remained unchanged during both levels of displacement.

As the wall approached a displacement of 26.4 mm, ($4\Delta_y$) in the pull direction, the outmost flexural reinforcing bar fractured. The displacement of the wall was 25.8 mm with a corresponding measured lateral load of 29.6 kN. Several cracks formed at this stage (See Figure 3.4 (i)). The majority of these were diagonal cracks. Pulling was stopped and the wall was unloaded to zero lateral load and then displaced in the push direction.

The target displacement for the wall was 33 mm, ($5\Delta_y$). However, as the wall reached a displacement of 25.0 mm, the East outmost bar fractured. Due to the damage incurred in the previous pulling phase, it was decided that this would be the last loading phase and therefore the wall could be pushed further. At approximately 31 mm displacement in the push direction, and a corresponding lateral load of approximately 19.5 kN, the second East outmost bar fractured. Immediately after this bar fracture, the displacement was recorded as 34.1 mm and corresponded to a lateral load of 12.5 kN. Due to the fractured reinforcement and the severely reduced capacity (37.4% of the maximum lateral load reached), the test was terminated at this point. The crack pattern at this stage is shown in Figure 3.4 (j).

As with the previous test, there was a permanent base uplift on the East end, of approximately 5-10 mm (See Figure 3.5 (a)), as well as some compression cracking of the West toe (see Figure 3.5 (b)). However, unlike the previous test, there was no masonry crushing in either wall toe.

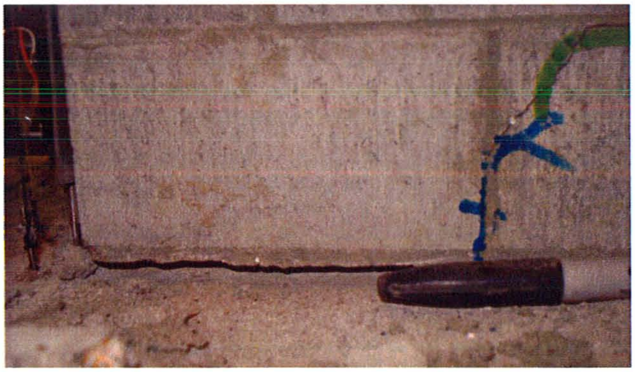

(a) Permanent Uplift of the East End of Wall 2

(b) Compression Damage of West Toe of Wall 2 (South Face)

Figure 3.5: Damage to Wall 2 at End of Test

3.3.2 General Observations

The behaviour of Wall 2 was dominated by flexure. This is apparent due to the large amount of horizontal bed joint cracking. Similar to the previous test, the wall exhibited symmetric responses in the push and pull directions. At equal levels of displacement above Δ_y, the resistances were approximately 13% higher in the push direction. Due to the level of yielding during first loading in the push direction, it is difficult to determine whether both the push and pull direction did in fact share the same yield displacement. However, test data showed that the yield loads for the push and pull direction differed by approximately 7%, favouring the pull direction whereas higher loads were observed in the push direction for larger displacements.

The desired failure mode of this wall was a flexural failure mode with yielding of the reinforcement followed by the eventual crushing, and spalling of the masonry. This was not achieved due to the lack of ductility present in the vertical reinforcement. Although use of the modified test procedure appeared to result in improved steel performance, the brittle failure of the steel after a few cycles of reversed cyclic loading led to the conclusion that the experimental procedure should be changed so that load reversals were only applied after the East outmost longitudinal steel had fractured. This effectively changed the testing procedure to a push-over test for both the East (pull) and West (push) loading directions.

The hysteresis loops for Wall 2 were plotted in Figure 3.6 with displacements also shown as the percentage drift. The load-displacement plot did not show any significant stiffness degradation up to displacing the wall to $4\Delta_y$ and it appeared that the behaviour of the steel had improved through the use of single cycles of reversed loading. However, once the load was reversed and the wall approached a displacement of $4\Delta_y$ in the pull direction, the previously observed steel behaviour was exhibited again. The fracture of the West outmost bar resulted in a sharp decrease in capacity.

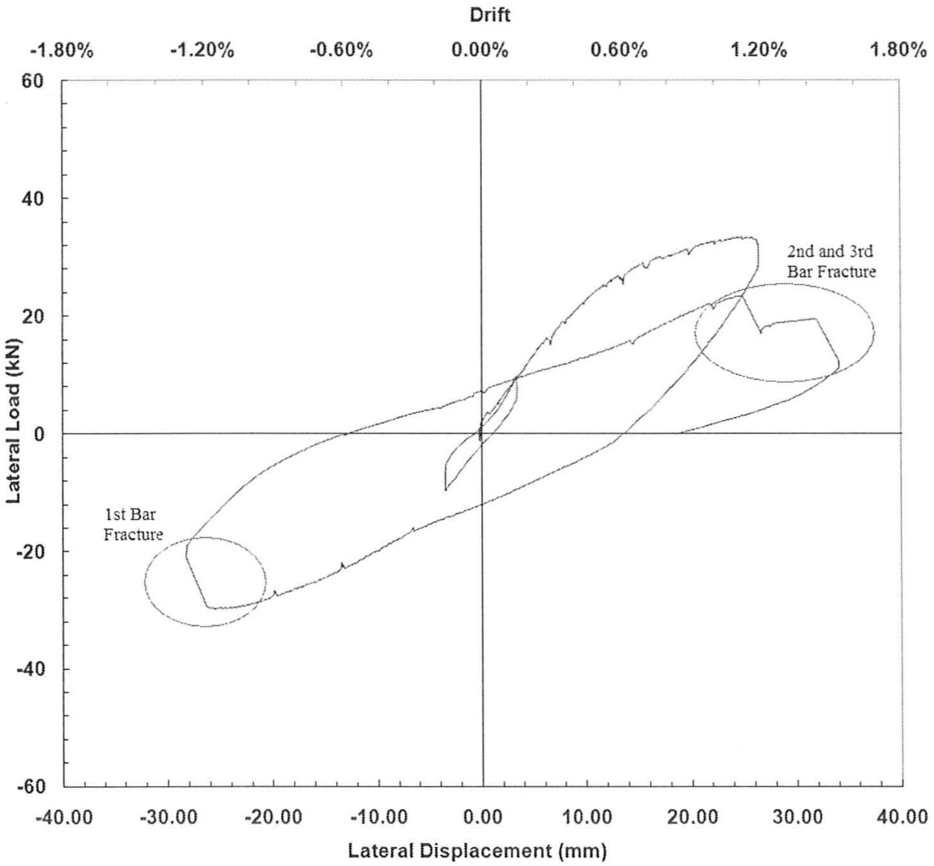

Figure 3.6: Hysteresis Load-Displacement Loops for Wall 2

Pushing the wall to the next level of displacement ($5\Delta_y$) presented another difficulty as the East outmost steel fractured at a slightly lower level of displacement. This resulted in a sharp decrease in capacity. In an attempt to achieve higher displacement, the wall was pushed further. During this process, the wall regained some stiffness. However fracture of the second East outmost bar resulted in another sharp decrease in capacity. With 3 out of 7 vertical bars fractured, the test was terminated.

3.4 Wall 3

3.4.1 Test Documentation and Description of Test

The testing procedure adopted for Wall 3 closely resembled a pushover test with the exception of eventual load reversal. In choosing this loading procedure, the ultimate wall capacity under cyclic loading was assumed to be comparable to the capacity when subjected to monotonic loading as shown by Jamison (1997). Similarly, the monotonic load deflection curve was assumed to be similar to the envelope of the cyclic test results. It was decided that the wall would be loaded monotonically until the outmost bar fractured and then the load was to be reversed and similarly tested in the opposite direction of loading until fracture occurred in a vertical reinforcing bar.

The wall was initially laterally loaded in both directions at 50% lateral yield load in order to ensure proper functioning of instrumentation. After this cycle, the wall was loaded in the push direction.

The theoretical lateral yield load was calculated as 108.4 kN with a corresponding yield displacement of 3.57 mm. Yield was experimentally achieved at a lateral load of 81.1 kN and a displacement of 4.0 mm. This was identified by electrical strain gauge readings on the outmost tensile reinforcement. While the experimental yield displacement was relatively close to the predicted theoretical displacement, the experimental lateral yield load was only approximately 75% of the predicted theoretical yield load. Conversely, when it came to predicting the ultimate lateral load, the maximum experimental lateral load of 151.5 kN was approximately 4% higher than the predicted theoretical lateral load of 145.7 kN. This would seem to indicate that the strain reading in the outermost reinforcing bar might have been in error. Such an error would affect identification of yield load during the test but not influence the prediction of ultimate load. As will be discussed later, the maximum experimental displacement achieved was 26.8 mm.

The "C" shape geometry of Wall 3 presented a unique challenge due to the unsymmetric axis in the plane of the wall which increased the possibility of torsional moment as the result of off-shear centre loading. Considering the behaviour of the proposed symmetric conceptual structure, and neglecting the impact of accidental eccentricities, Wall 3 would not be representative of actual behaviour if it was allowed to twist. For this reason, the rollers used to prevent out-of-plane displacement were placed in light contact with the first storey floor slab. However, the contact forces were small enough that the rollers could be hand turned indicating that very little resistance to in-plane deflection was introduced.

The loading beam for this wall was installed similarly to the previous tests with the centre of the loading beam aligned with the web of the wall. Thought was given to aligning the line of action of the loading beam and actuator with the elastic shear centre. However, the location of the shear centre changes as the wall cracks and loading produces inelastic behaviour. Fortunately shear centre loading

(a) First Storey Bed Joint Cracking Pattern of Wall 3 at Δy

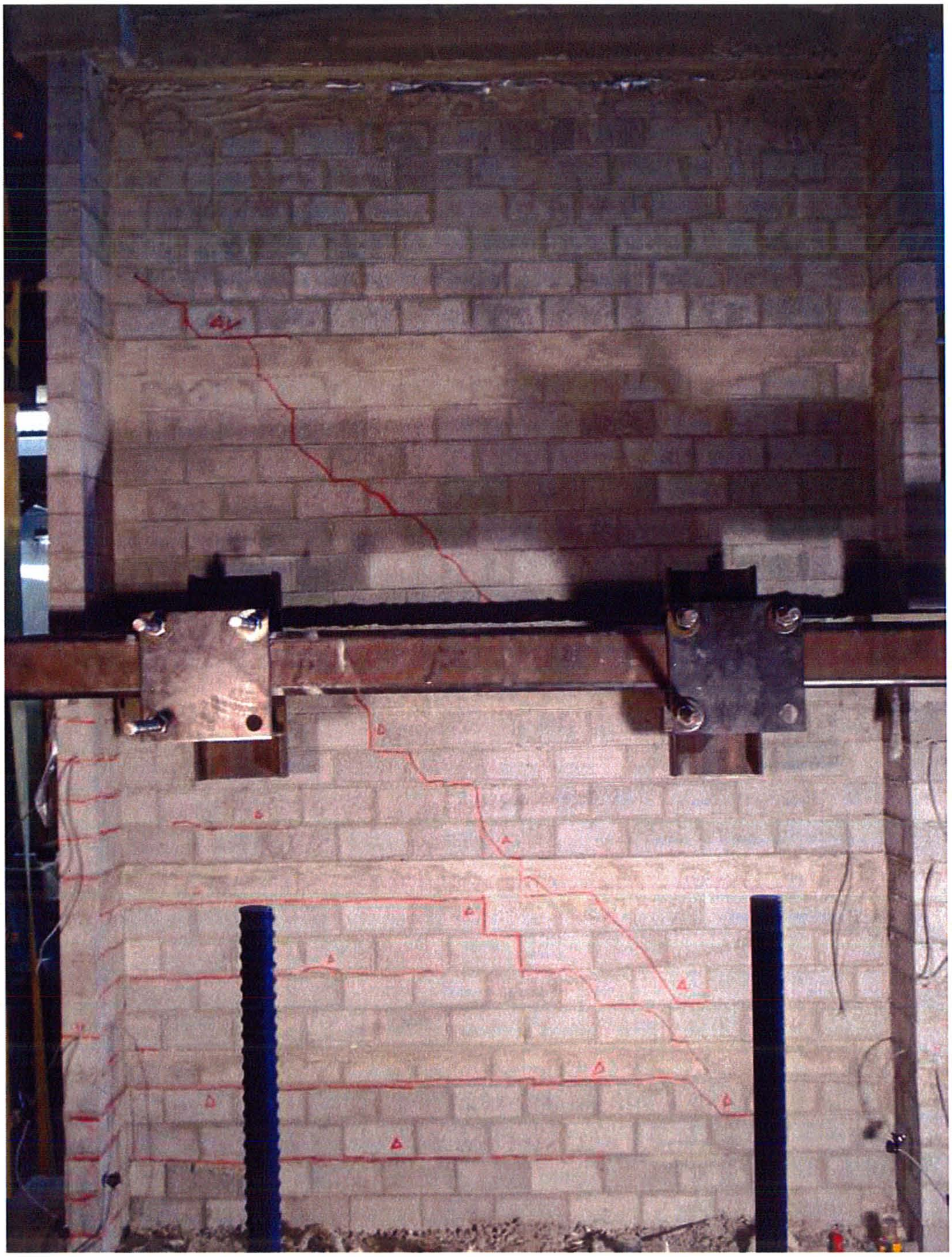

(b) Cracking Pattern of Wall 3 at Δy

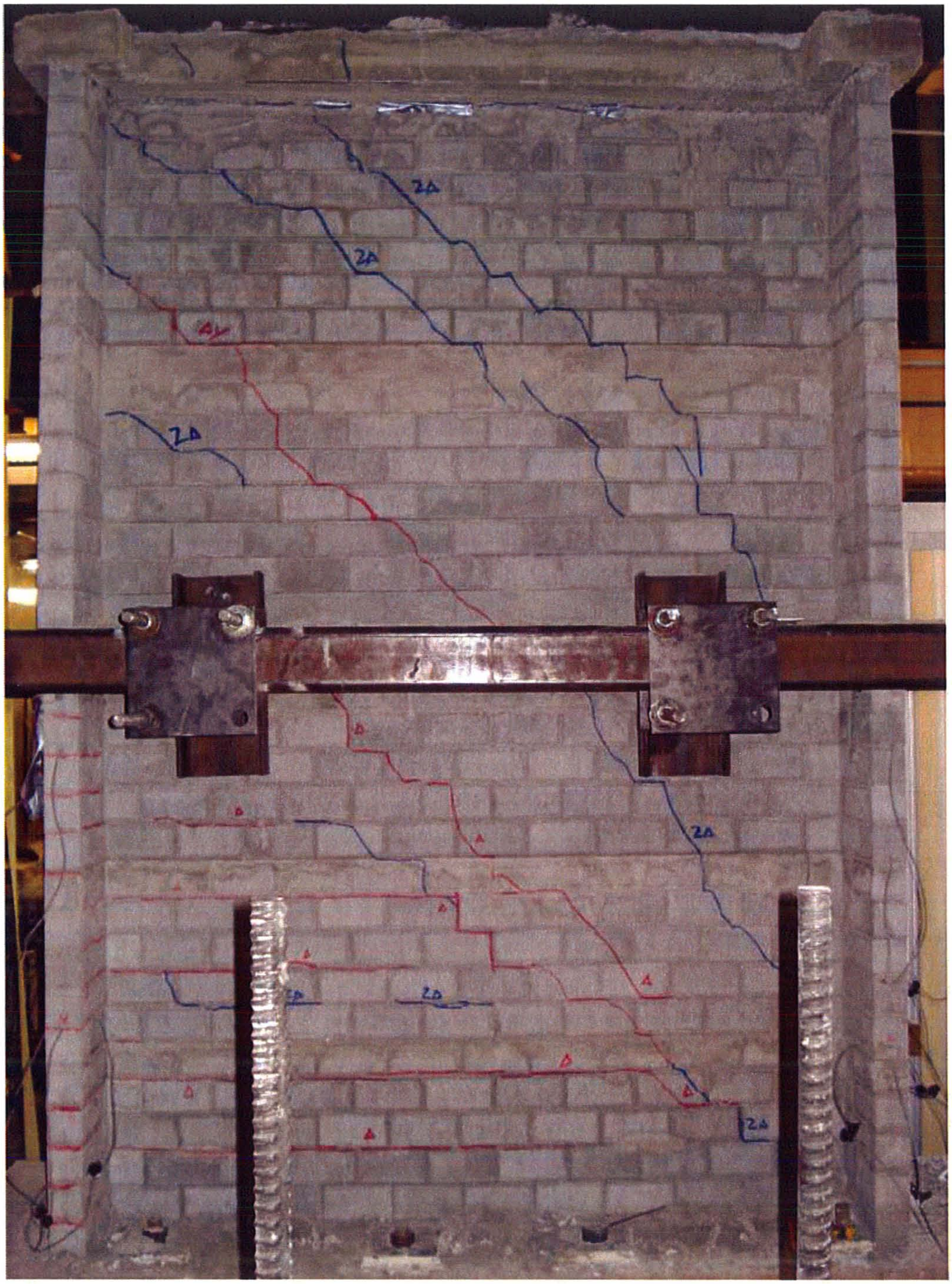

(c) Cracking Pattern of Wall 3 at 2Δy

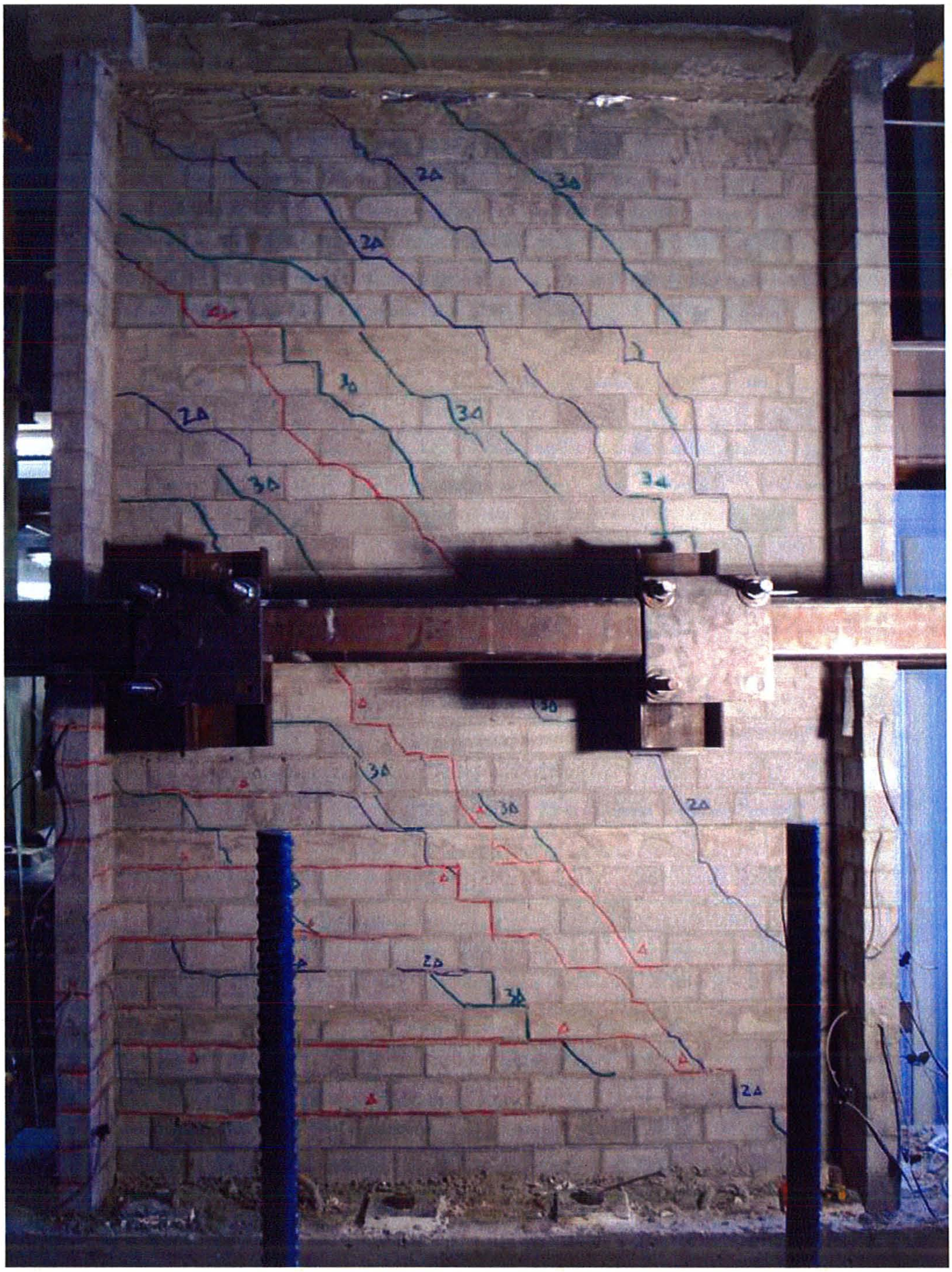

(d) Cracking Pattern of Wall 3 at 3Δy

(e) Cracking Pattern of West Flange of Wall 3 at 3Δy

(f) First Storey Cracking Pattern of Wall 3 at 4Δy

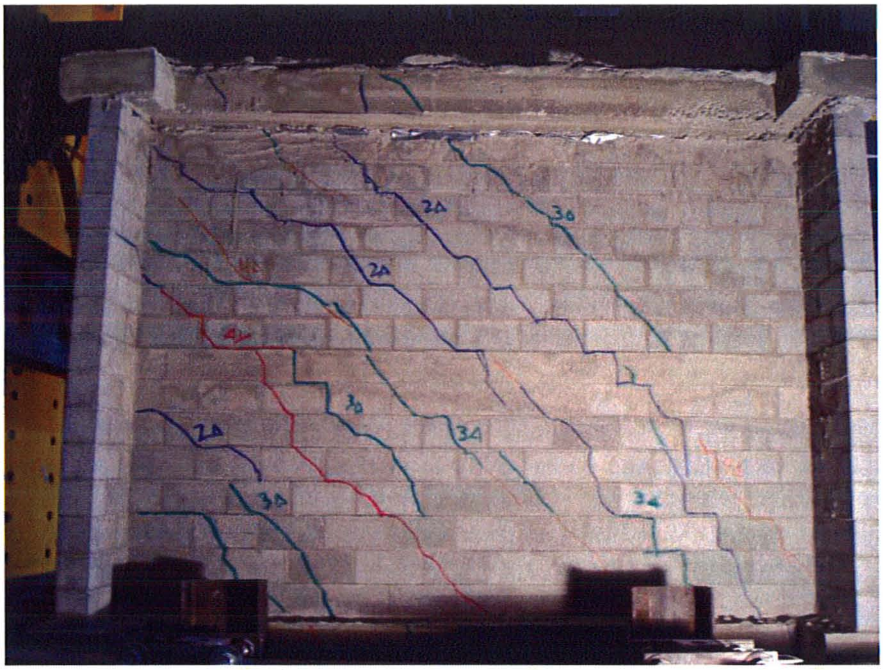

(g) Second Storey Cracking Pattern of Wall 3 at 4Δy

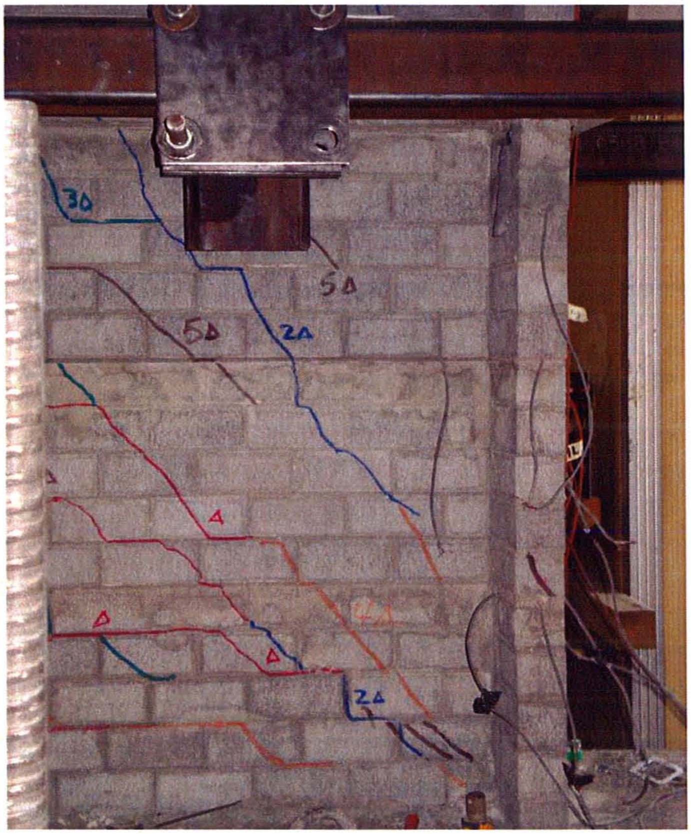

(h) Diagonal Cracking Pattern of Wall 3 at 5Δy

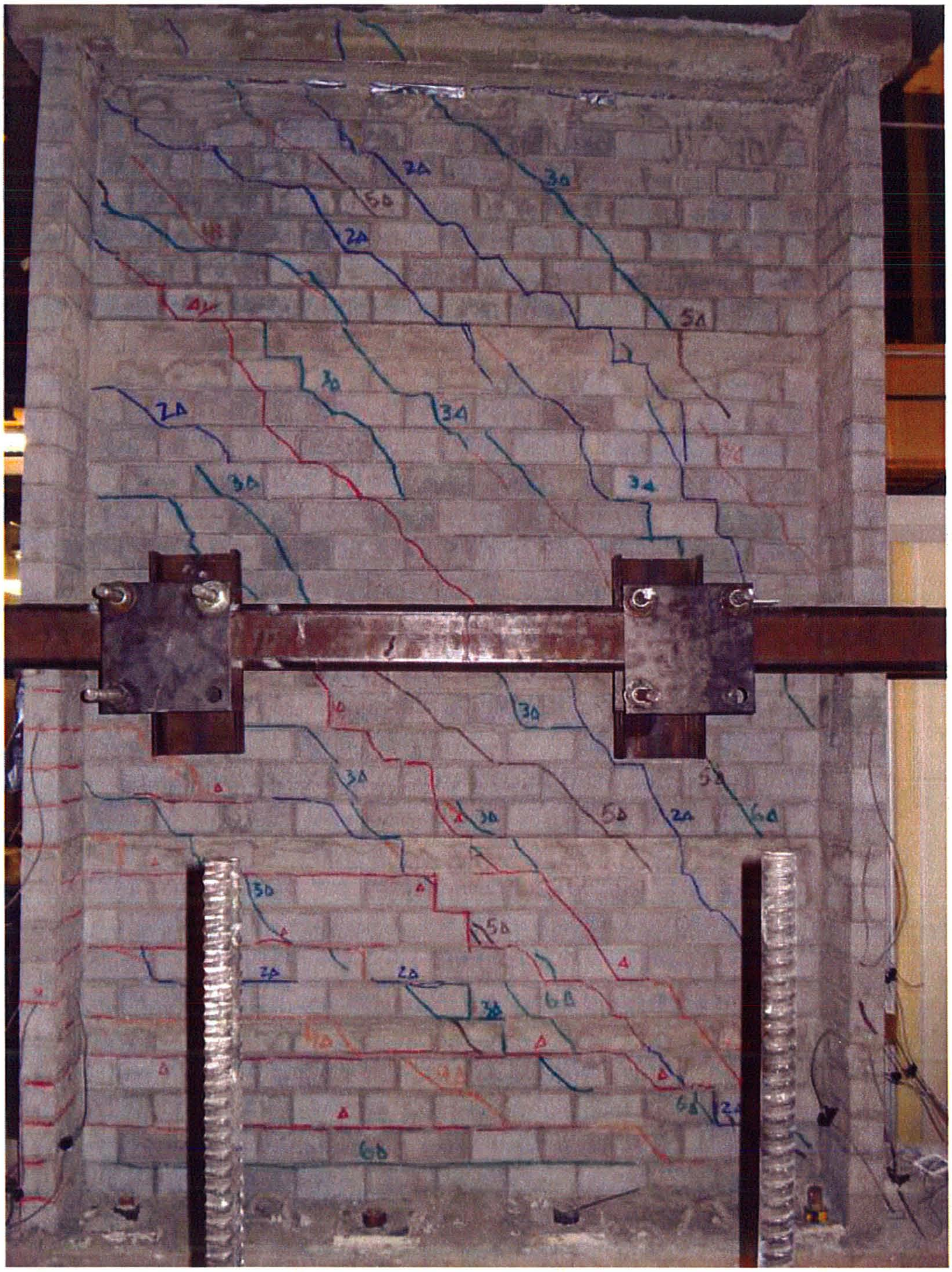

(i) Cracking Pattern of Wall 3 at 6Δy

Figure 3.7: Cracking Patterns for Wall 3

The lateral displacement was then increased to 7.9 mm (2 Δy) with a corresponding measured lateral load of 103.9 kN. At this displacement, there was significantly more stepped cracking in the second storey. Cracking propagated into the second storey floor slab (See Figure 3.7 (c)) and existing cracks, in the first and second storey, extended into the first storey floor slab. Less significant cracking was observed in the first storey. A single, large stepped crack formed along with three much smaller stepped cracks and some minor bed joint cracking.

At a displacement level of 11.9 mm, ($3\Delta_y$), the corresponding measured lateral load was 124.7 kN. The additional amount of stepped cracks which formed in the second storey was consistent with the increased cracking which occurred at previous displacements. Additional cracking in the first storey was less significant and consisted of 5 stepped cracks (See Figure 3.7 (d)). Upon inspecting the outer face of the flange, a large crack was observed (See Figure 3.7 (e)). At this point in the test, the second storey appeared to have a comparable amount of cracking to that of the first storey.

Continuing loading to a displacement of 16.0 mm, ($4\Delta_y$), the corresponding lateral load was 142.8 kN. At this displacement, existing cracks in the second storey extended. This was also observed in the first storey along with formation of additional stepped cracks (See Figure 3.7 (f) and Figure 3.7 (g)).

Pushing further to a displacement of 20.0 mm, ($5\Delta_y$), the corresponding lateral load continued to increase to 149.4 kN. Minimal additional cracking occurred in the second storey with the two cracks formed being extensions of previous cracks. The first storey exhibited more damage. One large crack formed and, in the bottom right end of the linear web element, three diagonal cracks were observed (See Figure 3.7 (h)) and, as subsequent testing showed, these were the beginning of diagonal compression crushing.

The next level of displacement was 23.9 mm, ($6\Delta_y$). This displacement corresponded to a virtually unchanged measured lateral load of 149.0 kN. At this level of displacement, there was minimal additional cracking in the first storey and no additional cracking in the second storey (See Figure 3.7 (i)).

As the wall approached a displacement of 27 mm approximately 10 or 11 bars (4 bars contained within the flange as well as 6 or 7 bars within the web of the wall) fractured in rapid succession. Loading dropped from approximately 150 kN to a value of approximately 6 kN. The extent of failure of vertical reinforcing bars was easily observable due to the large amount of uplift which had occurred at the base of the wall. A thin strip of metal inserted through the wall at the bottom bed joint was used to check for bar continuity.

Testing was terminated at this point. The position of the neutral axis was such that the majority of the reinforcement experienced tensile stress. With so many bars having failed within the linear web portion of the wall, it was decided that loading in the reverse direction would not be similar to the loading in the push direction nor would it be representative of the initial geometry and reinforcement ratio of the specimen. In addition to this condition, the remaining sliding shear resistance of the wall was questionable. With the entire bed joint of the first course cracked and much of the flexural reinforcement fractured, there was significantly less sliding shear resistance offered by the wall.

Similar to the other wall specimens, there was permanent uplift but Wall 3 displayed significantly larger uplift, of between 20 to 25 mm (See Figure 3.8 (a)). Compressive toe crushing was observed as well as diagonal compression crushing. The latter was a behaviour which was not observed in the previous wall tests (See Figure 3.8 (b)).

(a) Permanent Uplift of East End of Wall 3

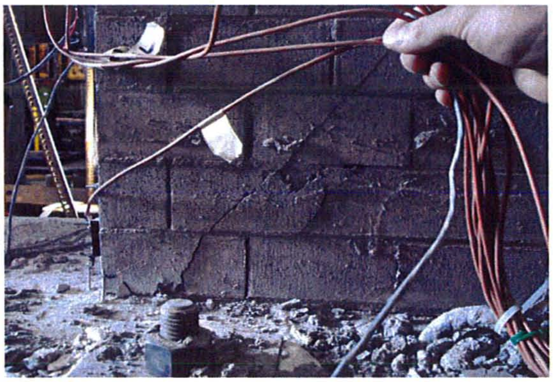

(b) Compression Damage of West Toe of Wall 3 (Photograph Taken From South Face)

Figure 3.8: Observed Damage at End of Test of Wall 3

3.4.2 General Observations

The behaviour and initial failure of Wall 3 was governed by flexure. However, as seen in the photographs, strut action was observed and post-peak load compression crushing was observed in the masonry adjacent to a diagonal crack. Unfortunately the specimen incurred sudden severe damage which prevented testing in the pull direction. For this reason, no comparison could be made as to whether push and pull directions of loading would have displayed symmetric responses.

In order to ensure that torsion was restricted, the out-of-plane bracing rollers had been placed in light contact with the first storey floor slab. Both before and during the test, the rollers were rotated by hand to ensure they were still functioning correctly and not providing additional resistance to lateral load. This suggested that the amount of torsion may have been low with the result that the amount of force exerted on the rollers to resist torsion was correspondingly low.

From the experience of previous testing, the method of testing had been refined further for this test. As mentioned earlier, the testing procedure was introduced to consist of pushing until reinforcement fracture, followed by displacing the wall in the pull direction. The extent of reinforcement fracture and the excessive reduction in capacity prevented testing in the pull direction.

In Figure 3.9, it can be seen that, as the test approached the theoretical ultimate lateral load of the wall, its stiffness decreased and the capacity reached a plateau. Shortly afterwards, at approximately 1.2% drift, the fracture of flexural reinforcement dramatically reduced the capacity of the wall. At failure, the lateral load had decreased from approximately 150 kN to approximately 6 kN and the displacement had approximately doubled, increasing from approximately 26 mm to a value of 56 mm despite using displacement control aimed at 28 mm. This extra displacement can be explained by the manner in which the experimental test set-up was built in conjunction with the displacement data of the actuator relative to the displacement of the wall. In this regard, it is important recall from Section 2.6, that the actuator reaction columns were bolted to the strong floor of the laboratory at their base and unsupported along their height. Hence, at a wall displacement of 26 mm, the actuator had actually displaced by 71 mm. A combination of bending and sliding displacements of the reaction columns accounted for the difference of 45 mm. Upon fracture of the vertical reinforcement and release of the reaction load on the columns, the displacement due to bending of the columns was transferred back to Wall 3 resulting in a jump in wall displacement of 30 mm with the remaining 15 mm being accounted for as permanent sliding displacement of the reaction columns.

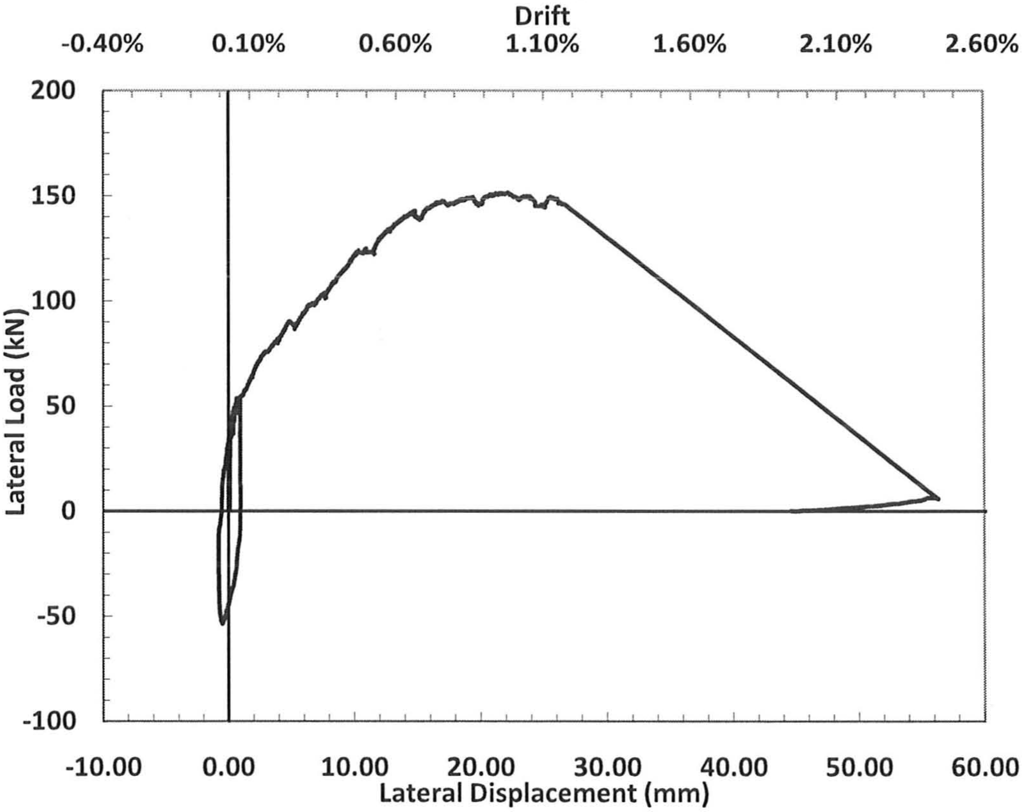

Figure 3.9: Pushover Curve for Wall 3

3.5 Wall 4

3.5.1 Test Documentation and Description of Test

Wall 4 was the final specimen in the test matrix and, due to coupling of the two similar sections, was also the most complicated in terms of testing and analysis of results. The testing procedure for Wall 4 was the same as the proposed plan presented for Wall 3. The wall would be displaced monotonically until fracture(s) occurred in the vertical tension reinforcement and then it would be displaced in the opposite direction.

Wall 4 possessed a unique consideration in terms of experimental testing related to the need for a specifically designed loading beam. Because it was necessary to avoid having the loading beam contribute to coupling of the individual shear walls, it could not be attached to both walls at the same time. Therefore, this loading beam was designed such that it directly loaded the East end of the floor slab during pushing and directly loaded the West end of the floor slab during pulling. This differs from the other loading beams that transferred the load through the vertical reinforcement. Since the loading beam was not attached mechanically to either wall, it was left 'floating' between the transition of pushing and pulling (i.e., when the lateral load was zero). The loading beam was able to be displaced freely in either direction until coming into contact with the floor slab. At this point, the loading beam would displace uniformly with the wall but transfer load only at the contact point. For this reason, unlike other tests, this wall was not cycled during the initial pre-yield phase of testing. In order to verify proper function of the instrumentation, the wall was pushed to a lateral load of 50% of the calculated yield capacity.

The focus of this test was to examine the effect of flexural coupling. The test of this wall was approached with the premise that the amount of flexural coupling was unknown. Through experimental testing, the effectiveness of the coupling would be evaluated. Therefore, as a choice between assuming either full coupling or no coupling, the latter assumption was used to calculate the lateral load at initial yielding of the two walls. Neglecting flexural coupling, the two walls should theoretically behave as two independent walls, possessing separate yet identical flexural strain profiles and, therefore, having a combined capacity which would theoretically be double that of similar Wall 2. The theoretical lateral load at yield for Wall 2 was 19.7 kN and doubling that value results in Wall 4 having a theoretical lateral load of 39.4 kN at initial yield.

Yielding of the outermost vertical reinforcing bars would be verified by electrical strain gauge readings on the outmost tensile reinforcement of each wall. These readings would also aid in determining the early coupling effects. However, during the initial phase of testing, the strain gauges malfunctioned and ceased to perform properly. Since they were displaying readings which were neither reasonable nor stable, strain gauge data was not available and nominal flexural yield was set as the point where the lateral load reached a value of 39.4 kN.

At the lateral load of 39.4 kN, there was a corresponding displacement of 3.42 mm. This point marked the nominal yield point of the wall. Bed joint cracks were observed only in the first storey, in both walls. While Wall A (East) displayed more cracking than Wall B (West), this difference was not considered to be significant (See Figure 3.10 (a)). Observation of the first storey floor slab revealed that it had cracked in the tensile face of the slab adjacent to the coupled ends of each wall (See Figure 3.10 (b)).

Loading to double the nominal yield displacement corresponded to a measured lateral load of 62.9 kN and a displacement of 7.0 mm. At this load, bed joint cracking was observed in the second storeys of both walls. Only minor additional cracking was observed in Wall A, and consisted of further propagation of previous bed joint cracks. Much more additional cracking was visible in Wall B and consisted of both bed joint and stepped cracking (See Figure 3.10(c)). The first storey floor slab exhibited more cracking (See Figure 3.10(d)) and the second storey displayed its first signs of cracking (See Figure 3.10(c) and Figure 3.10(e)).

At a displacement of 10.4 mm, ($3\Delta_y$), the measured lateral load was 74.0 kN and additional cracking was observed primarily in the second storey of Wall A and in the first storey of Wall B. A single new bed joint crack was noted in the first storey of wall A while the second storey of Wall B was unchanged (See Figure 3.10(f)). Cracking in the first and second storey slabs remained unchanged but the existing cracks widened.

At 13.9 mm displacement ($4\Delta y$) the corresponding measured lateral load was 82.6 kN. At this point, rotation was minimally noticeable in the first storey slab. Bed joint cracking was observed in both storeys of Wall A. Additional stepped cracks were noted in the first storey of Wall B. However, the second storey showed no change.

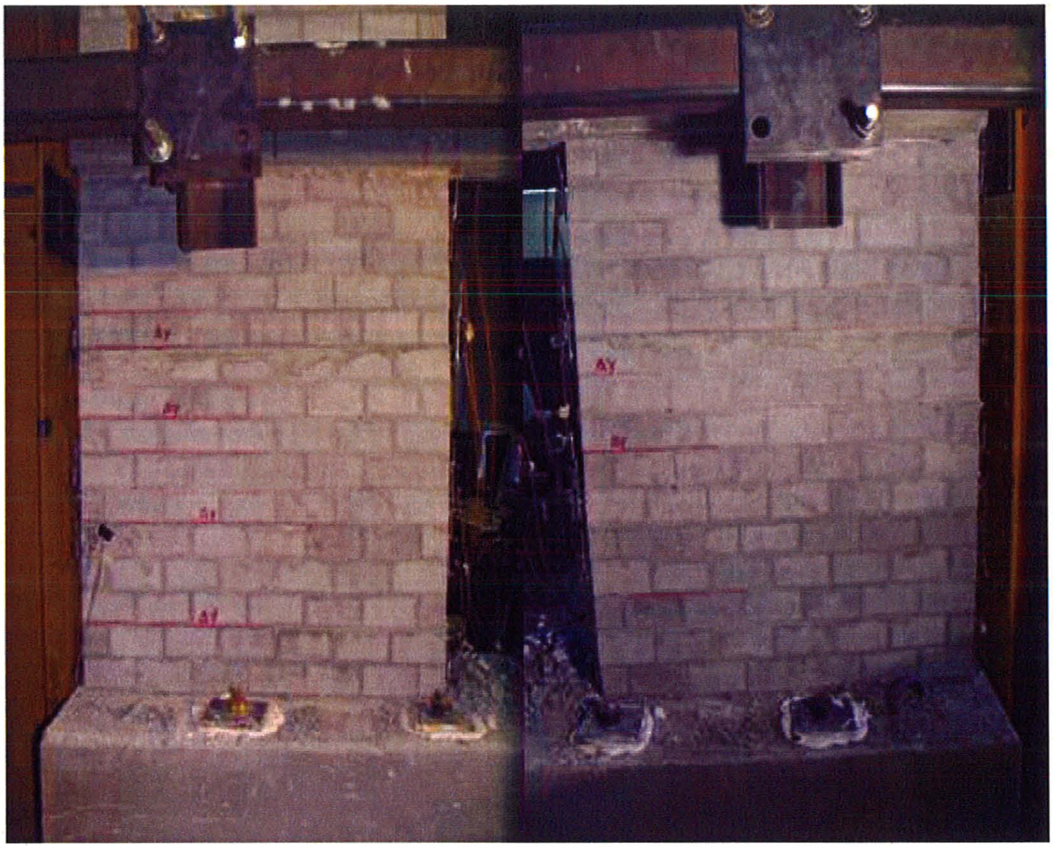

(a) **Cracking Pattern of East Wall (Left) and West Wall (Right) at Δy**

(b) **Cracking Pattern of first Storey Slab of Wall 4 at Δy**

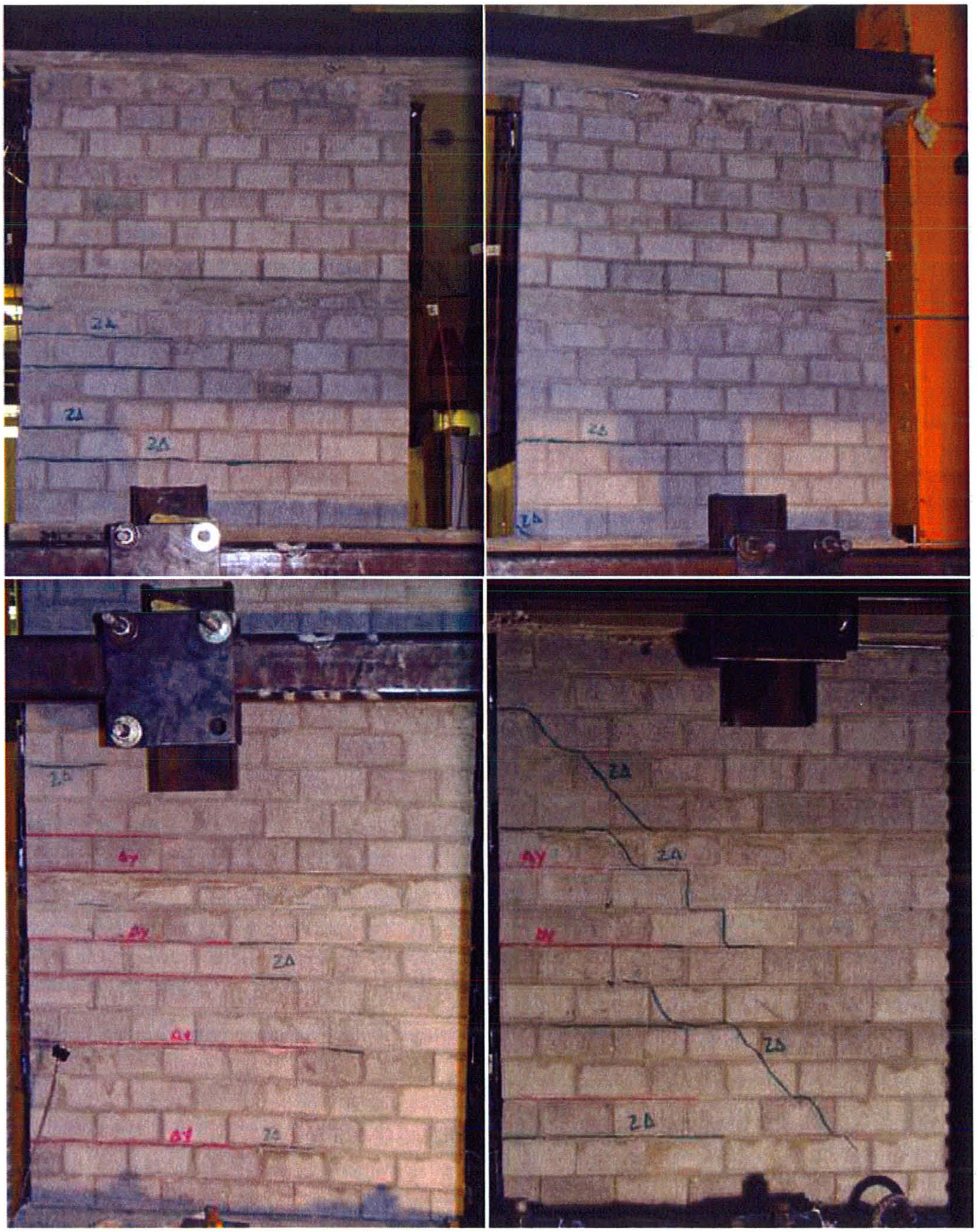

(c) Cracking Pattern of first and Second Storey of East Wall (Left) and of West Wall (Right) at 2 Δy

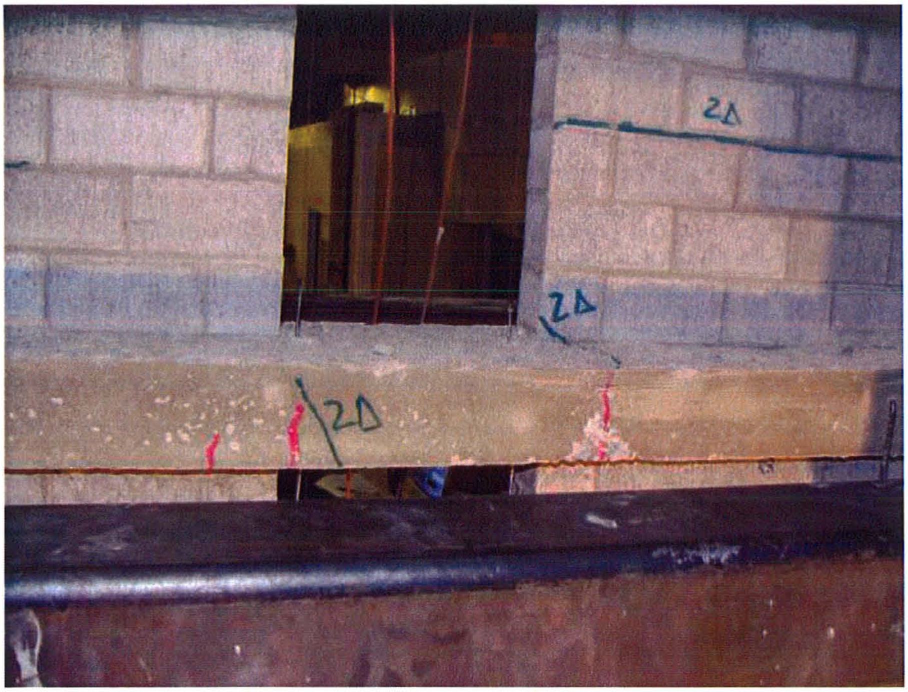

(d) First Storey Slab Cracking Pattern at 2Δy

(e) Second Storey Slab Cracking Pattern at 2Δy

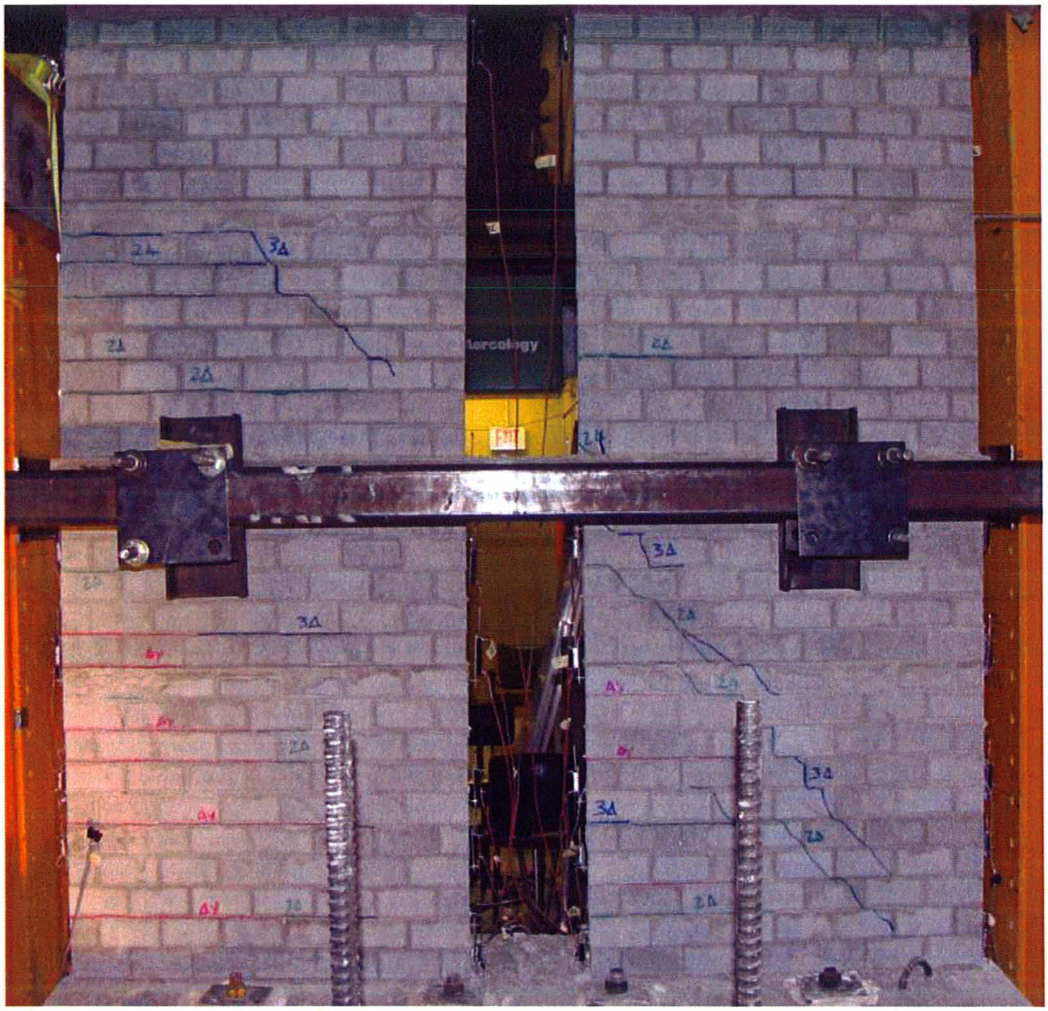

(f) Cracking Pattern of Wall 4 at 3Δy

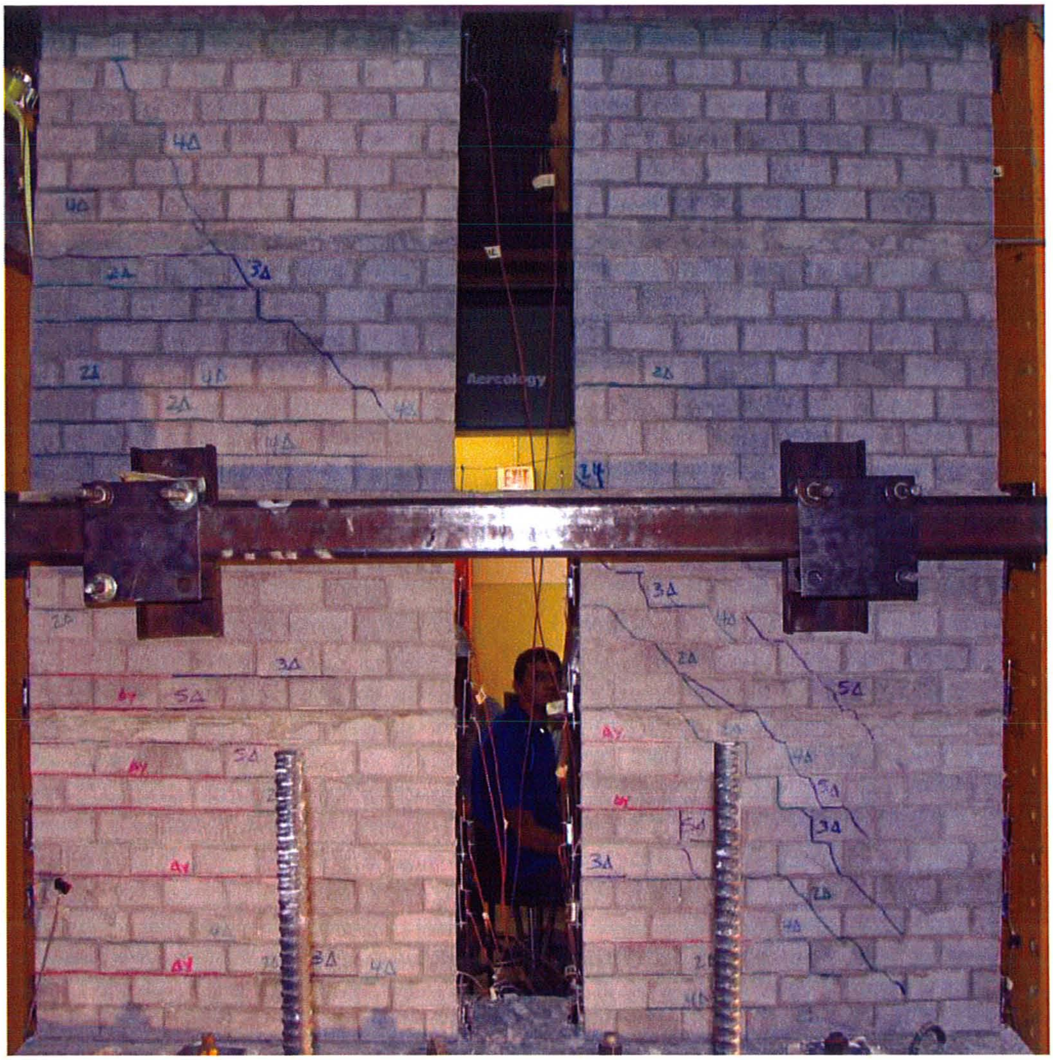

(g) Cracking Pattern of Wall 4 at 5Δy

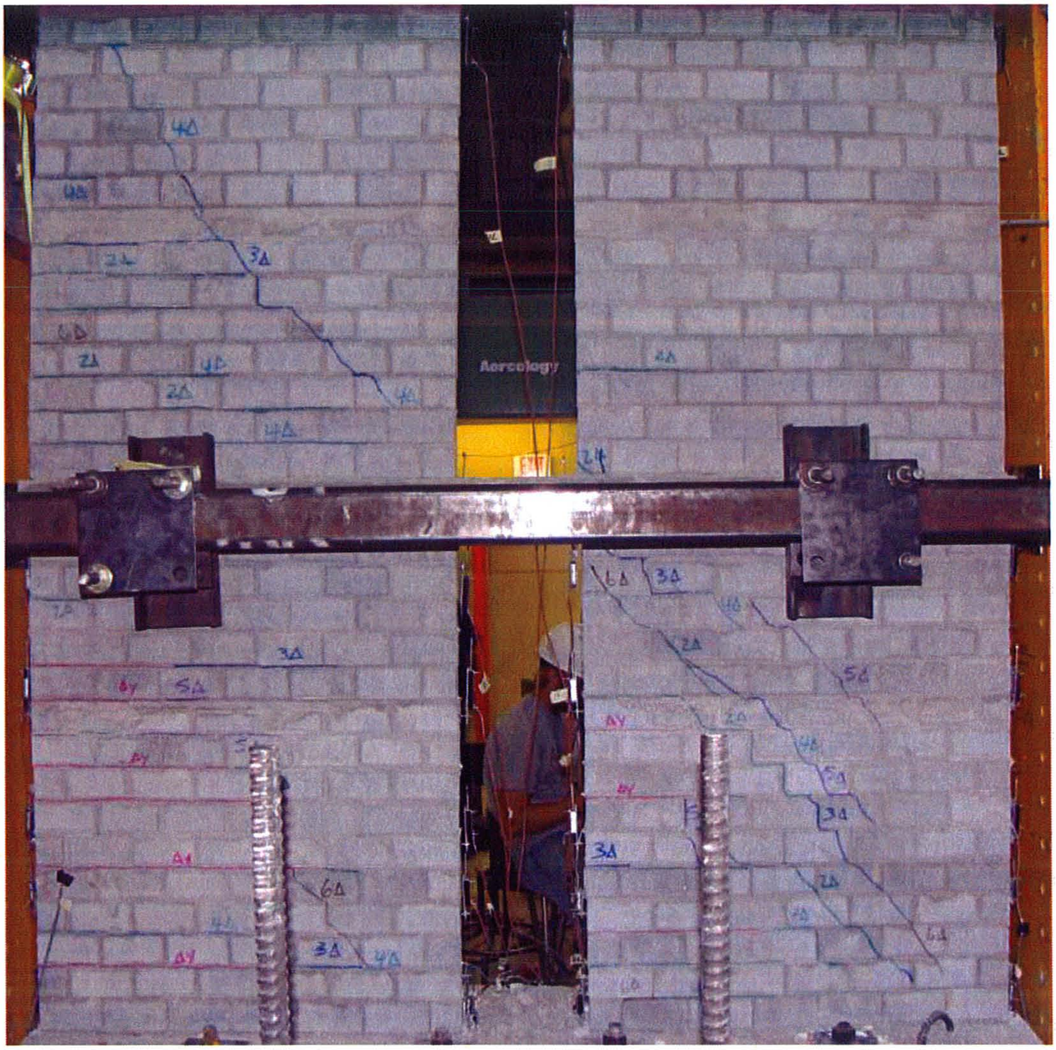

(h) Cracking Pattern of Wall 4 at 6Δy

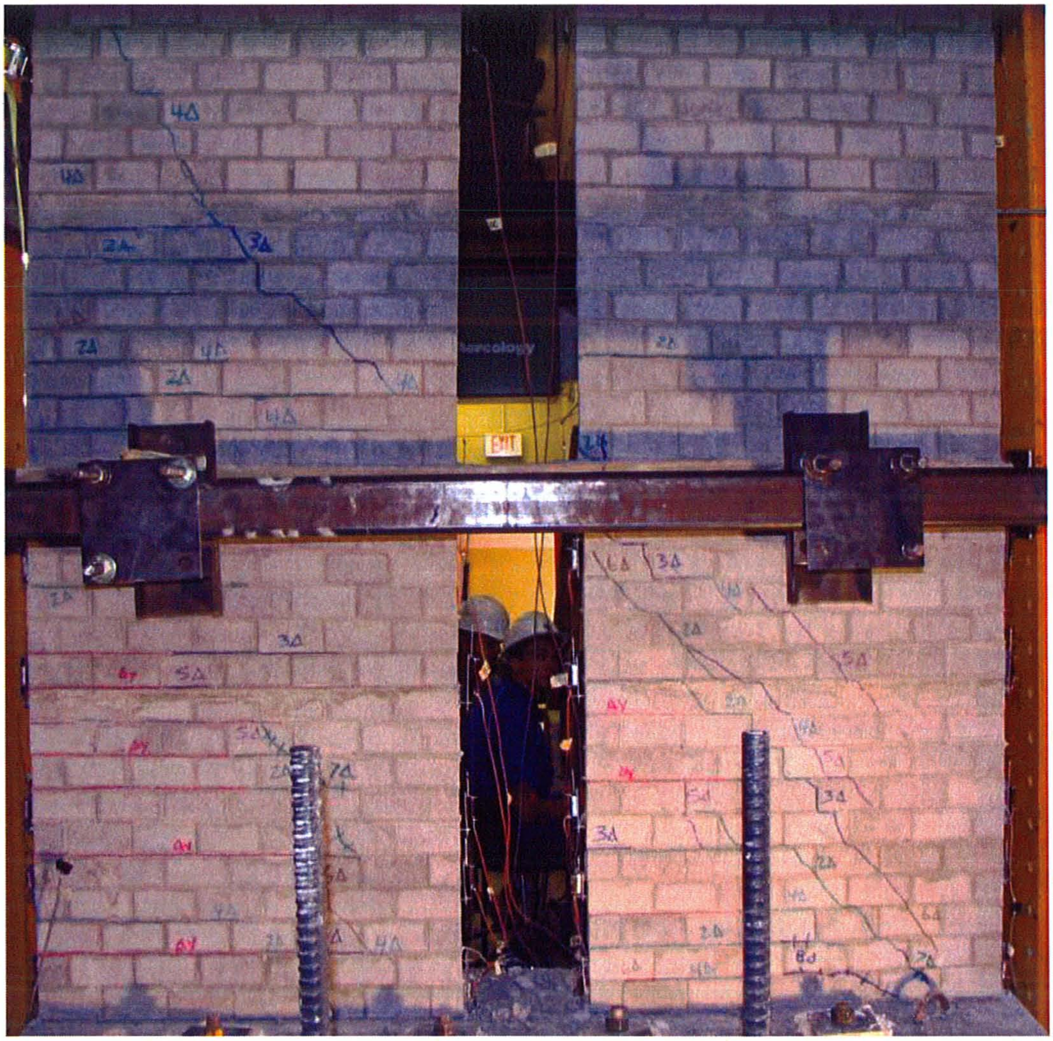

(i) Cracking Pattern of Wall 4 at 8Δy

Figure 3.10: Cracking Patterns in Wall 4

The displacement was then increased to 17.4 mm ($5\Delta_y$) with a measured lateral load of 84.6 kN. The first storey of both walls displayed additional cracking. However, bed joint cracking dominated Wall A whereas Wall B was dominated by a stepped cracking pattern. The second storey of both walls remained unchanged with no additional cracking and no propagation of existing cracks. The additional cracking for $4\Delta_y$ and $5\Delta_y$ are presented in Figure 3.10(g).

At the displacement to 21.1 mm, representing 6Δy, the measured lateral load was 87.5 kN, and additional cracking was observed in the first storey of Wall A. The cracking followed a stepped pattern and occurred in the bottom portion of the West end. A single additional bed joint cracked formed in the second storey of Wall A. The first storey of Wall B showed slightly more additional cracking consisting of 3 cracks in the form of a single bed joint crack and 2 diagonal cracks. The second storey of Wall B remained unchanged with no additional cracks being formed. The wall cracking pattern can be seen in Figure 3.10(h). The first storey floor slab remained unchanged however an additional crack was observed in the second storey floor slab. This crack formed within the area covered by the loading beam.

Increasing the displacement of Wall 4 to 24.7 mm ($7\Delta_y$), led to the corresponding lateral load dropping slightly to 87.3 kN. Additional cracks were observed at the mid-height of the first storey of Wall A. These cracks followed a diagonal pattern and extended through approximately 3 blocks. Additional cracking within Wall B consisted of a very minor crack located in the bottom course adjacent to the west toe.

Displacing the wall to 28.0 mm ($8\Delta_y$) led to the corresponding measured lateral load decreasing slightly to 84.8 kN. The lateral load reached at this level was approximately equal to the lateral load reached at 5 times yield (84.6 kN). Additional cracking was minimal and only observed in the middle of the bottom courses of Wall B. (See Figure 3.10(i)).

As the wall was being displaced toward the next level of displacement of 31.5 mm, an unknown amount of vertical reinforcement fractured. The outmost East vertical reinforcement within both walls had fractured and further inspection of the first storey floor slab revealed that the tensile reinforcement had fractured within the coupled end at Wall B (See Figure 3.11). As observed in the previous wall tests, there was permanent uplift of the east ends of the walls (See Figure 3.12). However, unlike previous testing, there appeared to be no damage within the toe of either wall.

After failure, the level of displacement increased to approximately 36 mm and rotation in the first storey slab was clearly noticeable as can be seen in Figure 3.13. This very well defined curvature indicated a coupling moment within the slab. Considerable cracking occurred at both moment regions where the slab connected to the walls and the failure of the slab was dominated by flexure as observed by the rupture of the tensile reinforcement within the slab.

Figure 3.11: Reinforcement Fracture of First Storey Slab

Figure 3.12: Permanent Uplift at East End of East Wall (Left) and West Wall (Right)

Due to the failure of the floor slab as well as the fracture of vertical reinforcing bars in the walls, the push phase of the test was concluded. At this point, there was some debate as to whether the loading should be reversed.

However, due to the amount of damage, specifically that of the coupling mechanism, it was decided to terminate the test and the wall was unloaded to zero lateral load.

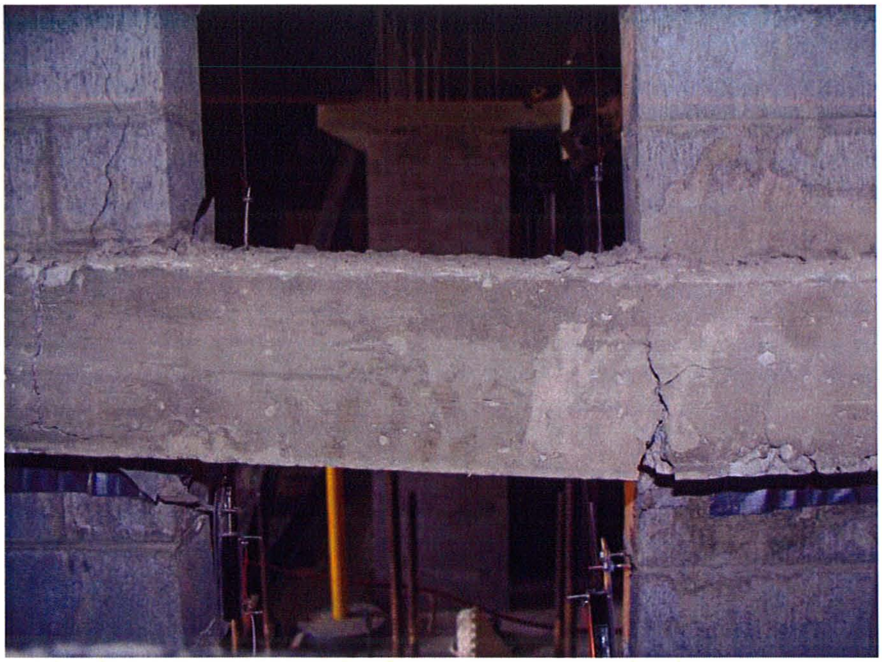

Figure 3.13: First Storey Slab Rotation (Photograph Taken of South Face)

3.5.2 General Observations

The failure mode of the wall was flexural in nature and included near simultaneous failure of the coupling beam at the first storey as well as vertical tension reinforcement within both walls. The cracking pattern of this specimen was similar to the diagonal cracking observed in Wall 3 and seemed to define a crack running diagonally across the wall. From examination of the figures in the previous section, it appeared as if the diagonal cracking originated in the second storey of Wall A and, if the cracking pattern was visualized as extending across the gap between the walls, it appeared to continue in the first storey of Wall B for this push loading.

Throughout the test, the second storey of Wall B did not appear to experience any significant damage. Beyond $3\Delta_y$ displacement, no additional cracks formed. Compared to Wall A and the lower storey of Wall B, this region incurred the least amount of masonry damage whereas the first storey of Wall B appeared to be the most damaged. Similarly to the test of Wall 3, the extent of the damage prevented the specimen from being loaded in the opposite direction and, therefore, no comparison between push and pull behaviour can be made.

During the design and construction phase of Wall 4, it was thought that the behaviour of the coupling beam would likely be dominated by shear rather than flexure. Therefore, because flexural failure was the preferred behaviour, a lightly reinforced section was chosen to minimize shear but from shear strength calculations, it could not be guaranteed that shear failure would not occur. In this respect, due to the fact that the flexural reinforcement within the slab failed in tension it is clear that the slab behaviour was governed by flexure.

Similarly to the previous wall tests, the properties of the reinforcing steel governed failure. As was the case with the previous specimens, the reinforcing steel fractured prior to the masonry undergoing significant levels of compression damage. This was especially evident during the test of Wall 4 as there was virtually no damage within the compression zone of either wall.

From the load-deflection curve (See Figure 3.14), it can be seen that the capacity of the wall was greater than the uncoupled value predicted using twice the ultimate lateral load of Wall 2 (or 66.8 kN). Due to coupling, Wall 4 reached a maximum lateral load of 88.3 kN suggesting that the coupling was in fact significant. Similar to previous tests, fracture of reinforcement resulted in a sudden decrease in capacity from 88 kN to 56 kN. The sudden jump of 5 mm of wall displacement can again be explained by a transfer of load from the reaction columns as their deflection due to bending decreased rapidly as the wall resistance decreased. The analysis of extent of coupling is included in Section 4.6.1.

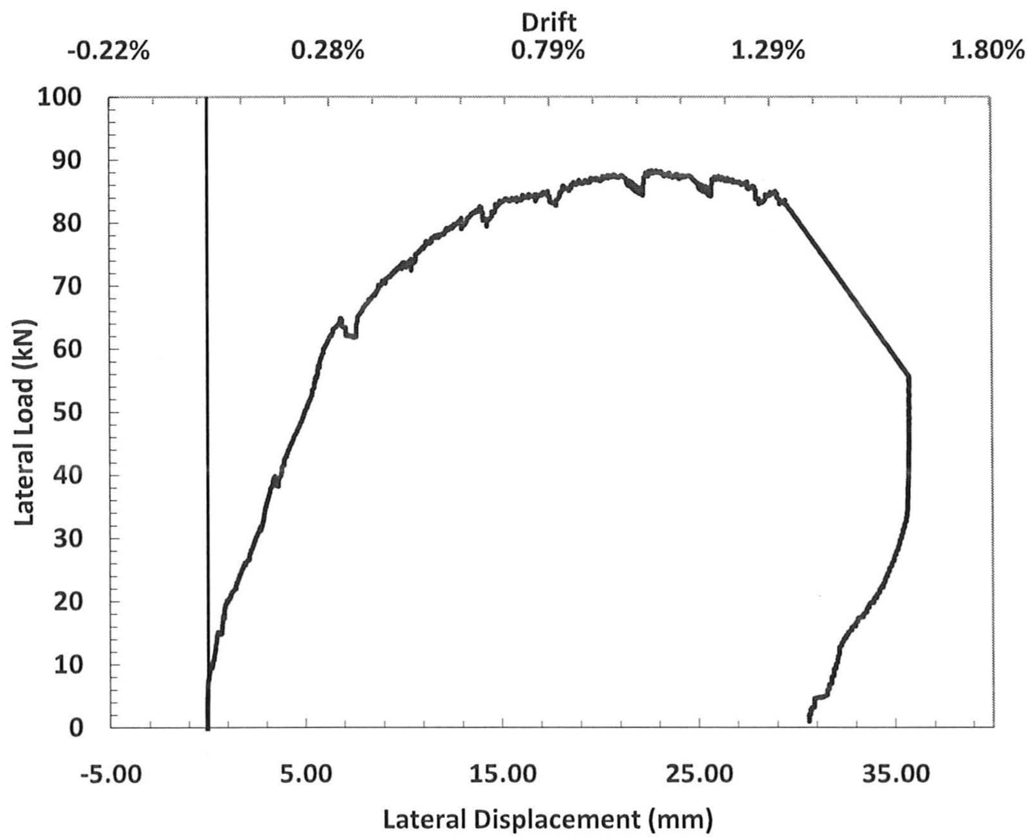

Figure 3.14: Pushover Curve for Wall 4

3.6 Conclusions

This chapter provides documentation of the experimental results of the wall tests. The experimental procedure for each specimen, experimental observations, and relevant graphs and photographs were presented.

From the information presented, it can be seen that the testing procedure had an impact on the behaviour of the specimens but more importantly their behaviour was governed by the properties of the vertical reinforcing steel. The comparatively low ductility of the reinforcing steel caused the specimens to exhibit a somewhat brittle behaviour and, rather than allowing damage to occur within the masonry, the wall specimen failures were governed by the reinforcement's inability to undergo moderate plastic deformations. With this limit on the amount of plastic behaviour, particularly as it relates to the ultimate displacement, the observed displacement ductility of the wall was less than otherwise might be expected with usual ductile reinforcement. Obviously, the ability of the reinforcing steel to undergo large plastic deformations is critical to ductile behaviour.

As a consequence of premature failure of the reinforcement, the masonry was not able to undergo large compressive strains and toe damage to produce increased ductility. Masonry damage not only influences the ductility of shear walls but also energy dissipation and equivalent viscous damping. With only minor masonry damage, there was only very minor energy dissipation within the masonry. As a result, the majority of the energy dissipation came from yielding of the reinforcing steel.

Another consequence of having relatively brittle steel is a lack of post peak data for all of the walls. Upon fracture of reinforcing bars, there was a sudden decrease in load resistance and, of course, a decrease in stiffness. This can be seen in the load displacement behaviours by the presence of nearly linear post peak behaviours. In reality, this plotted linear behaviour is actually the result of the graphing software connecting two data points as the scanning time of the data acquisition software did not have the resolution necessary to capture the behaviour in the brief instant when fracture occurred. Thus the linear behaviour shown in the load-displacement figures is not actually the behaviour of the specimen as the only recorded data lies at the moment before fracture and the moment after fracture. It would be expected that the initial loss of resistance and stiffness would have been much more rapid than shown by the connecting line.

Although the relatively brittle steel presented these complications, when considered as lower bound results they provide a positive indication of the resistance of ductile reinforced masonry shear walls subjected to seismic forces.

Analysis of the wall specimen data and a discussion of the analysis are presented in the following chapter.

Chapter 4

Analysis of Results

4.1 Introduction

The analysis of the experimental results presented within this chapter consists of an examination of various parameters related to seismic performance. The purpose is to evaluate whether the force modification factor, R_d, presented within CSA-S304.1 and the National Building Code of Canada (NBCC) are, in fact, underestimated. Underestimated values lead to design for higher equivalent lateral forces. In order to evaluate the performance of each specimen, there are several criteria which need to be studied.

4.2 Discussion of Seismic Performance Factors

4.2.1 Plastic Behaviour and Equivalent Plastic Hinge Length

Plastic behaviour involving the magnitude and the extent of plasticity is an important aspect of the analysis of seismic behaviour. Plasticity creates a means of energy dissipation through yielding of reinforcing steel and damage to the masonry. In this regard, the extent of plasticity which refers to the height over which plastic behaviour occurs and, more specifically, the equivalent plastic hinge length which is used to represent the cumulative effect of all of the plastic behaviour, is of great importance as this ultimately determines the magnitude of plastic displacement and, therefore, the ultimate displacement. Since the plastic deformations contribute directly to the ultimate displacements, they directly affect the displacement ductility which, in turn, directly affects the ductility related force modification factor, R_d.

Through the use of experimental data collected at specific locations, it is possible to calculate the average curvature for each location and generate an average curvature profile which can be plotted and from which the extent of plasticity may be examined. Lateral displacements, collected at various positions along the height of the wall, also can be used to estimate the extent of plasticity by examining a plot of lateral displacement versus wall height, at each level of displacement at the top of the wall recorded during testing.

Of the various approximations used to determine an equivalent plastic hinge length, 3 will be discussed below:

1. An approximation from Paulay and Priestley (1992) is based on rearranging Equation 4.1 to solve for the equivalent plastic hinge length, l_p, based on the equal energy elastic-plastic idealization of the load-deflection data to determine Δ'_y and P_y' as shown in Figure 4.1. In this case, the maximum displacement was the value corresponding to ultimate displacement but various drift limits or limits to the amount of strength degradation could be used.

$$\mu'_\Delta = 1 + 3\,(\mu'_\varphi - 1)\,(l_p / h_w)\,(1 - 0.5\, l_p / h_w) \qquad \text{Eq. 4.1}$$

where:
$$\mu'_\Delta = \Delta_{max} / \Delta'_y$$
$$\mu'_\varphi = \varphi_y / \varphi'_y$$
$$\Delta'_y = \Delta_y P_y' / P_y \text{ and } \varphi'_y = \varphi_y P_y' / P_y$$

Figure 4.2 contains a sketch showing the plastic hinge length and constant plastic curvature assumptions used to develop Equation 4.1.

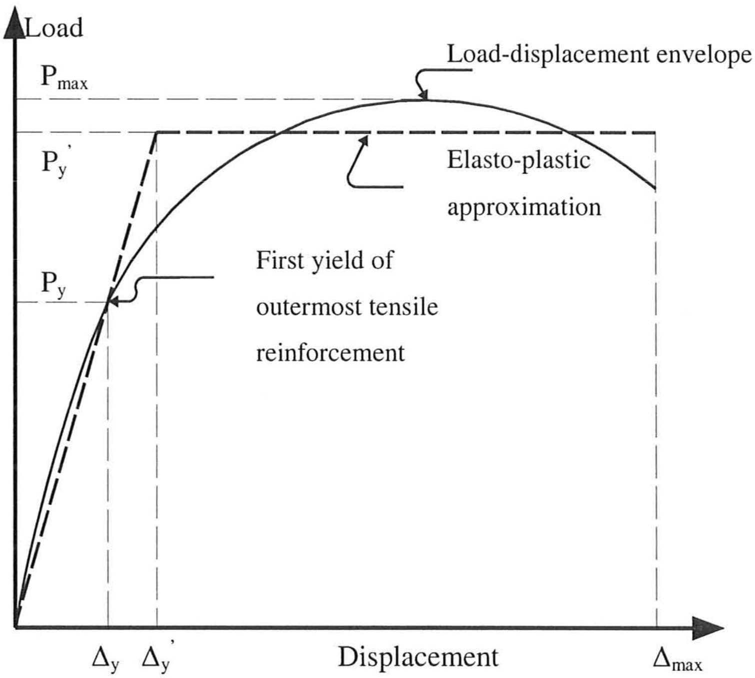

Figure 4.1 Elastic-plastic Idealization of the Load-Displacement Data for a Masonry Wall Specimen (from Shedid (2006))

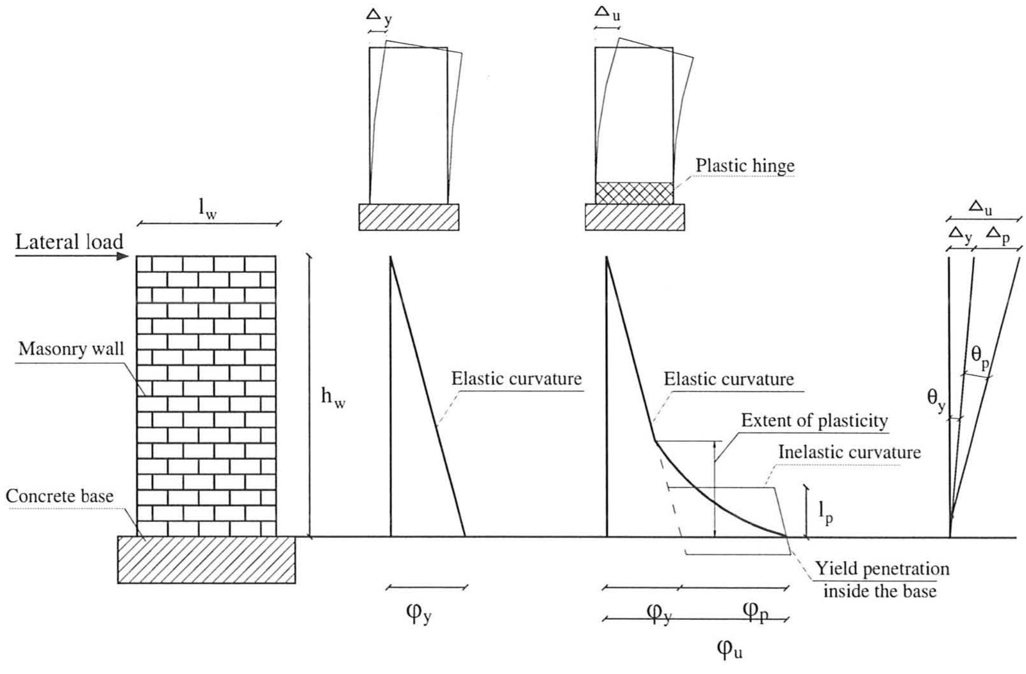

Figure 4.2: Curvature and Deflection Relationship for a RM Cantilever Shear Wall (from Shedid (2006))

2. Equation 4.2 also comes from Paulay and Priestley (1992) and is based solely on the diameter and yield strength of the reinforcement. This approximation was chosen because of the different characteristics used to describe the equivalent plastic hinge length. This approximation accounts for various heights of walls and bar diameter but does not include any influence of changes in aspect ratio (h/l_w) or the amount of vertical reinforcement placed in the wall.

$$l_p = 0.08h_w + 0.022d_bf_y \qquad \text{Eq. 4.2}$$

where : d_b = The bar diameter in mm;

f_y = The yield stress of the reinforcement in MPa;

h_w = Wall height;

l_p = Equivalent plastic hinge length.

3. The third approximation, also suggested by Paulay and Priestley (1993), is based on the aspect ratio and length of the wall (Eq. 4.3). This approximation, unlike approximation 2, accounts for the aspect ratio of the wall. However, it does not account for the amount of vertical reinforcement.

$$l_p = (0.20 + 0.044\ A_r)l_w \qquad \text{Eq. 4.3}$$

where: A_r = Aspect ratio of the wall= h/l_w

l_w = Wall length

Another approximation that was adopted in CSA S304.1 (2004) recommends that the length of the plastic hinge be the greater of l_w or $h_w/6$ for the case of a moderately ductile shear wall.

In interpreting the wall data from Chapter 3, it is suggested that the extent of plasticity can be qualitatively interpreted from plotted curves of lateral displacement versus wall height. By assuming that two zones exists, a zone of plasticity and a zone of elasticity, the plotted curves ideally consist of two distinct parts with the first part containing the zone of plasticity and the second part being more linear for the elastic region of behaviour. By assuming that the function consists of $f(x)_1$ for $0 < x<x_p$ and $f(x)_2$ for $x_p<x<h_w$, the extent of plasticity can be interpreted as the value x_p. However, because the displacements are measured only at fairly widely spaced points, the apparent extent of plasticity may fall between two points. Therefore, the extent of plasticity is presented as falling in the range between these values.

Using the average curvature profiles, the extent of plasticity also can be interpreted as the point at which the average curvature value is equal to the theoretical yield curvature value.

4.2.2 Wall Strength and Stiffness Degradation

For a building to effectively withstand seismic excitation, there must be adequate ductility and energy dissipation capabilities, and an adequate amount of strength. Large ductility is achieved when the ultimate displacement is several times larger than the yield displacement. However, for the required level of ductility, it is essential that a large part of the lateral capacity be retained to ensure the stability of the structure as it also supports the gravity load. Also, it is important that lateral displacement (drift) be limited within reasonable values.

In terms of dynamic response, it is also important to examine the effective stiffness as well the stiffness degradation. In order to do this, the secant stiffness, defined as the ratio between the lateral resistance and the corresponding wall displacement at the top of the wall, can be calculated and plotted against lateral displacement. The natural frequency (and the period) is directly related to the stiffness of the element or structure. A decrease in stiffness of 50% for stiff masonry structures with periods ranging between 0.4 and 0.8 seconds will result in an increased period ranging from 0.6 to 1.1 seconds (Drysdale and Hamid (2005)). This change is significant in terms of seismic demand due to the fact that a building with a longer period will typically show a reduced response to seismic ground motion than a stiffer building with a shorter period. The reduced response results in lower seismic forces in the longer period structure.

4.2.3 Normalized Period

As mentioned above, the period of a structure, or element, is an important aspect of seismic behaviour. In the absence of a dynamic analysis, a normalized period was calculated using Eq. 4.4 in order to determine the change in period with respect to lateral displacement. While the calculated initial period was not the true initial period, the relative change indicates that, as the shear wall is damaged, the period of the wall and possibly the structure increases. In turn, this typically results in decreases in the seismic forces; seismic demand decreases at higher displacements.

$$T_{norm} = \sqrt{\frac{K_{initial}}{K_i}} \qquad \text{Eq. 4.4}$$

where: $K_{initial}$ = the initial stiffness

K_i = the secant stiffness at drift level (i)

4.2.4 Wall Capacity and Displacement

Prior to experimental testing, the theoretical behaviour of each specimen was calculated. To facilitate accurate predictions of the yield force as well as displacement, actual material test data for the masonry was used in the calculations. In addition to measuring the compressive strength using tests on fully grouted block prisms, Young's modulus was determined as the slope of the line joining the 10 percent and 50 percent strength points in the stress-strain curve. The observed modulus of elasticity in conjunction with the assumption of elastic behaviour was used to model the stress and strain state in the masonry compression zone. Similarly, the yield stress, yield strain, and modulus of elasticity of the reinforcing steel were determined experimentally by tensile testing. The test data was then idealized into an elastic-perfectly plastic curve and used to characterize the stress and strain state of the reinforcement up to initial yield of the outermost bar.

The lateral force and strain profile, at yield, were calculated using simple beam theory assuming elastic behaviour of the masonry and idealized yield stress and strain conditions of the outmost tensile reinforcement. Reinforcement which experienced compression was included in the calculations. Elastic behaviour of the masonry up to initial yielding of the reinforcement in the walls was verified afterwards using stress-strain plots corresponding to data collected from material testing. Once the strain profile and yield force were determined, the yield curvature was calculated using the strain profile. From this, the theoretical yield displacement was calculated by assuming a constant moment-curvature relationship. Tensile strength of the masonry was ignored in all calculations.

The ultimate capacity was calculated using simple beam theory as well as the equivalent rectangular stress block set forth in CSA S304.1 (2004). Similar to the yield calculations, reinforcement which experienced compression was included in the calculations because, even though excluded in CSA S304.1 (2004) because of lack of tie support, it has been found to be effective up to very large deformations even corresponding to damage, decreased capacity, and very large drift (Shedid, 2006). In the ultimate strength calculations, the steel stress was determined using the nominal yield strength calculated using the 0.2% offset method as describe in Section 2.2.5 with a strain of 0.0027. The ultimate masonry strain was set conservatively as 0.0025 which is the value for moderately ductile shear walls within CSA S304.1-04 and the value used in block masonry in the MSJC Code (2005). Material reduction factors were not used. The strain profile at ultimate capacity was determined and subsequently the ultimate curvature was calculated.

Using the relationship that the sum of the yield and plastic curvatures is equal to the ultimate curvature, the plastic curvature was determined. Then, to predict ductility according to CSA S304.1-04, the plastic hinge length was estimated using the greater of $h_w/6$ and l_w requirement for a moderately ductile shear wall. The predicted plastic displacement was then calculated using the plastic curvature and the hinge height, assuming that plastic rotation occurred at the mid-height of the plastic hinge.

4.2.5 Displacement Ductility

It is generally accepted that, for members exhibiting nearly ideal elastic-plastic load-deflection behaviour, the displacement ductility, $\mu_\Delta=\Delta_u/\Delta_y$, can be calculated accurately using the actual yield displacement (Shedid et al. (2008)). Inspection of the load-displacement behaviours presented in Chapter 3 reveals that these load-displacement behaviours do not resemble ideal elastic-plastic behaviour. Therefore, an equivalent elastic-plastic load-displacement curve was needed in order to calculate the displacement ductility. Although several other options were considered, the four illustrated in Figure 4.3 were chosen and are discussed below.

Method 1: This method is similar to one presented by Shing et al. (1989). In this method, the yield resistance is selected to be the ultimate resistance of the specimen with an elastic stiffness, *k*, based on the initial stiffness during a small amplitude displacement cycle in which the peak load is approximately 50% of the ultimate resistance. However, in these calculations, the stiffness was calculated based on a load which is less than 50% of the ultimate resistance to ensure that the elastic stiffness, *k,* corresponds to a section which is behaving elastically.

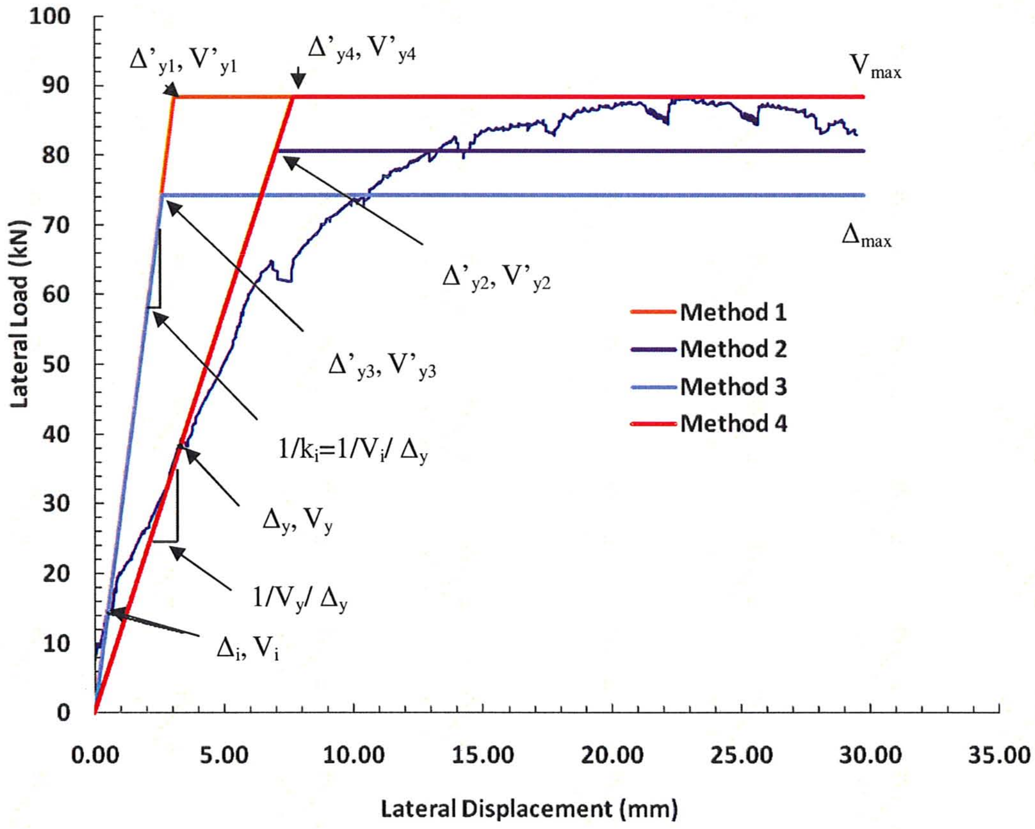

Figure 4.3: Idealization Techniques for Load-Deflection Curves

Method 2: Method 2 is consistent with *Option 7* presented by Shedid et al. (2008). This method consists of defining an effective yield displacement as the value which produces equal energy under the curves, up to a prescribed level of displacement (Shedid et al. (2008)), with an idealized elastic stiffness value of V_y/Δ_y.

Method 3: Method 3 is a modification of Method 1 similar to that presented by Vasconcelos and Lourenço, (2009). In this method, the effective yield displacement and yield resistance are defined as the values which produce equal energy under the load-displacement curves. The initial stiffness of the idealization is consistent with Method 1.

Method 4: Method 4 is a modification of Method 2, proposed by the Author. In this method, the yield resistance is selected as the ultimate resistance of the specimen with an idealized elastic stiffness value of V_y/Δ_y. Equal energy, as represented by the area under the curves, is not considered in this method. This method was chosen to complete the idealization patterns presented by Methods 1 to 3. Method 1 and Method 3 share the same initial stiffness value, *k*, with Method 1 using the ultimate resistance to describe yield and Method 3 using the equal energy approach to describe yield. Method 2, however, uses an initial stiffness of V_y/Δ_y but only describes yield in terms of equal energy. By creating Method 4, there is now an idealization technique which produces an initial stiffness of V_y/Δ_y but also describes yield in terms of the ultimate resistance.

Once the experimental load-displacement curves are transformed into idealized elasto-plastic curves, the displacement ductilities can be readily calculated using the ultimate displacement and the idealized yield displacement. Idealized curvature ductility was calculated based on Equation 4.1. However, since Methods 1 and 3 do not rely on experimental yield data, the curvature ductility cannot be calculated as Equation 4.1 requires a value for yield curvature.

4.3 Analysis of Wall 1

4.3.1 Predicted and Experimental Wall Capacities and Displacements

As stated in Section 2.4.1, the theoretical yield and ultimate forces were 32.4 kN and 50.4 kN, respectively. During the wall test, a force equal to the theoretical yield force was applied. However, the corresponding displacements were not equal to the predicted displacement of 5.0 mm. In fact, the measured displacements were approximately 2.6 mm greater in the push direction and 1.6 mm greater in the pull direction. This is not surprising and the larger displacements observed during testing can be explained by a number of factors. Firstly, predicted values were based on flexural displacements whereas the measured total lateral displacements were the sum of the displacements created by sliding, shear and flexural deformations. Additionally, debonding of reinforcing steel (or tensile strain penetration) within the concrete base would contribute to the lateral displacement (Paulay and Priestley (1992)). Thirdly, the nominal yield stress and strain were used to calculate the theoretical lateral load at yield as well as the theoretical lateral displacement at yield whereas, in fact, significantly higher strains were required to reach the nominal yield stress level.

The maximum displacement reached by the wall was 22.0 mm whereas the predicted ultimate displacement was 34.4 mm. Due to the brittle behaviour of the reinforcement and the related fact that very little masonry compressive damage was present, it is not surprising that these values differ significantly. Had the wall been able to undergo larger steel strains and, consequently, more significant masonry damage, it is entirely possible that the lateral displacement could have reached the 34.4 mm or more as observed in similar tests using standard reinforcing bars (Shedid, 2009). In other circumstances, the overestimated ultimate deflection also could have been attributed to the plastic hinge length approximation as is discussed in a following section.

The achieved maximum lateral resistance of 50.7 kN is in close agreement with the predicted value of 50.4 kN. While use of the equivalent rectangular compression stress block would have resulted in an overestimation of the compression moment arm, this would have been counteracted by the fact that, as can be seen from the stress-strain curves for the reinforcing, the steel stress at failure would have exceeded the nominal yield value used in the calculation.

4.3.2 Stiffness Degradation and Normalized Period for Wall 1

The initial stiffness was taken as the secant stiffness during a low level of lateral load for both directions of loading. The secant stiffness was calculated also at each level of displacement. The experimentally determined displacements, secant stiffnesses, and corresponding stiffness degradations are presented in Table 4.1

Table 4.1: Stiffness Degradation of Wall 1

Stage	Top Deflection (mm)		Secant Stiffness (kN/mm)		Stiffness Degradation (%)**	
	Push	Pull	Push	Pull	Push	Pull
Initial	1.97	-1.76	4.42	5.05	-	-
Δ_y	7.40	-6.91	4.14	4.09	16.3	19.0
2 Δ_y	14.54	-14.37	3.21	3.05	27.4	39.6
3 Δ_y	21.98	-21.78	2.07	1.96	53.2	61.1
4 Δ_y	26.61*	-29.05	1.28	1.16	71.0	77.4

*Recall from Section 3.2.1 that the outmost reinforcement fractured at a displacement of 21.4 mm, not reaching a displacement of $4\Delta_y$. This was the highest level of displacement achieved while attempting a displacement of $4\Delta_y$.

** Expressed cumulatively as a percentage of the initial stiffness

It can be seen that the stiffness degradation increased as the displacement increased with the largest incremental decrease in stiffness occurring during the increase from $2\Delta_y$ to $3\Delta_y$. Considering that the average incremental decrease in stiffness between $3\Delta_y$ and $4\Delta_y$ was 17.0% of the initial stiffness, and the total average degradation in secant stiffness was 74.2%, when compared to the initial pre-yield secant stiffness, it can be seen that the rate of decrease was fairly uniform but slightly less at the larger displacement. This trend can be seen graphically in Figure 4.4 where the curves appear to be approximately linear. Plotting a linear best fit results in an R^2 value of 0.982 and 0.994 for the push and pull directions of loading, respectively, which statistically indicates a nearly uniform rate of stiffness degradation.

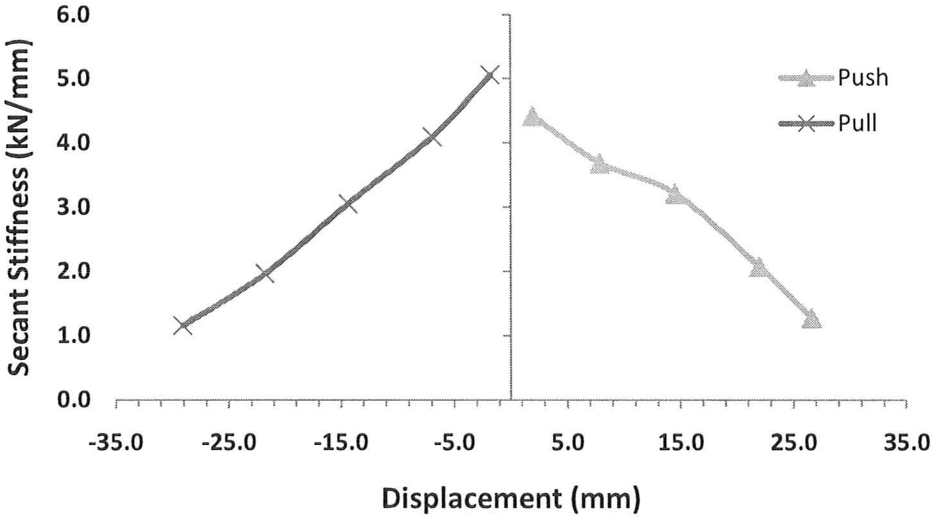

Figure 4.4: Stiffness Degradation of Wall 1 (Push direction denoted by positive displacement)

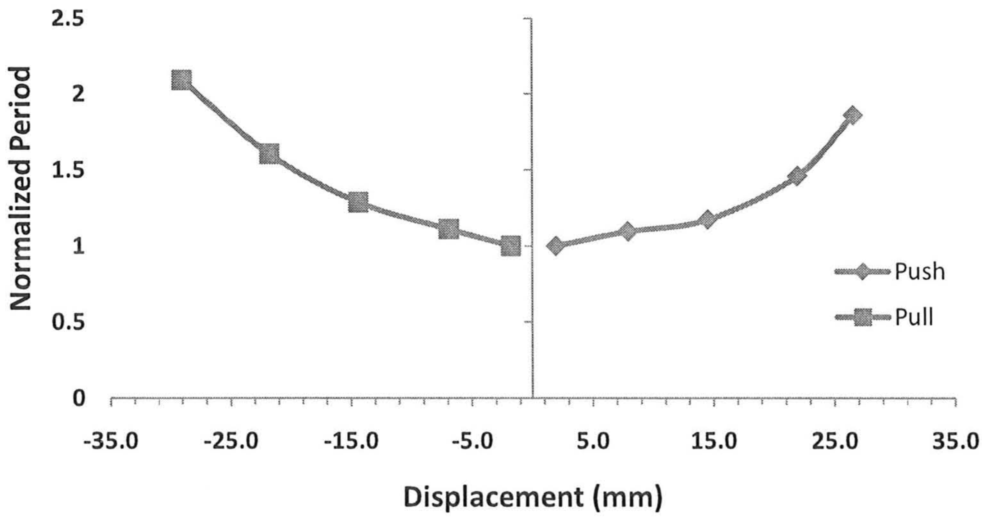

Figure 4.5: Normalized Period versus Displacement for Wall 1 (Push direction denoted by positive displacement)

Looking at the normalized period, calculated as described in Section 4.2.3, plotted against the lateral displacement (See Figure 4.5), it can be seen that, as the lateral displacement increased, the normalized period increased due to the decreasing secant stiffness. These calculations show an increase in normalized period of approximately 100% at 4 Δ_y compared to the initial level.

4.3.3 Plastic Behaviour of Wall 1

The first aspect that will be looked at related to plastic behaviour is the average curvature. At first yield, the predicted curvature at the base of the wall was calculated as 3.1x10^{-6} rad/mm whereas the measured average curvatures at the base of the wall were 6.1x10^{-6} rad/mm (Push) and 8.8x10^{-6} rad/mm (Pull). The values were 1.97 (Push) and 2.84 (Pull) times the predicted value. One reason for this discrepancy can be explained by debonding of the vertical reinforcement within the concrete base as this would add to the tensile displacement measured over the first 100 mm above the base. As an illustration, if bond is assumed to add an elongation equal to the effect of 100 mm unbonded length in the foundation, the (f_y/E_s)100 mm elongation divided by the segment height of 100 mm would result in an apparent increase in tensile strain to f_y/E_s mm/mm and an increase in curvature equal to $\varepsilon_y/(d - kd)$ rad/mm, where d is the distance from the distance from the extreme compression fibre to the centroid of the outmost tensile bar and kd is the depth of the compression zone. As indicated earlier, the other main reason for actual curvature at first yield load being larger than predicted is that significantly higher steel strain was required to reach the nominal yield stress than was used in the calculations based on an idealized elastic-plastic relationship.

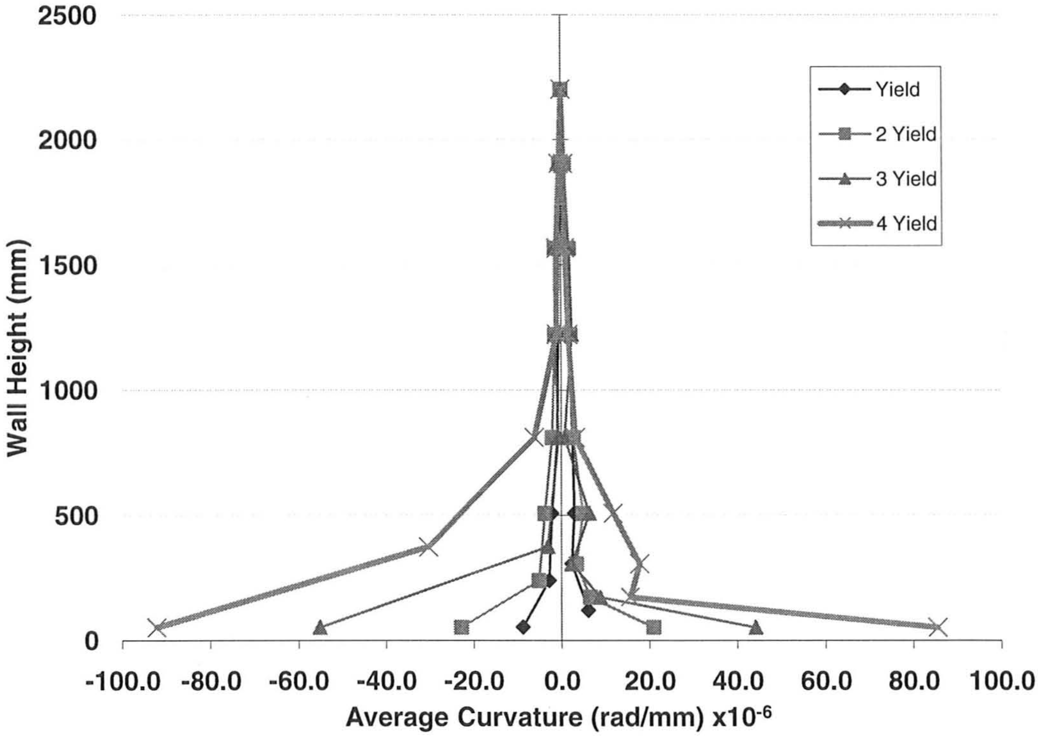

Figure 4.6: Average Curvature Profiles for Wall 1 at Various Displacement Levels (Push direction denoted by positive displacement)

The theoretical ultimate curvature was calculated as $19x10^{-6}$ rad/mm whereas, from Figure 4.6, it can be seen that this value was surpassed even before the wall reached $2\Delta_y$. Again, the fact that the measured average curvatures were much higher than the predicted curvature could be due to bar debonding (or strain penetration) within the base (Paulay and Priestley (1992)) leading to a higher effective average strain over the bottom segment of the wall. The extent of plasticity can be simplistically estimated by looking at both the average curvature profile and a plot of lateral displacement versus wall height. From Figure 4.6, the extent of plasticity could be interpreted as being approximately 800 to 1000 mm above the base in both directions of loading as this is the location where average curvature values become less than the measured yield curvature. From the lateral displacements plotted in Figure 4.7, the extent of plasticity was interpreted as being within the range of 270 mm to 540 mm in the push direction and approximately between 540 mm to 820 mm in the pull direction. In this regard, it can be seen that such an interpretation is difficult to make and it should be noted that the plastic behaviour at highest usable deflection is of most interest.

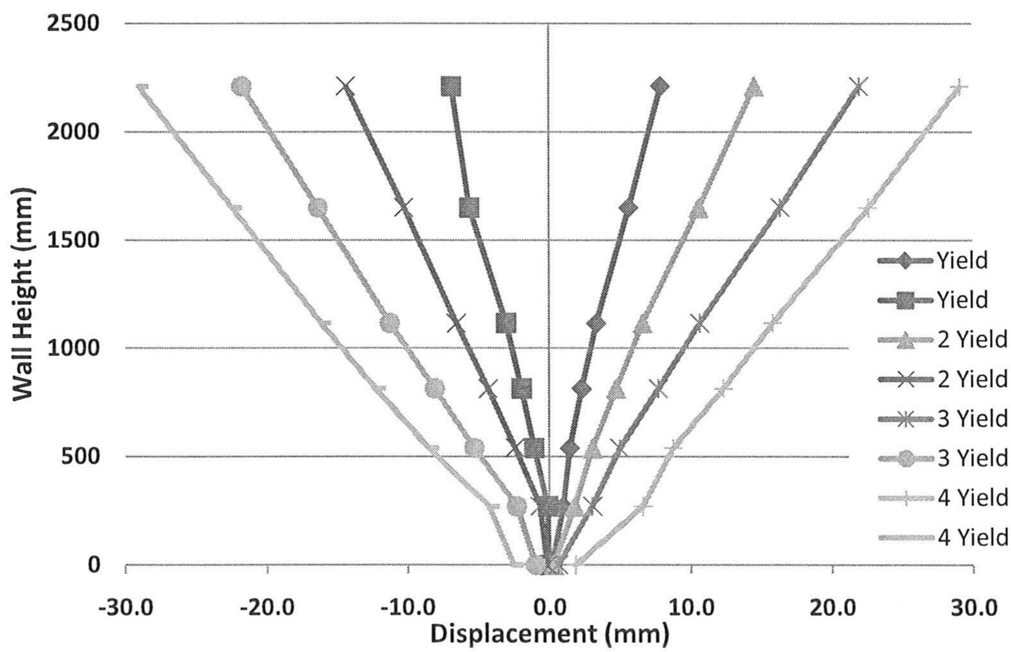

Figure 4.7: Lateral Displacement Profiles at Various Displacement Levels for Wall 1 (Push direction denoted by positive displacement)

As discussed in Section 4.2.1, various approximations have been used for determining the equivalent plastic hinge length. Since equivalent plastic hinge lengths are considered to have constant plastic curvature, these lengths should not be confused with or expected to equal lengths of zones of plasticity. The calculated values corresponding to the four approximations (described in Section 4.2.1) are presented in Table 4.2 where it can be seen that the CSA S304.1-04 approximation provides the largest estimate of plastic hinge length. While this is not surprising when it is considered that the measured ultimate curvature is usually much larger than used in the theoretical analysis, it should be remembered that this wall suffered failure of reinforcing bars at very low curvatures with masonry compressive and steel tension strains well below normal expectations (Shedid (2006)). Therefore, compared to the extent of plasticity and the results of the other approximations, it appears that this approximation results in a plastic hinge length which is unreasonably large. Estimates using Equation 4.1 and Equation 4.3 bracket the range of the remaining predicted equivalent hinge lengths while Equation 4.2 is approximately the average of the two.

Table 4.2: Calculated Equivalent Plastic Hinge Lengths for Wall 1

	Eq. 4.1	Eq. 4.2	Eq. 4.3	CSA S304.1
Lp (mm)	192 (Method 2) 184 (Method 4)	266	323	1132

4.3.4 Ductility of Wall 1

As described in Section 4.2.5, four displacement ductilities were calculated based on the 4 chosen idealization techniques. The 4 idealizations are illustrated in Figure 4.8 with key values presented in Table 4.3.

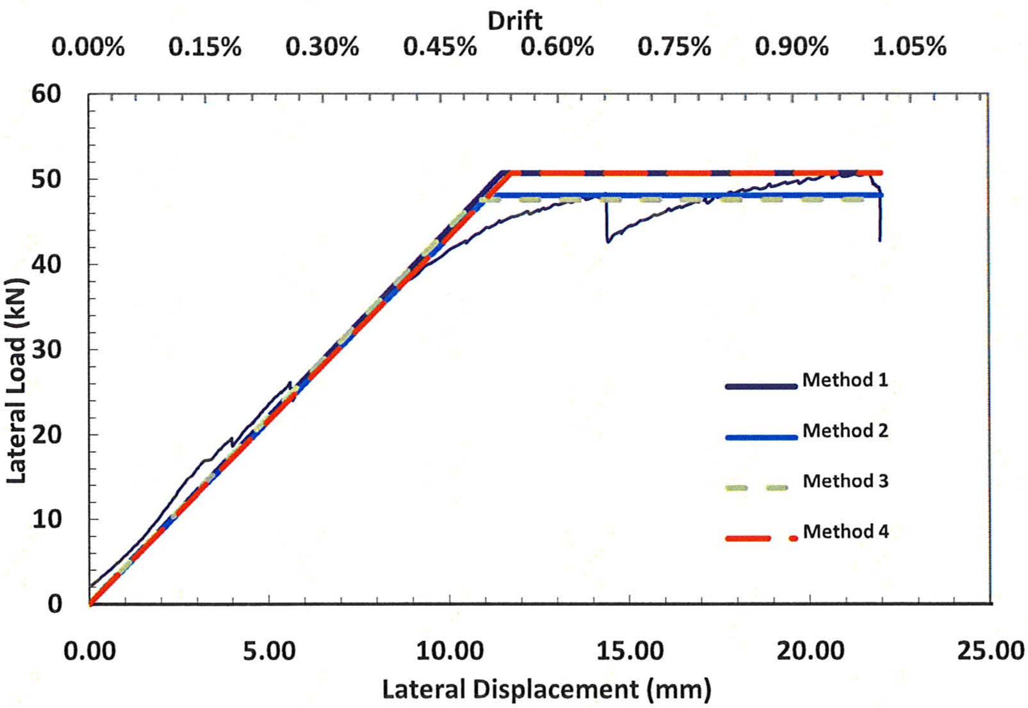

Figure 4.8: Elasto-Plastic Idealizations for Wall 1 (Push direction denoted by positive displacement)

Table 4.3: Ductilities for Wall 1 Calculated using Various Idealizations

	Method 1	Method 2	Method 3	Method 4
V'y (kN)	50.69	48.07	47.53	50.69
Δ'y (mm)	11.48	11.14	10.76	11.74
Δu (mm)	22.00	22.00	22.00	22.00
μ_Δ	1.92	1.98	2.04	1.87
μ_φ	N/A	4.89	N/A	4.64

From Table 4.3, it can be seen that all 4 methods of elasto-plastic idealization resulted in similar evaluations of displacement ductility with Method 3 producing the highest value of displacement ductility and Method 4 producing the most conservative value. In terms of curvature ductility, Methods 2 and 4 are similar but Method 2 gave a slightly higher value. Compared to NBCC 2005 values for R_d, this specimen exceeded the required value of 1.5 and was close to the value of 2.0 corresponding to a moderately ductile shear wall. However, since the ultimate condition was reached prematurely due to comparatively brittle steel properties, it is likely that R_d values much greater than 2.0 would have been achieved. Also, since very little post-peak behaviour was observed, the differences between values resulting from Method of calculation were not very pronounced. Existence of a post-peak behaviour would illustrate the impact of choice of method.

4.4 Analysis of Wall 2

4.4.1 Predicted and Experimental Wall Capacities and Displacements

As stated in Section 2.4.2, the theoretical yield and ultimate lateral forces were 19.7 kN and 29.9 kN, respectively. During the wall test, the force was applied until the strain gauge located at the foundation-shear wall interface of the outmost tensile bar reached the nominal yield strain. At this strain level, the measured displacement was 6.6 mm and the corresponding lateral load was 15.3 kN. In terms of theoretical predictions versus experimental observations, this measured displacement is equal to the theoretical displacement of 6.6 mm but the lateral load does not correspond with the predicted value. In fact, the observed lateral load was 22% lower than the predicted value. Considering this magnitude of load difference, it seems that the strain gauge readings may not have been accurate and the agreement in displacements was the result of other discrepancies as discussed earlier for Wall 1. For instance, the predicted values were based on flexural displacements whereas the total measured lateral displacement measured was the sum of the displacements created by sliding, shear and flexural deformations. Also, as mentioned before for Wall 1, at the nominal yield strain, the actual steel would be less than the yield value.

The maximum displacement reached by the wall was 26.4 mm including shear deformations whereas the predicted ultimate displacement was 38.5 mm considering only flexural deformations. As was the case for Wall 1, due to the relatively brittle properties of the reinforcement and the fact that very little masonry compressive damage was present, it is difficult to compare these values but, clearly, limiting the tensile strain in the reinforcement would result in a much reduced predicted ultimate displacement. Had greater strains in the reinforcement been possible and the masonry subjected to more significant damage, it is entirely possible and considered likely that the lateral displacement could have reached in excess of the 38.5 mm predicted displacement. The overestimated ultimate deflection, in part, also can be attributed to the plastic hinge length approximation discussed in a following section.

The maximum lateral resistance achieved was 33.4 kN, which is 12% higher than the predicted value. Most of this discrepancy can be explained by the fact that the reinforcing steel did not display perfectly plastic behaviour and large steel strains could result in steel stresses of up to 590 MPa, which is 9.25% percent higher than the idealized yield of 540 MPa.

4.4.2 Stiffness Degradation and Normalized Period of Wall 2

The initial stiffness for Wall 2 was taken as the secant stiffness at the low level of lateral load of 9.7 kN in the push direction and 9.2 kN in the pull direction which represent 29% and 28% percent of maximum observed lateral resistance. The secant stiffness was also calculated at each multiple of yield level of displacement. The displacements, secant stiffnesses and corresponding stiffness degradations are presented in Table 4.4.

Table 4.4: Stiffness Degradation of Wall 2

Stage	Top Deflection (mm)		Secant Stiffness (kN/mm)		% Degradation	
	Push	Pull	Push	Pull	Push	Pull
Initial	3.32	-3.32	2.92	2.77	-	-
Δ_y	6.59	-6.54	2.34	2.53	19.9	8.6
2 Δ_y	13.17	-13.11	2.04	1.74	30.2	37.0
3 Δ_y	19.71	-19.64	1.59	1.40	45.5	49.3
4 Δ_y	26.08	-26.30	1.26	1.12	56.7	59.7

Wall 2 displayed a steady increase in stiffness degradation. The only discrepancy was at Δ_y in the pull direction, where the stiffness degradation was much less pronounced than in the push direction of loading. This trend is plotted in Figure 4.9. Compared with Wall 1, it does not display the same linearity. With a linear regression analysis, the resulting R^2 values are 0.957 and 0.959 for the push and pull directions of loading, respectively, thus indicating that the trend is not truly linear.

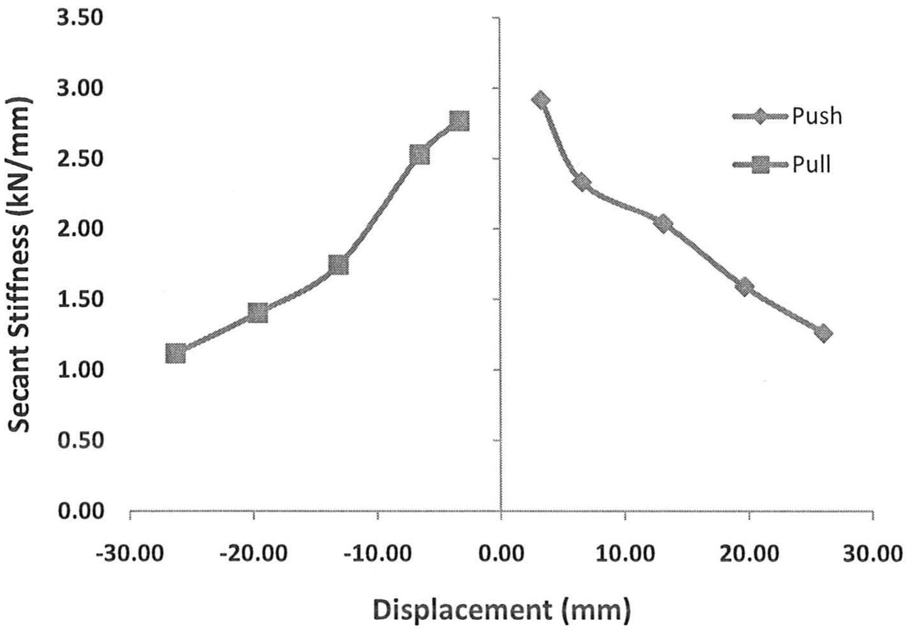

Figure 4.9: Stiffness Degradation of Wall 2 (Push direction denoted by positive displacement)

Considering the normalized period versus displacement plotted in Figure 4.10, the trend is not the same as that displayed by Wall 1 (See Figure 4.5). The change in normalized period for Wall 2 resembles a linear function rather than the parabolic shape seen for Wall 1. The increase in normalized period for Wall 2 was approximately 60% at a displacement of $4\Delta_y$ whereas Wall 1 had displayed an increase of approximately 100% over a similar displacement. While this increase for Wall 2 seems dramatic, it represents a 0.4-0.5 second period difference between Wall 1 and Wall 2.

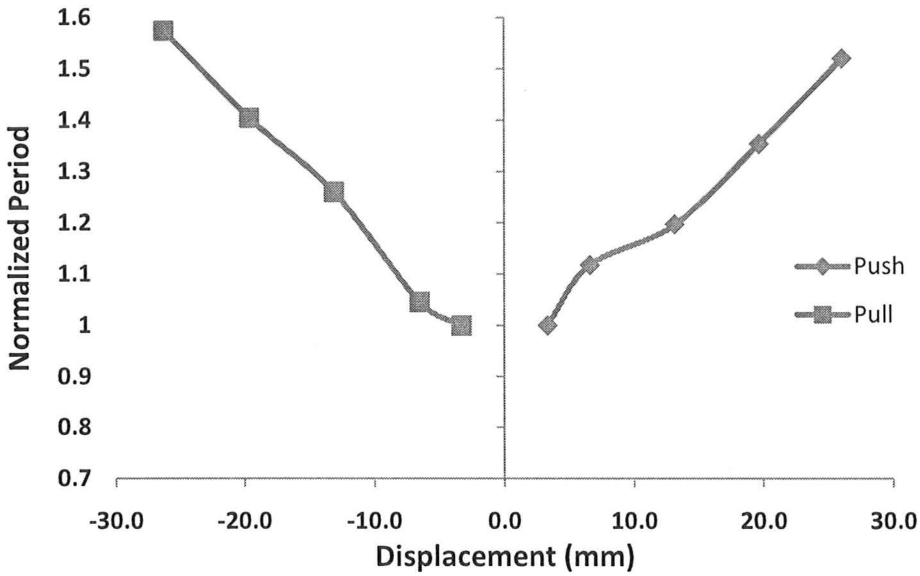

Figure 4.10: Normalized Period versus Displacement for Wall 2 (Push direction denoted by positive displacement)

4.4.3 Plastic Behaviour of Wall 2

The theoretical curvature at first yield of the outermost reinforcement was calculated as 4.10×10^{-6} rad/mm whereas the measured average curvatures at first yield of the outermost reinforcement whereas 7.98×10^{-6} rad/mm and 15.2×10^{-6} rad/mm for the push and pull directions of loading, respectively. The measured average curvature in the push direction was 1.95 times the predicted value. This was consistent with Wall 1 which displayed a measured average curvature value that was 1.97 times the predicted value. As mentioned in Section 4.3.3, the very large curvature values measured at yield may be due to tensile strain penetration into the reinforced concrete base due to vertical bar debonding. Also the difference between the nominal yield strain and the actual value adds significantly to the curvature.

The discrepancy between the measured average curvature values in the push and pull directions can be attributed to the testing procedure. It is suggested that damage to the wall during loading in the push direction caused much larger curvatures to be measured in the pull direction of loading.

The ultimate curvature for Wall 2 was predicted to be 25.0×10^{-6} rad/mm. However, from the plotted average curvature profiles within Figure 4.11, this value was surpassed at the $3\Delta_y$ level of displacement in the push direction, and prior to the $2\Delta_y$ level of displacement in the pull direction. Therefore, the measured average curvatures were much higher than the predicted curvature. This could be due to the same reasons as discussed for Wall 1 in Section 4.3.3. From consideration of the yield curvature, the extent of plasticity may be interpreted as having a length of about 600 mm in both directions of loading.

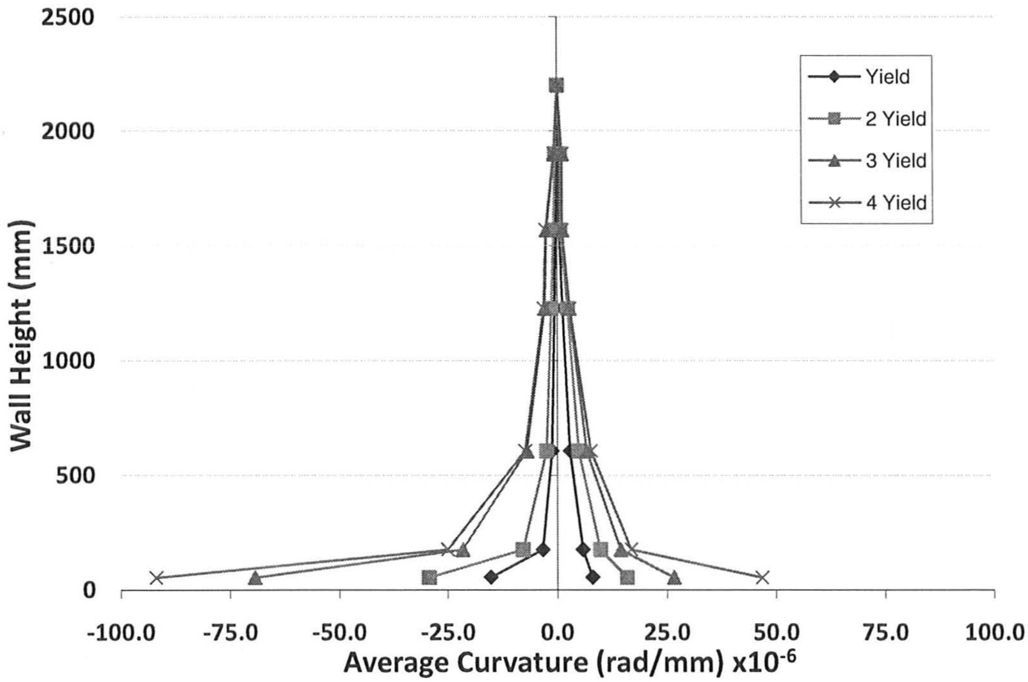

Figure 4.11: Average Curvature Profile for Wall 2 at Various Displacement Levels (Push direction denoted by positive displacement)

The shape of the plot of lateral displacement versus wall height (See Figure 4.12) suggests that the extent of plasticity may be at a wall height of approximately 530 mm to 805 mm and is consistent for both directions of loading.

As previously mentioned, 4 methods were used to determine the equivalent plastic hinge length. These calculated values are summarized in Table 4.5. Equations 4.2 and 4.3 estimated the smallest equivalent plastic hinge lengths whereas CSA S304.1-04 estimated the highest equivalent plastic hinge length and Equation 4.1 estimated a value between them. Unlike the approximations for Wall 1 where the highest estimate of equivalent plastic hinge length (produced by

Equation 4.1) was 29% of the CSA S304.1-04 estimate, the highest estimate for Wall 2 was 48% of the CSA S304.1-04 estimate.

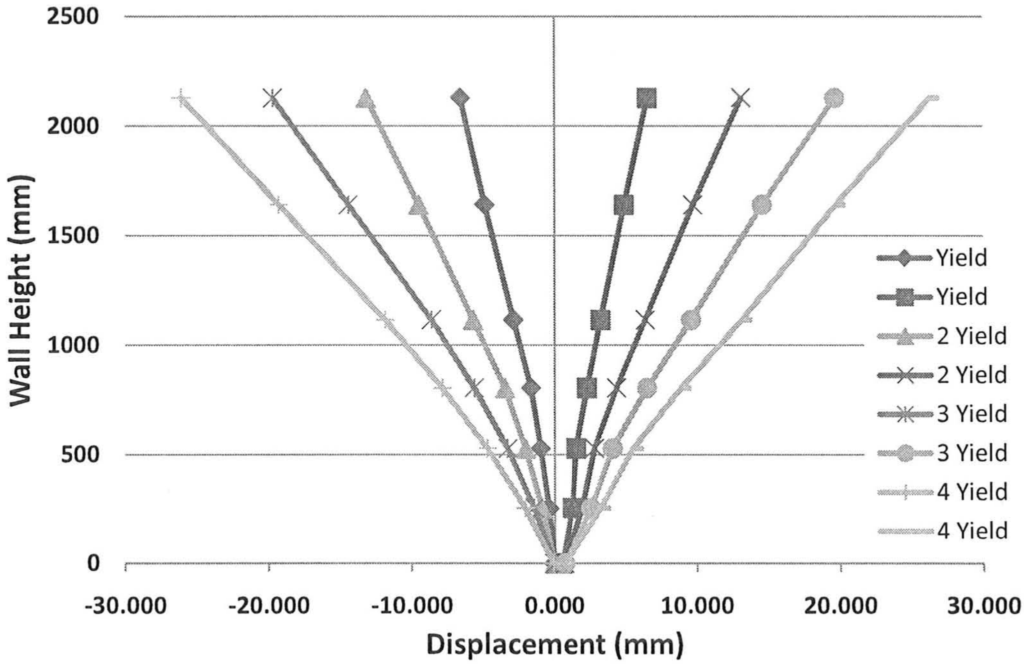

Figure 4.12: Lateral Displacements at Various Displacement Levels for Wall 2 (Push direction denoted by positive displacement)

Table 4.5: Calculated Equivalent Plastic Hinge Lengths for Wall 2

	Eq. 4.1	Eq. 4.2	Eq. 4.3	CSA S304.1
Lp (mm)	418 (Method 2) 402 (Method 4)	266	270	865

4.4.4 Ductility of Wall 2

As discussed in Section 4.2.5, the displacement ductility was calculated based on 4 chosen idealization techniques. The 4 chosen techniques are presented in Figure 4.13 for the load-top deflection data for Wall 2. Due to the pronounced difference in the initial stiffness determined for Methods 1and 3 versus 2and 4, Methods 1and 3 result in the highest level of displacement ductility as opposed to Methods 2 and 3 from Wall 1. Table 4.6 contains a summary of the key values. Displacement ductility was highest using Method 3, with a value of 2.68, and lowest using Method 4, with a value of 1.84. Curvature ductility was highest using Method 2 with a value of 2.88 while Method 4 resulted in a value of 2.70. According to Method 3, this wall achieved a displacement ductility which was 34% higher than the NBCC value of 2.0 for moderately ductile walls. Using Method 4, this specimen did not meet the R_d=2.0 ductility value. However, it is expected that use of reinforcing steel possessing a greater level of ductility would have produced results surpassing these values.

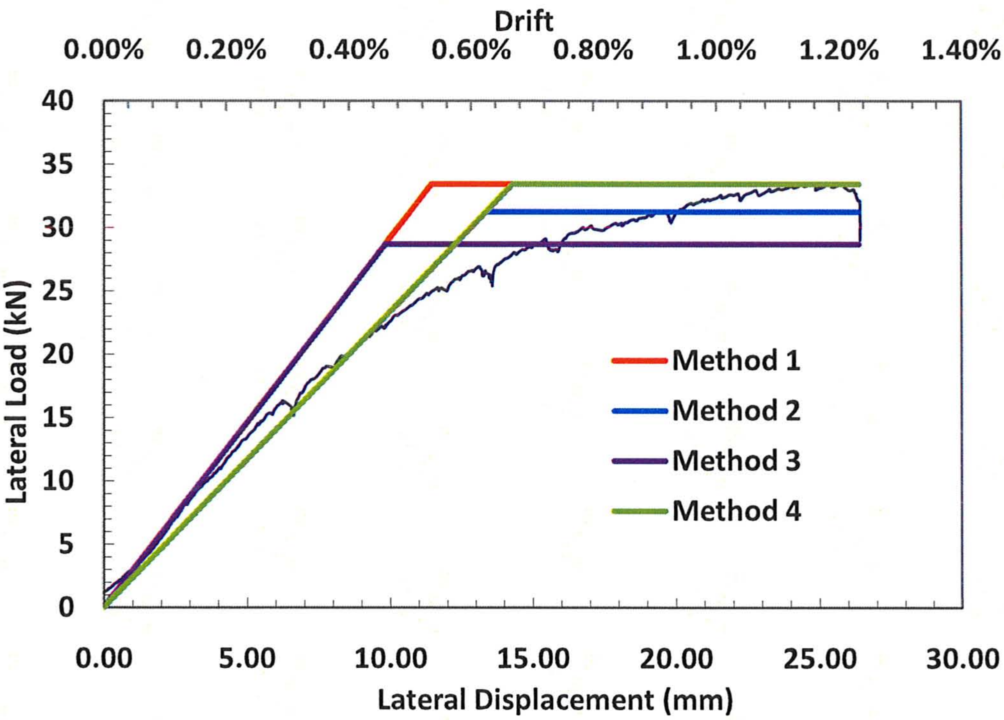

Figure 4.13: Elasto-Plastic Idealizations for Wall 2 (Push direction denoted by positive displacement)

Table 4.6: Ductilities for Wall 2 Calculated using Various Idealizations

	Method 1	Method 2	Method 3	Method 4
V'y (kN)	33.45	31.26	28.70	33.45
Δ'y (mm)	11.47	13.38	9.84	14.32
Δu (mm)	26.40	26.40	26.40	26.40
μ_Δ	2.30	1.97	2.68	1.84
μ_φ	N/A	2.88	N/A	2.70

4.5 Analysis of Wall 3

4.5.1 Predicted and Experimental Wall Capacities and Displacements

As stated in 2.4.3, the theoretical yield and ultimate forces were 108.4 kN and 146.9 kN, respectively. During the wall test, a lateral force was applied until the strain gauge located at the foundation-shear wall interface of the outmost tensile bar reached the nominal yield strain. At this strain level, the measured displacement was 4.0 mm with a lateral load of 81.1 kN. This load point was relatively close to the theoretical displacement of 3.6 mm but did not correspond closely with the predicted value for lateral load. The observed lateral load was 25% lower than the predicted value. As was the case for Walls 1 and 2, the use of a nominal yield strain based on elastic-perfectly plastic modeling can account for the fact that lower stress in the reinforcement and , therefore, lower lateral load corresponded to the lower force in the reinforcement. That is, steel stress prior to yielding was overestimated using the idealized stress-strain curve.

The maximum displacement reached by the wall was 26.8 mm whereas the predicted ultimate displacement was 91.0 mm. One reason for the largely overestimated ultimate deflection can be attributed to the overly large plastic hinge length approximation. The hinge length approximation, from CSA S304.1-04 for Wall 3, was equal to the length of the wall (1532 mm) which is 70% of the total wall height so that it extended to half the height of the second storey. Of course, the other reason is that the reinforcement failed at relatively low steel strain with the result that the masonry under compression did not reach high strains and did not suffer compression damage. The related effects were that the amount of plastic deformation was relatively low.

The maximum lateral resistance achieved was 151.5 kN, which is 3% higher than the predicted value. Although there is a slight discrepancy, this can be explained by the fact that the reinforcing steel did not display perfectly plastic behaviour and steel strains higher than the actual strain at nominal yield stress would produce stresses in excess of the nominal yield. Slightly larger values than the idealized yield stress of 540 MPa could account for the 5 kN difference.

4.5.2 Stiffness Degradation and Normalized Period for Wall 3

The initial stiffness was taken as the secant stiffness at a low level of lateral load. The secant stiffness was calculated also at each level of displacement. The displacements, secant stiffnesses, and corresponding stiffness degradations are presented in Table 4.7.

Table 4.7: Stiffness Degredation of Wall 3

	Δ (mm)	Secant Stiffness (kN/mm)	Degradation(%)
Initial	0.98	43.31	-
Δ_y	4.01	20.32	53.1
2 Δ_y	8.00	12.86	70.3
3 Δ_y	11.92	10.48	75.8
4 Δ_y	16.01	8.92	79.4
5 Δ_y	19.98	7.47	82.7
6 Δ_y	23.94	6.22	85.6

It can be seen from the above table that the largest stiffness degradation occurred between initial stiffness and that at Δ_y. This large initial decrease in stiffness is consistent with the observations of Drysdale and Hamid. (2005) where cracking is the main factor. Graphically this trend can be observed (See Figure 4.14). Compared with the plots in Figure 4.4 and Figure 4.10 for Walls 1 and 2, respectively, the graph in Figure 4.14 does not display the same linearity. In fact, it displays a pronounced curve.

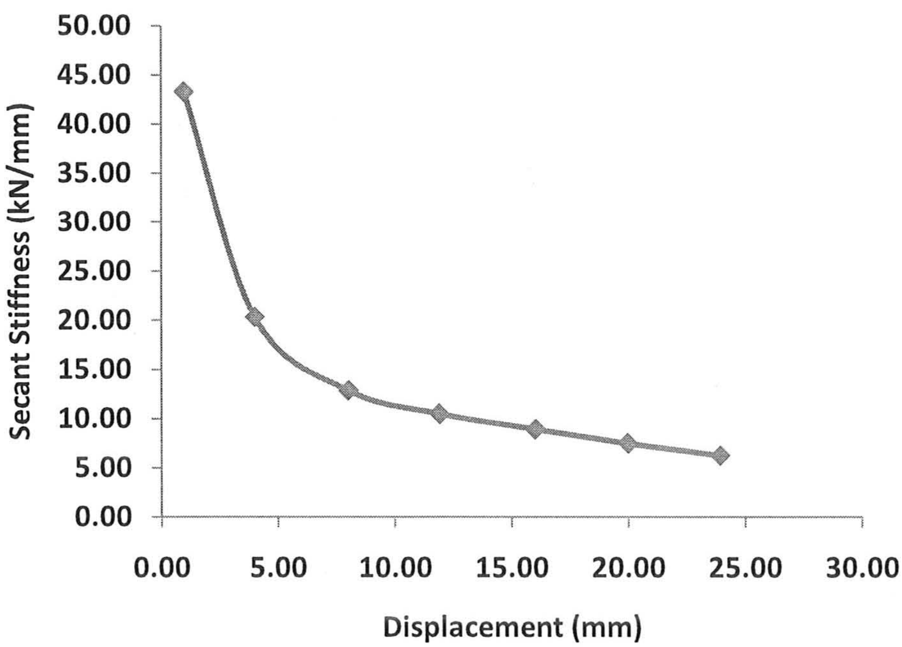

Figure 4.14: Stiffness Degradation of Wall 3 (Push direction denoted by positive displacement)

Looking at the normalized period versus the displacement (See Figure 4.15), the trend was not the same as that displayed by Walls 1 and 2. The normalized period resembles a polynomial and, in fact, performing a third order polynomial regression resulted in an R^2 value of 0.999, indicating that the relationship between normalized period and displacement can be described by a third order polynomial function. The normalized period for this specimen was significantly larger than for Wall 1 and Wall 2 with an increase in the range of 160-165% which represents a period which would typically have a positive effect on the seismic performance of the shear wall.

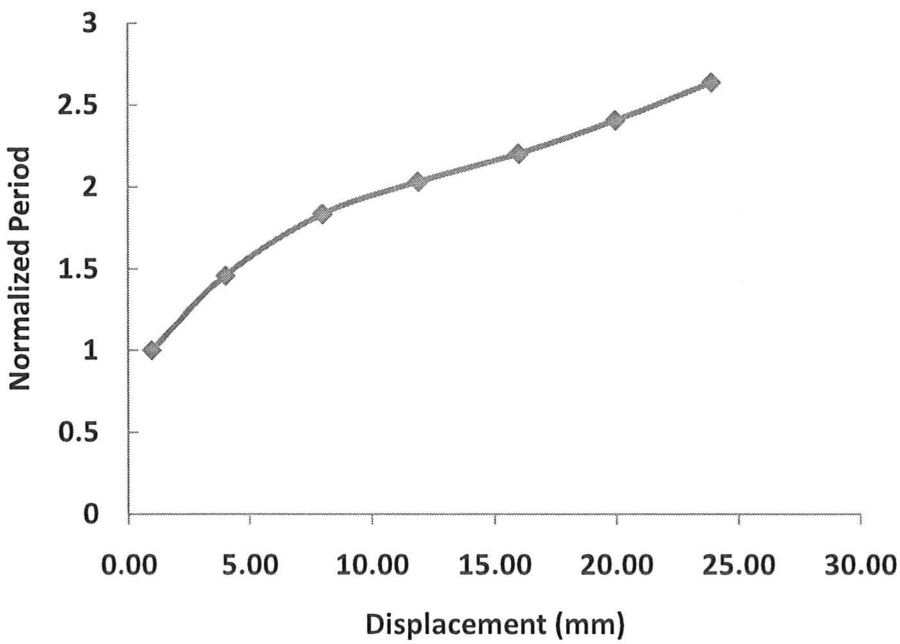

Figure 4.15: Normalized Period versus Displacement for Wall 3 (Push direction denoted by positive displacement)

4.5.3 Plastic Behaviour of Wall 3

The theoretical curvature at yield was calculated as 2.21×10^{-6} rad/mm whereas the measured average curvature at yield was 4.74×10^{-6} rad/mm. Compared to the measured curvature, this value is 2.14 times the value predicted and is consistent with Wall 2 which displayed a curvature value that was 1.95 times the predicted value. As mentioned in Section 4.3.1, the large curvature values measured at yield may be due to tensile strain penetration into the base slab and to the fact that higher steel strains were required to reach the nominal yield stress than was accounted for in the theoretical calculations using a perfectly elastic-plastic idealization.

The predicted ultimate curvature was $42.0\text{x}10^{-6}$ rad/mm. However, it can be seen from Figure 4.16 that this value was never reached. If it is recalled from Section 3.4.1 that the measured ultimate displacement was much lower than the theoretical displacement, the above result is not surprising since the ultimate curvature prediction is based upon the predicted ultimate displacement. In addition, the relatively brittle behaviour of the reinforcement limited the maximum strains reached in the reinforcement and the masonry. Also, this higher theoretical ultimate displacement may be due, in part, to the estimation of the plastic hinge length provided by CSA S304.1 (2004).

From Figure 4.16, the extent of plasticity may be interpreted as being within the wall height range of approximately 175 mm to 310 mm as this is the range where the measured average curvatures becomes less than the predicted curvature at first yield. An examination of the shape of the plot of lateral displacement versus wall height (See Figure 4.17) suggests that the extent of plasticity may be interpreted as having a length of approximately 240 mm to 510 mm.

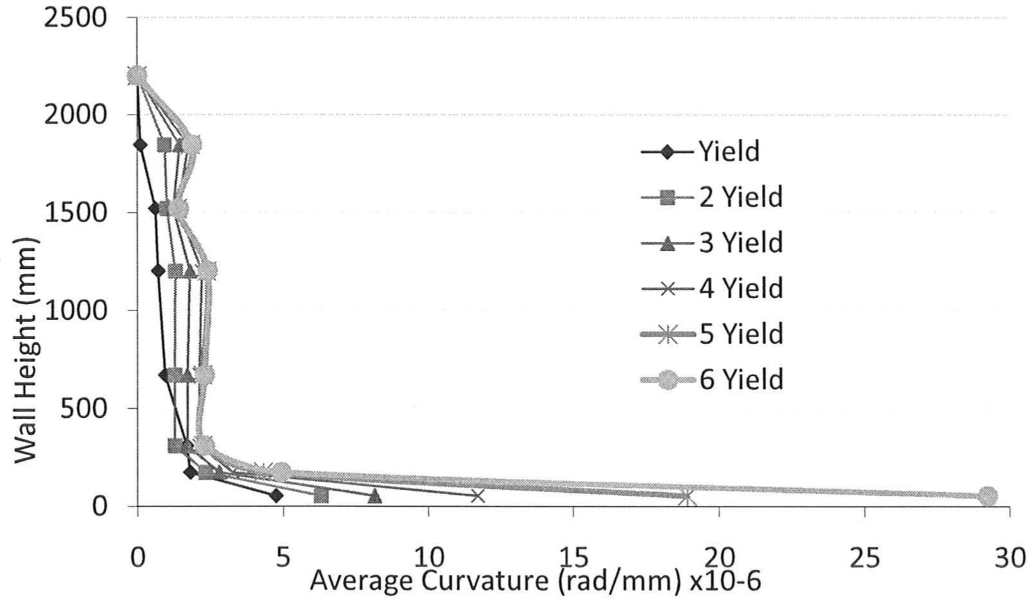

Figure 4.16: Average Curvature Profile for Wall 3 at Various Displacement Levels (Push direction denoted by positive displacement)

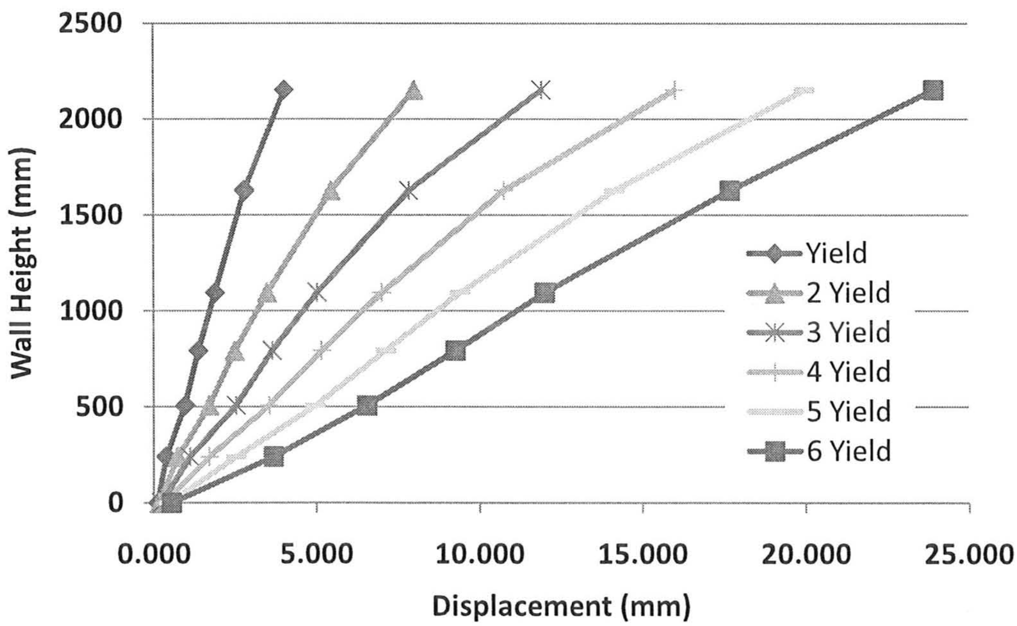

Figure 4.17: Lateral Displacements at Various Displacement Levels for Wall 3 (Push direction denoted by positive displacement)

As previously mentioned, 4 methods of determining the equivalent plastic hinge length were chosen, the results of which are summarized in Table 4.8. Equations 4.2 and 4.3 resulted in the smallest equivalent hinge lengths whereas the CSA S304.1-04 length was the largest; the Equation 4.1 estimation gave a value nearest the specified CSA S304.1-04 value.

Table 4.8: Calculated Equivalent Plastic Hinge Lengths for Wall 3

	Eq. 4.1	Eq. 4.2	Eq. 4.3	CSA S304.1
Lp (mm)	1093 (Method 2) 1100 (Method 4)	266	403	1532

4.5.4 Ductility of Wall 3

As described in Section 4.2.5, displacement ductilities were calculated based on the 4 chosen idealization techniques. The results using the 4 techniques are presented in Figure 4.18. Due to the pronounced difference in the initial stiffness between Methods 1 and 3 versus 2 and 4, Methods 1 and 3 result in the highest level of displacement ductility, a result similar to Wall 2. From Table 4.9, the resulting displacement ductility was highest using Method 3 with a value of 9.04, and lowest using Method 4 with a value of 3.59. In terms of curvature ductility, Method 2 resulted in the highest value of 3.59 while Method 4 resulted in a value of 3.30. According to the results of Method 3, this wall achieved a significant displacement ductility which was 3.52 times the NBCC specified value of 2.0 for moderate ductility. Using Method 4, this specimen also surpasses the

2.0 ductility by 80%. The key values for each idealization technique are summarized within Table 4.9. Based on the idealization techniques presented, it is reasonable to say that the NBCC restriction of R_d = 2.0 severely underestimated the ductility of Wall 3 even though, because of the relatively brittle reinforcement, this wall did not experience as much deformation as would be expected had normal reinforcement been used.

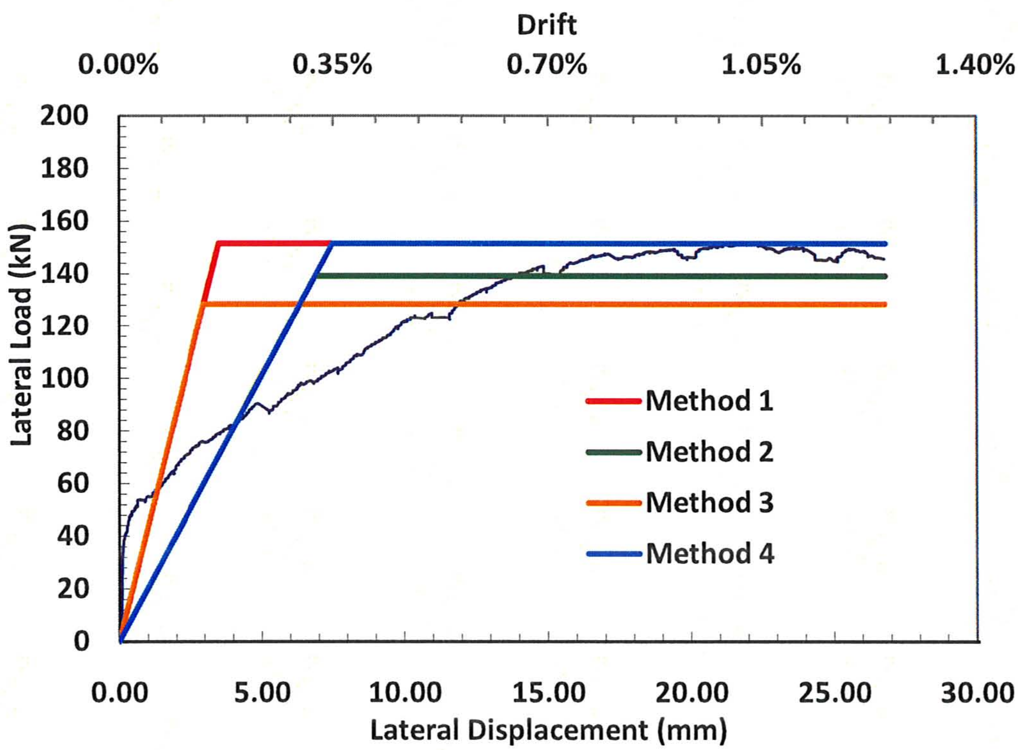

Figure 4.18: Elasto-Plastic Idealizations for Wall 3 (Push direction denoted by positive displacement)

Table 4.9: Ductilities for Wall 3 Calculated using Various Idealizations

	Method 1	Method 2	Method 3	Method 4
V'y (kN)	151.45	139.03	128.33	151.45
Δ'y (mm)	3.50	6.86	2.96	7.47
Δu (mm)	26.80	26.80	26.80	26.80
μ_Δ	7.66	3.91	9.04	3.59
μ_φ	N/A	3.59	N/A	3.30

4.6 Analysis of Wall 4

4.6.1 Predicted and Experimental Capacities and Displacements

As described in Section 2.4.4, originally the theoretical yield load and theoretical ultimate load were not calculated due to the unknown contribution of flexural coupling to lateral load capacity. During the wall test, a lateral load equal to two times the theoretical yield force of similar Wall 2 was applied as representative of yielding. At this 39.5 kN load, the corresponding displacement was 3.4 mm. If no flexural coupling was present, the coupling beams could be modeled as link members possessing pin-pin end conditions rather than fixity, or partial fixity. For this uncoupled case, the theoretical yield load, corresponding to yielding of the outermost bars in both of the similar walls would have been calculated as 39.5 kN.

Although strain readings indicating yielding of the outermost vertical bars in the coupled walls would have provided an indication of load and displacement at first yield, these readings were found to be unreliable. The alternative option of calculated first yield of the coupled walls was also thought not to be reliable because of the inability to accurately model the necessary variable load-deformation properties of the cracked walls and coupling slab at yield point. However, if the average of the yielding load for both walls is considered to define initial yielding, then the effect of coupling should be mainly on increasing the load resistance at yield rather than the displacement. This conclusion is based on the fact that the opposite tensile and compressive axial forces in the two similar walls due to the coupling action of the floor slabs will be equal and fairly small. Therefore, yield of the wall with the axial tension force would occur at a lower displacement than similar Wall 2 and initial tensile yielding of the wall with the axial compressive force will be delayed to a slightly higher displacement. Since these decreased and increased displacements will be roughly equal, the yield displacement value from Wall 2 with no axial load seems to be a reasonable compromise between the alternatives of using either first yield of the wall with axial tension versus the later first yield of the second wall due to the presence of axial compression. Thus the yield load would be the measured load corresponding to the 6.6 mm yield displacement recorded for Wall 2.

The maximum lateral resistance achieved was 88.3 kN and the corresponding maximum lateral displacement was 29.8 mm. Assuming that flexural coupling is negligible, the measured ultimate resistance should have been comparable to twice that of the ultimate load reached by Wall 2. Recalling from Section 4.4.1 that the measured ultimate lateral load reached by Wall 2 was 33.4

kN, this would result in a 66.8 kN ultimate resistance for Wall 4. Considering the other extreme of fully plastic flexural coupling by the coupling beams, the corresponding theoretical ultimate lateral resistance became 86.1 kN compared to the 59.8 kN value predicted for the 2 walls simply linked together (2 x 29.9 kN predicted capacity of Wall 2). This theoretical difference of 26.3 kN is close to the observed difference of 21.5 kN which seems to indicate that the full coupling capacity of the coupling beams (or very close to full coupling) was achieved.

A weak-beam strong-column mechanism (See Figure 4.20) was used for the theoretical ultimate lateral load capacity calculations. Since this theoretical value is only 5% lower than the experimentally observed value, it was concluded that the coupling beams contributed a coupling effect equal to 100% of their flexural capacity. Recalling from Section 3.4.1 the flexural reinforcement within the coupling beam fractured in the regions adjacent to the shear walls where moment magnitude is expected to be a maximum value, this indicates that the failure of the beam was governed by flexural behaviour as opposed to shear behaviour.

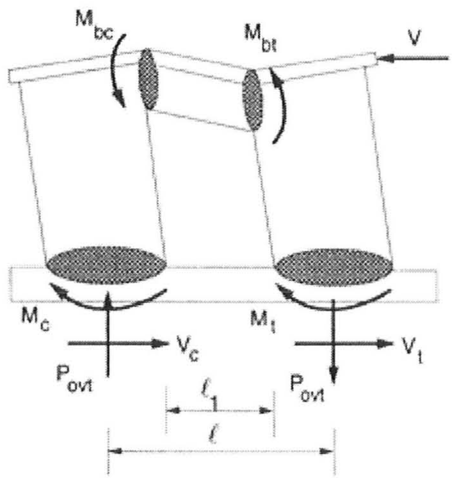

Figure 4.19: Weak Beam Strong Column Mechanism for a Single Storey Wall (from Drysdale, R., and Hamid, A. (2005))

Where:

M_c, M_t	= flexural strengths of base sections for the compression and tension piers, respectively.
P_{ovt}	= pier force due to overturning moment and is equal to shear force in the coupling beam.
M_{bc}, M_{bt}	= flexural strengths of compression pier end and tension pier end of the coupling beam, respectively
ℓ_1	= clear length of the coupling beam
ℓ	= distance between center lines of piers.

$$V = \frac{M_c + M_t + P_{ovt}\,\ell}{h} \qquad P_{ovt} = \frac{M_{bc} + M_{bt}}{\ell_1}$$

The theoretical ultimate displacement was calculated by analysing Wall 2 with the addition of axial forces, P_{ovt}, created due to coupling. The theoretical ultimate curvature of Wall B (compressive axial force) was 20.24×10^{-6} rad/mm whereas the theoretical ultimate curvature Wall A (tensile axial force) was 31.47×10^{-6} rad/mm, indicating that Wall B governs the ultimate condition of Wall 4. As stated earlier, the displacement at first yield was 6.6 mm which was the theoretical yield displacement of Wall 2. Therefore, the theoretical yield curvature calculated for Wall 2 was valid for Wall B. Using the theoretical yield curvature for Wall 2, the theoretical ultimate curvature of Wall B, and the equivalent plastic hinge length from CSA S304.1, the resulting theoretical ultimate lateral displacement was 31.3 mm. With an ultimate measured displacement for Wall 4 of 29.8 mm, this represented the most accurate prediction of ultimate displacement. However, the measured value of 29.8 mm included shear deformations in addition to flexural deformations whereas the theoretical predictions considered only flexural deformations.

4.6.2 Stiffness Degradation and Normalized Period for Wall 4

The initial stiffness was taken as the secant stiffness during a low level of lateral load. The secant stiffness was calculated initially as well as at each level of displacement. The displacement, secant stiffness and corresponding degradation are presented in Table 4.10.

Table 4.10: Stiffness Degradation of Wall 4

Load Stage	Displacement (mm)	Secant Stiffness (kN/mm)	Degradation%
Initial	0.51	28.41	-
Δy	3.43	11.48	59.6
2 Δy	7.07	8.96	68.5
3 Δy	10.41	7.12	74.9
4 Δy	13.92	5.93	79.1
5 Δy	17.39	4.89	82.8
6 Δy	21.32	4.08	85.6
7 Δy	24.68	3.54	87.6
8 Δy	27.98	3.03	89.3

The largest stiffness degradation occurred over the Δy displacement increment. This large decrease in stiffness is consistent with the observed stiffness degradation of Wall 3. Graphically the trend of decreasing stiffness can be observed in the plot presented in Figure 4.20. Compared with the plot presented in Figure 4.14 for Wall 3, the shapes of the smooth curves are similar; the curves appear to become fairly linear after yielding has been well developed.

The trend present in the normalized period versus displacement (See Figure 4.21) is also similar to that displayed by Wall 3. It is fairly linear after yielding is well developed. The normalized period and the increase in normalized period for Wall 4 are significantly larger than the previous specimens with an increase of approximately 206%. This increase would typically have a positive effect on the seismic performance of the shear wall or a building made up of similar shear walls.

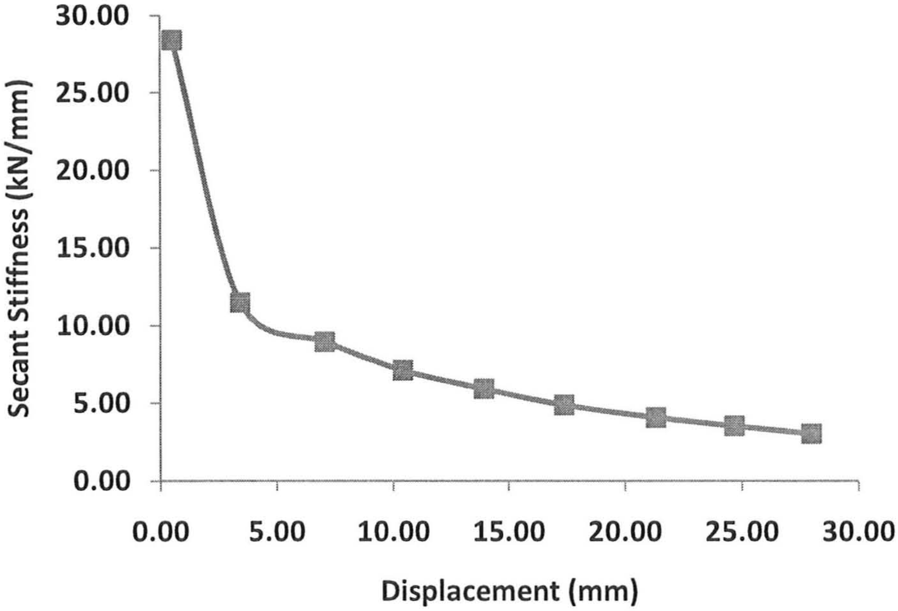

Figure 4.20: Stiffness Degradation of Wall 4 (Push direction denoted by positive displacement)

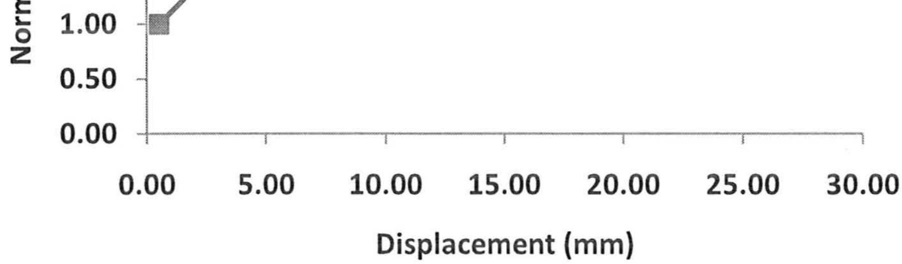

Figure 4.21: Normalized Period versus Displacement for Wall 4 (Push direction denoted by positive displacement)

4.6.3 Plastic Behaviour of Wall 4

At the time of testing Wall 4, as indicated in Section 3.5.1, the nominal yield was chosen to correspond to the uncoupled condition. However, since there was coupling, it is more rational to define the yield point at the measured lateral displacement of 6.6 mm corresponding to the measured displacement at yield for Wall 2. The measured average curvatures at the yield displacement of 6.6 mm were 8.81×10^{-6} rad/mm and 12.35×10^{-6} rad/mm for Walls A and B, respectively, while the measured average curvature at yield for Wall 2 (Push direction of loading) was 7.98×10^{-6} rad/mm. Compared to the measured curvature of Wall 2, the measured curvature of Wall A was similar whereas the measured curvature of Wall B was 1.55 times that of Wall 2. Although such differences would be considered to be unusual, the number of cracks that exist within the height of wall being measured will significantly affect the average strain over that gauge length. A study of the photograph of the 2 walls at initial yield seems to show differing crack patterns with more cracking in Wall B. Recalling from Section 4.4.3, that the predicted ultimate curvature for Wall 2 was 25.0×10^{-6} rad/mm, it can be seen from Figure 4.22 and Figure 4.23 that this value was reached at displacements of $6\Delta y$ and $5\Delta y$ for Walls A and B, respectively.

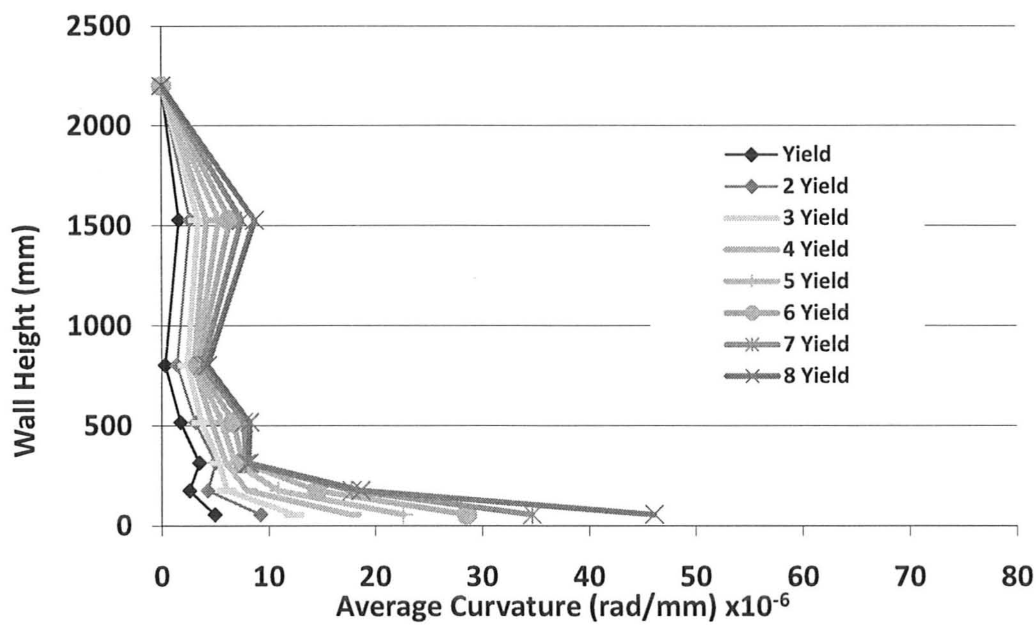

Figure 4.22: Average Curvature Profile: Wall A of Wall 4 (Push direction denoted by positive displacement)

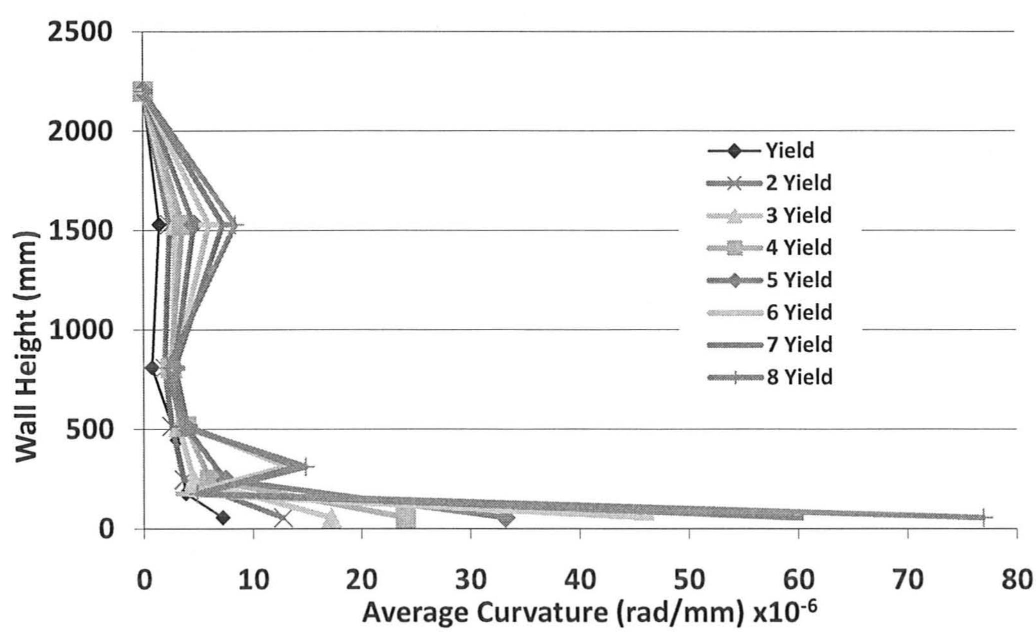

Figure 4.23: Average Curvature Profile: Wall B of Wall 4 (Push direction denoted by positive displacement)

From Figure 4.22 and Figure 4.23, the extent of plasticity may be interpreted as having a length of between 315 mm to 520 mm for Wall A and between 245 mm to 515 mm for Wall B. This assessment is based on the point at which the measured average curvature became less than or equal to the predicted curvature at yield for similar Wall 2. An examination of the plot of wall height versus lateral displacement (See Figure 4.24) suggests that the extent of plasticity was approximately between 500 mm to 800 mm. This assessment is based on identifying the point at which there is no longer a visible change in the slope of the deflection profile.

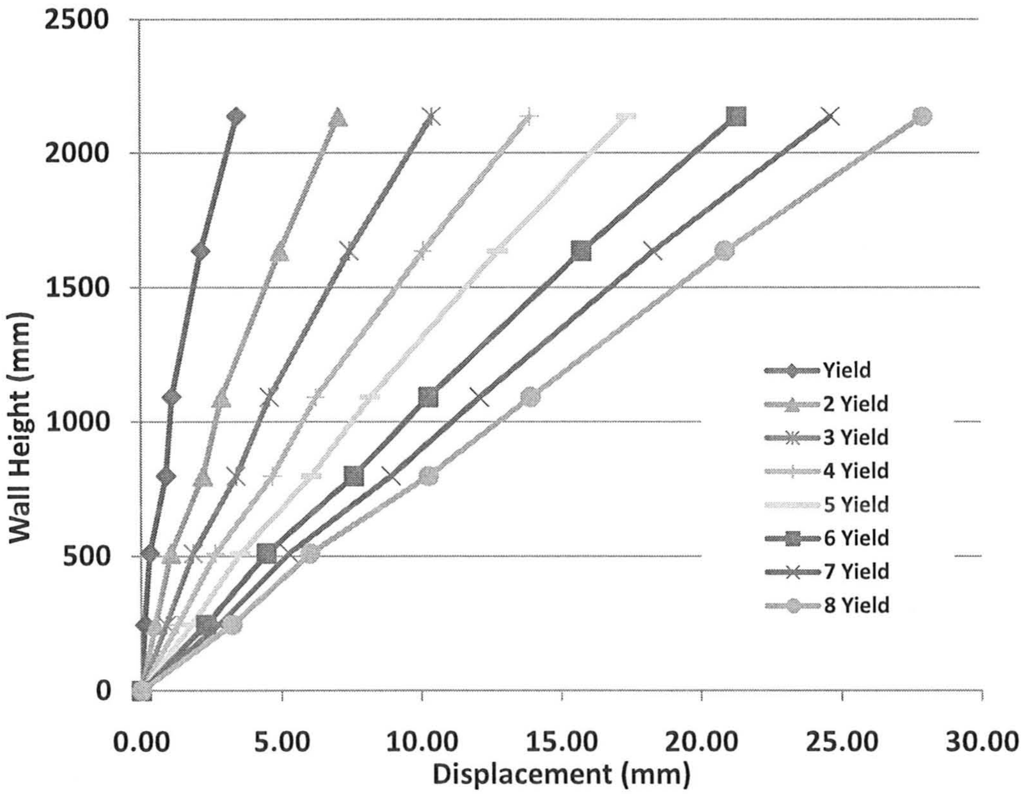

Figure 4.24: Lateral Displacements for Wall 4 at Various Displacement Levels (Push direction denoted by positive displacement)

As previously mentioned, 4 methods of determining the equivalent plastic hinge length were chosen as representative of the range of methods and values in use. However, the elasto-plastic idealization used in Method 1 requires that Walls A and B be considered as behaving identically. In this regard, the curvature at yield is the value corresponding to a top deflection of 6.6 mm and the curvature at ultimate similarly corresponds to the value from the walls at the ultimate stage. Since Walls A and B had different values of measured average curvature, two values are presented when using Equation 4.1. The value denoted with an '(A)' corresponds to the equivalent plastic hinge length resulting from the measured average curvatures at yield and ultimate condition of Wall A. Similarly, the notation '(B)' signifies that the measured average curvatures at yield and ultimate condition of Wall B were used. These two values mark the upper and lower bound of equivalent plastic hinge lengths when using Equation 4.1.

Table 4.11: Calculated Equivalent Plastic Hinge Lengths for Walls A and B of Wall 4

	Eq. 4.1	Eq. 4.2	Eq. 4.3	CSA S304.1
Lp (mm)	718 (A) (Method 2) 547 (B) (Method 2) 714 (A) (Method 4) 541 (B) (Method 4)	266	270	865

4.6.4 Ductility of Wall 4

As discussed in Section 4.2.5, the displacement ductility was calculated based on 4 chosen idealization techniques. The 4 techniques are presented in Figure 4.25. Due to the pronounced difference in the initial stiffness between Methods 1 and 3 and Methods 2 and 4, Methods 1 and 3 result in the highest level of displacement ductility. This is similar to the result for Wall 3. From Table 4.12, it can be seen that the resulting ductility was highest using Method 3, with a value of 11.40, and lowest using Method 4, with a value of 3.88. According to the results of Method 3, this wall achieved a significant displacement ductility of 5.70 times the NBCC specified value of 2.0 for moderately ductile walls. Using Method 4, this specimen surpassed the 2.0 ductility by 94%. The key values of each idealization technique are summarized within Table 4.12.

Based on the idealization techniques presented, it is reasonable to say that the NBCC restriction of $R_d = 2.0$ severely underestimated the ductility of Wall 4. It is interesting to note that the maximum ductility achieved by Wall 2 was 2.68 (Method 3) whereas the maximum ductility achieved by Wall 4 was 11.40. This represents an increase in displacement ductility of 325%. Considering that Wall 4 also did not benefit from large steel and masonry strains and eventual masonry damage, due to the relatively brittle behaviour of the steel, this result is a good indication of the benefits of flexural coupling.

In making the decision as to whether or not flexural coupling should be considered during performance based design, it is clear from this result that flexural coupling significantly improved the displacement ductility and therefore would result in decreased seismic design force.

For the reasons stated regarding the equivalent plastic hinge length approximation using Equation 4.1, two values are presented for the curvature ductility. Similar to Table 4.11, (A) denotes the use of measured average curvatures values from Wall A whereas (B) denotes the use of measured average curvature values from Wall B.

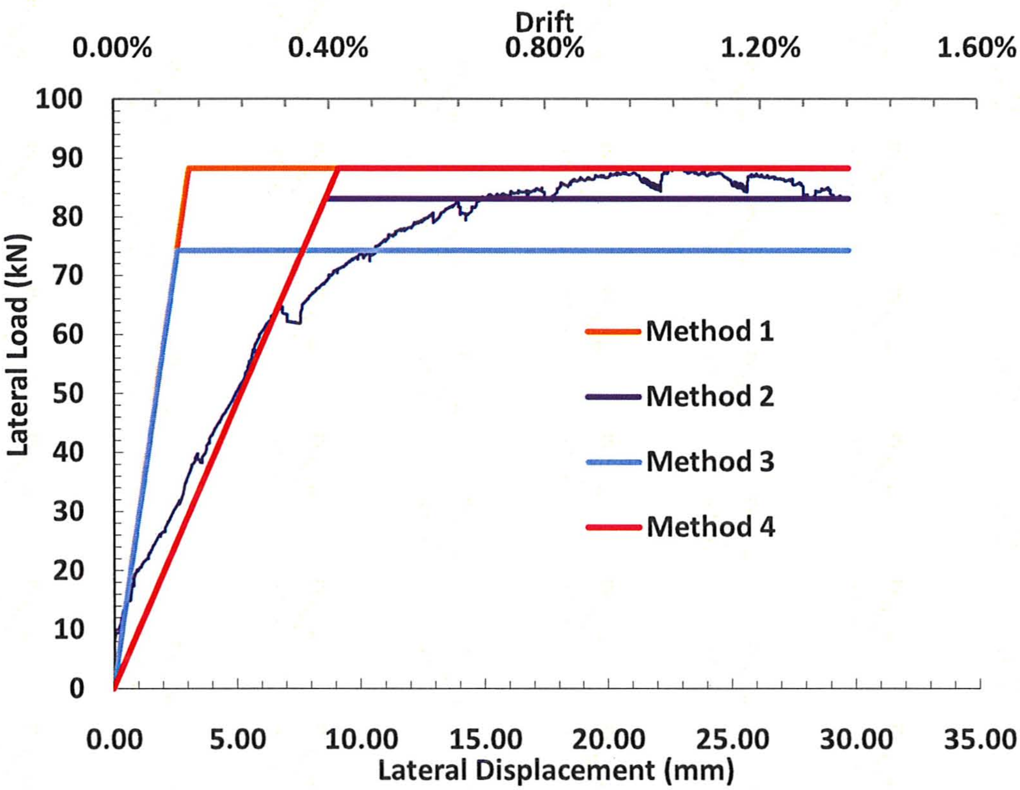

Figure 4.25: Elasto-Plastic Idealizations for Wall 4 (Push direction denoted by positive displacement)

Table 4.12: Ductilities for Wall 4 Calculated using Various Idealizations

	Method 1	Method 2	Method 3	Method 4
F'y (kN)	88.26	83.08	74.30	88.26
Δ'y (mm)	3.11	8.62	2.61	9.16
Δu (mm)	29.80	29.80	29.80	29.80
μ_{Δ}	9.59	3.46	11.40	3.25
μ_{φ}	N/A	4.00(A) 4.76(B)	N/A	3.76(A) 4.48(B)

4.7 Load-Displacement Response of Conceptual Structures

In order to assess the effect of combining several different wall types on a structure's theoretical load-displacement response, the experimental load-displacement envelopes presented earlier were used to produce the load-displacement responses for 3 different structures. The combinations of walls used in these conceptual structures can be seen below in Table 4.13.

Table 4.13: Combinations of Walls used in Conceptual Structures

Structure	Number of Specimens Included			
	Wall 1	Wall 2	Wall 3	Wall 4
Structure 1a	2	2	2	2
Structure 1b	2	6	2	0
Structure 2a	0	2	2	2
Structure 2b	0	6	2	0
Structure 3a	2	2	0	2
Structure 3b	2	6	0	0

For analysis purposes, all structures are assumed to be perfectly symmetric and, therefore, torsion was not considered. It is also assumed that, aside from the

Wall 4 coupled wall configuration, coupling between walls does not occur, meaning that the placement or spacing of in-plane and out-of-plane walls does not affect the flexural behaviour of individual walls.

Load-displacement curves were created for each structure by summing the resistance of each wall at the same level of displacement. Upon reaching the measured ultimate lateral displacement of a Wall, the structure was said to have failed with the load-displacement curve ending at that limiting displacement. In order to conveniently sum the experimental load-displacement behaviours, a trend-line was plotted for each load-displacement envelope. Trend-lines were chosen based on the Author's interpretation when compared to the experimental load-displacement response. The equation of the trend-line was used to determine the experimental lateral resistance at 0.5 mm increments.

Structures 1a and 1b were created to examine the difference between including flexural coupling and neglecting it. Therefore, for Structure 1a, Wall 4 was included whereas for Structures 1b Wall 4 was replaced with the equivalent number of Wall 2. The load-displacement response for Structures 1a and 1b was plotted in Figure 4.26. The shape of the load-displacement response curve for both structures was similar with the lateral resistance of Structure 1a being greater than Structure 1b.

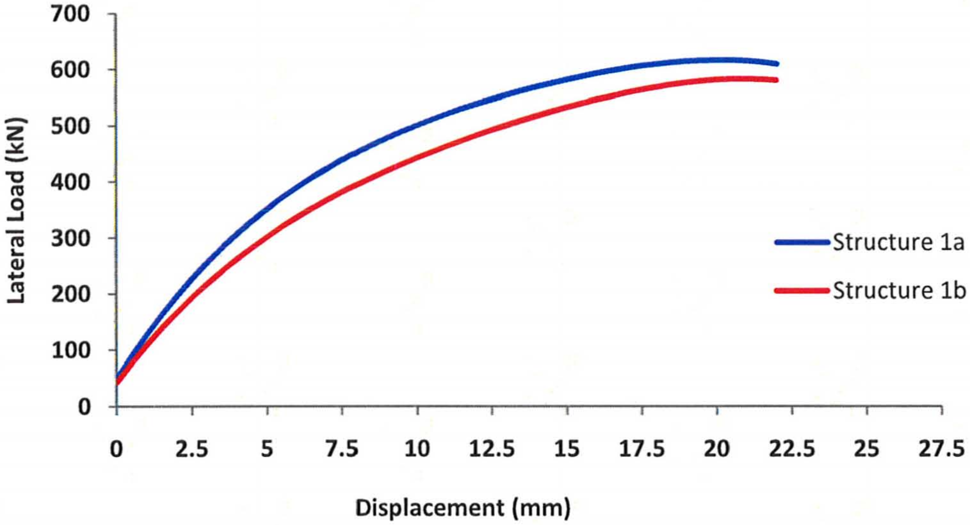

Figure 4.26: Load-Displacement Response for Structures 1a and 1b

From Section 4.3, it may be recalled that Wall 1 had a measured ultimate displacement of 22.0 mm which was the smallest displacement of the 4 shear walls and, as such controlled the ultimate displacement of Structure 1. Therefore, Structures 2a and 2b were created to examine the impact of the premature failure of Wall 1 and (again) to examine the difference between including and excluding flexural coupling. The load-displacement responses for Structures 2a and 2b were plotted in Figure 4.27.

The shapes of the load-displacement responses are similar with the most noticeable difference coming from the increased lateral load resistance of Structure 2a containing the coupled pair of Wall 4. From the figure, it can be seen that omitting Wall 1 had an effect at the higher levels of displacement where there was a distinct degradation in both stiffness and lateral resistance. While there was minor post-peak degradation in Walls 2 and 4, the magnitude of this degradation may have been influenced, in part, by the trend line chosen to represent the experimental load-displacement response.

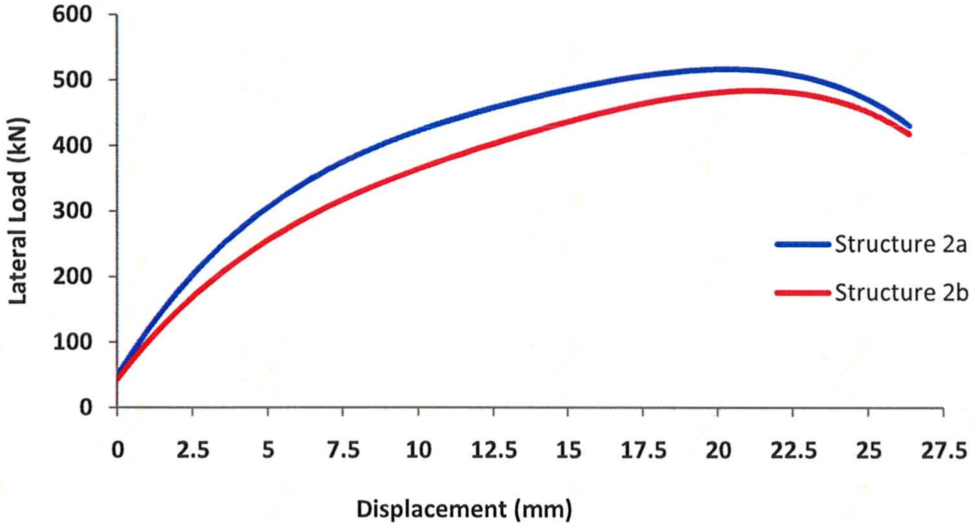

Figure 4.27: Load-Displacement Response for Structures 2a and 2b

Structures 3a and 3b were created to examine the effect of Wall 3 and, because Wall 3 was the dominant wall, to again examine the difference between including and excluding flexural coupling in a structure where this wall was now the dominant wall. Therefore, for Structure 3a, Wall 4 was included whereas for Structure 3b, Wall 4 was replaced with equivalent repetitions of Wall 2. The load-displacement responses for Structures 3a and 3b were plotted in Figure 4.28. From the load displacement response, a trend similar to Structures 1a and 1b can be seen. However, the shapes of the load-displacement curves differed slightly and the difference in lateral load resistance was more pronounced as the result of coupling. Also, Structure 3a had a visible post-peak degradation whereas Structure 3b did not.

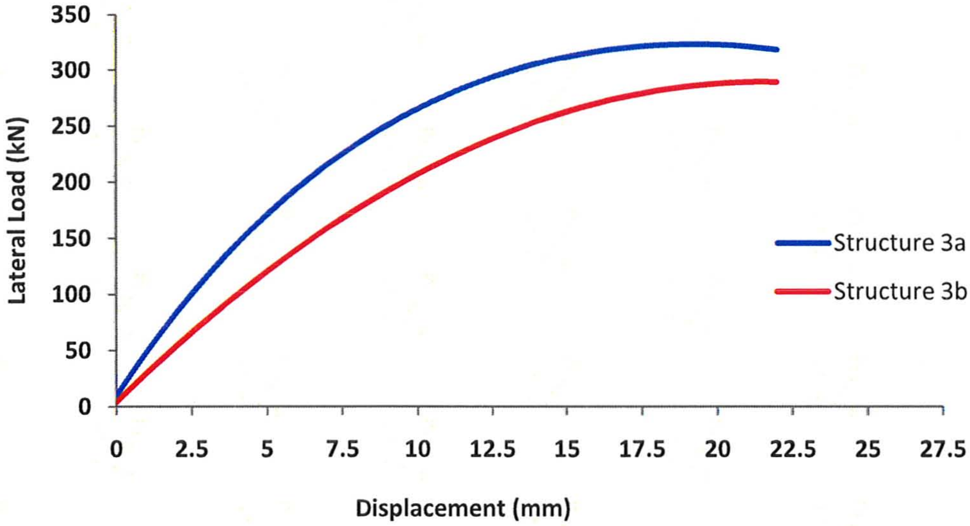

Figure 4.28: Load-Displacement Response for Structures 3a and 3b

4.8 Conclusions

4.8.1 Predicted and Experimental Wall Capacities and Displacements

In comparing the theoretical and experimental yield points, two factors should be considered. The first is that predicted displacements do not include shear and slip. The other factor is that nominal yield strain was used in the predictions whereas experimentally much larger strain was required to reach the 0.2 % offset defined yield strength. Both of these factors would be expected to result in the observed higher experimental displacement values. The predicted ultimate lateral load values are in reasonable agreement with the experimental ultimate lateral loads where, at ultimate conditions, the effect of the non-ideal elastic-plastic stress- strain curve would be minimal.

4.8.2 Stiffness Degradation and Normalized Period

Examining the trends of stiffness degradation among the 4 specimens (See Figure 4.29) revealed that the stiffer Walls 3 and 4 (also having the lowest aspect ratio) were similar. In terms of initial degradation, the values were similar (53% and 59% respectively). A similar curve was observed for Walls 1 and 2 except that the curve was more linear. Conversely, the walls with higher aspect ratio and lower stiffness displayed much lower initial stiffness degradation (19% and 20% for Walls 1 and 2, respectively).

As can be seen in Figure 4.30, normalized period for all specimens increased significantly with increased displacement. Walls 1 and 2 displayed increases in normalized period of 100% and 50-60%, respectively. However for the much stiffer Walls 3 and 4, the increase in normalized period was significantly higher. Wall 3 displayed a 160-165% increase while Wall 4 displayed an increase of 206%.

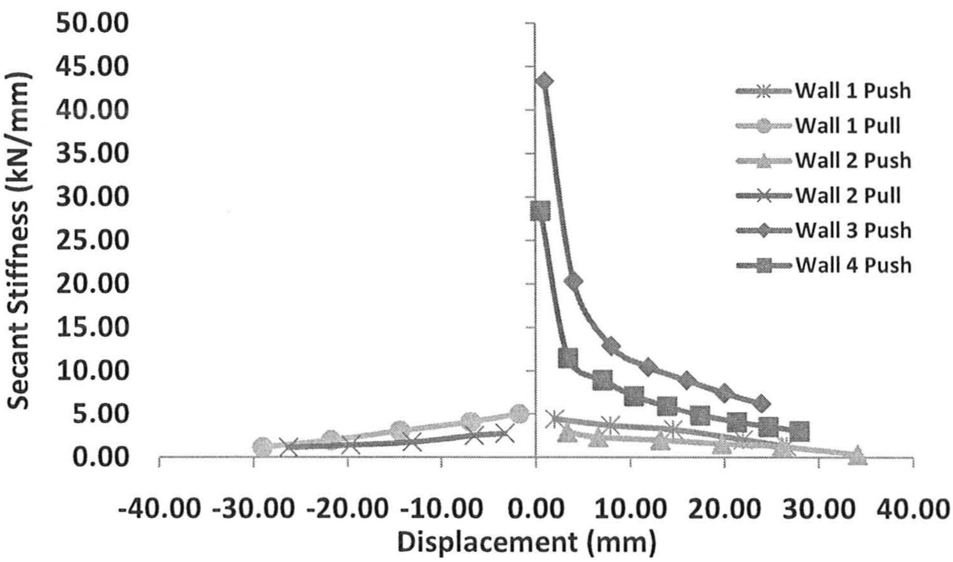

Figure 4.29: Stiffness Degradation Comparison

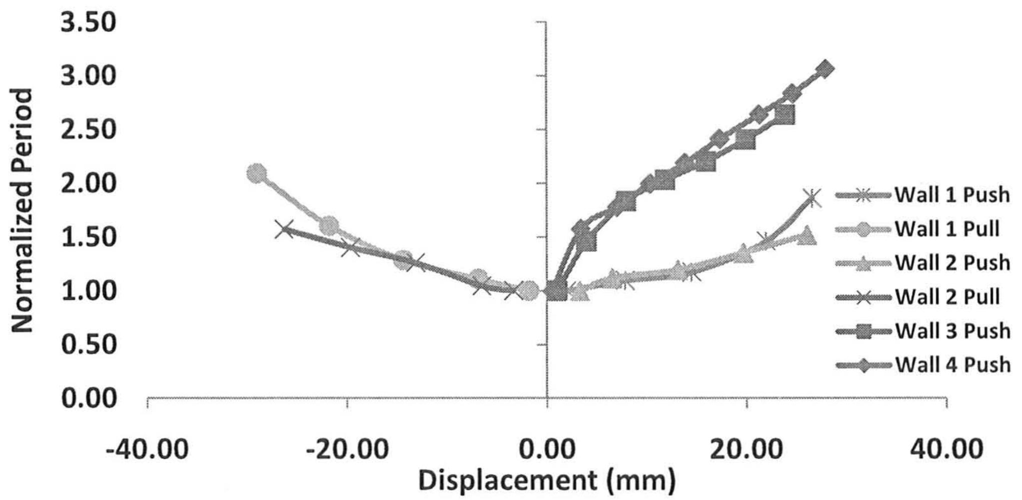

Figure 4.30: Normalized Period Comparison

4.8.3 Ductility

It is clear that, in terms of idealized displacement ductility, Wall 1 displayed the least ductile behaviour. Reaching a ductility value only slightly above 2.0, it can be said that this wall provides little argument against the existing code values for the ductility related force modification factor, R_d. Although one idealization method led to a ductility value above 2.0 the three remaining idealization techniques resulted in values less than 2.0. However, Wall 1 was subjected to the most cycles of reversed cyclic loading which accentuated the impact of the brittle reinforcement. Wall 2 also displayed a relatively low level of ductility. With the highest displacement ductility value being 2.68, the two idealization techniques which resulted in a value less than 2.0 leave doubt as to the true ductility of this specimen. It would seem that the linear walls, excluding Wall 4, achieved a ductility level which was below the expected level.

Walls 3 performed well in terms of displacement ductility. The displacement ductility of Wall 3 was bracketed by the values 3.59 and 9.04. When compared to the current force modification factor, the observed ductility is approximately 80 to 352% higher. This leads to the conclusion that perhaps the current value for the force modification factor is not accurate when applied to a flanged section.

Of the four specimens, it can be said that Wall 4 displayed the highest level of ductility. When compared to the results obtained from Wall 2, it is clear that the flexural coupling due to the floor slab provided a significant increase in ductility. Comparing the ductility of two identical Wall 2s with Wall 4, the difference in the design forces used for each of the 3 elements leads to the conclusion that, regardless of the idealization method, taking flexural coupling into consideration results in a much higher R_d value and, therefore, a lower seismic design force. From Table 4.14, it can be seen that there is an increase in displacement ductility due to flexural coupling. Based on these findings, it appears that the current value of the force modification factor, $R_{d,}$ may not be suitable when applied to a coupled shear wall. The upper bound values of ductility were 4.80 and 5.70 times the current R_d value and represent design forces which are 10.4% and 8.8% of the elastic design force.

Table 4.14: Comparison of the Effect of Flexural Coupling on Displacement Ductility

Displacement Ductility	Method 1	Method 2	Method 3	Method 4
Wall 2	2.30	1.97	2.68	1.84
Two Repetitions of Wall 2	2.30	1.97	2.68	1.84
Wall 4	9.59	3.46	11.40	3.25

4.8.4 Plastic Behaviour

In terms of theoretical prediction versus experimental results related to magnitude and extent of plasticity, the predicted values underestimated the experimental results. As mentioned previously, tensile strain penetration into the base and incorrect strain measurements may account for this discrepancy. The extent of plasticity could not be determined independently but rather it was interpreted based on the measured average curvature profiles and the profile of lateral displacements. For each wall there were discrepancies between the two methods in what could be interpreted as the extent of plasticity. In this regard, values based on deflected profile were determined in a much more subjective process and are not considered to be very reliable.

In lieu of plastic hinge length calculations, several equivalent plastic hinge length approximations were used. Although it cannot be said conclusively which method provided the most accurate result, it appears that CSA S304.1-04 overestimates the equivalent plastic hinge length. However, in assessing this observation, it should be remembered that the corresponding underestimation of magnitude of plasticity is a compensating factor.

4.8.5 Evaluation of Conceptual Structure Results

Three unique conceptual structures were created from combinations of the tested walls. These structures were created to examine the impact of each wall as well as the effect of coupling when combined to produce a conceptual structure. From experimental load-displacement envelopes of the three unique structures, it was observed that there was an impact due to the load-displacement behaviour of specific walls. The effect of coupling could also be seen as increased lateral load resistance.

Chapter 5
Conclusions and Recommendations

5.1 Conclusions

The historical performance of low rise masonry structures during seismic events has warranted further investigation into the behaviour of masonry. Past research has shown that reinforced masonry construction can perform with adequate strength and safety during seismic excitation and can also maintain an adequate level of strength and safety after the event. The study of plastic behaviour, energy dissipation, viscous damping, and ductility are used to evaluate the performance of masonry construction.

While reinforced concrete and reinforced masonry shear walls possess similar attributes, currently there is a distinct advantage to designing with reinforced concrete due to the flexibility in reinforcement detailing as well as the magnitude of the ductility related allowable force reduction modification factor. While current Canadian standards allow a maximum force reduction factor of 2.0, past and present research suggests that this value is overly conservative and may cause masonry construction to be economically uncompetitive.

From the literature reviewed, it is clear that additional research needs to be conducted in this field. In particular there is a lack of research conducted in the area of tall walls and the area of structural systems. The research use of third scale masonry units and third scale shear walls and shear wall buildings offers a practical option to rectify this lack.

Construction of the walls presented a unique challenge arising from the fact that the dimensions of 1/3rd scale masonry are rather small. The associated errors in laying the masonry units (i.e., bed joint and head joint thickness, in-plane and out-of-plane alignment of individual units) are very sensitive to the skill of the mason. Fortunately, these wall specimens were built by a mason with experience in scaled masonry construction.

While bed joint thickness is critical to achieving correct wall height, the head joint thickness is critical to proper bar alignment. With the small tolerances present, cumulative errors in head joint thickness could lead to improper bar alignment within the cell of the unit or, in severe cases, may result in bars interfering with the web of the unit. Once this occurs, there is no choice but to remove the units and lay them again. Additionally, improper bar alignment can lead to a void in the grout column as the bar prevents grout from flowing between it and the web of the unit.

The testing procedure had an impact on the behaviour of the specimens but more importantly their behaviour was governed by the properties of the vertical reinforcing steel. The comparatively low ductility of the reinforcing steel caused the specimens to exhibit a somewhat brittle behaviour and, rather than allowing damage to occur within the masonry, the wall specimen failures were governed by the reinforcement's inability to undergo moderate plastic deformations. With this limit on the amount of plastic behaviour, particularly as it relates to the ultimate displacement, the observed displacement ductility of the wall was less than otherwise might be expected with usual ductile reinforcement. Obviously, the ability of the reinforcing steel to undergo large plastic deformations is critical to ductile behaviour.

As a consequence of premature failure of the reinforcement, the reinforcement prevented recording of the much higher experimental ultimate displacements usually observed because the masonry was not able to undergo large compressive strains and toe damage to produce increased ductility. Masonry damage not only influences the ductility of shear walls but also energy dissipation and equivalent viscous damping. With only minor masonry damage, there was only very minor energy dissipation within the masonry itself. As a result, the majority of the energy dissipation came from the reinforcing steel.

Examining the trends of stiffness degradation among the 4 specimens revealed that the stiffer Walls 3 and 4 (also having the lowest aspect ratio) were very similar. In terms of initial stiffness degradation, the values were similar (53% and 59% respectively). Conversely, the walls with higher aspect ratio and lower stiffness displayed much lower initial stiffness degradation (19% and 20% for Walls 1 and 2, respectively).

Normalized period for all specimens increased significantly with increased displacement. Walls 1 and 2 displayed increases in normalized period of 100% and 50-60%, respectively. However for the much stiffer Walls 3 and 4, the increase in normalized period was significantly higher. Wall 3 displayed a 160-165% increase while Wall 4 displayed an increase of 206%.

It is clear that, in terms of idealized displacement ductility, Wall 1 displayed the least ductile behaviour. Reaching a ductility value only slightly above 2.0, it can be said that this wall provides little argument against the existing code values for the ductility related force modification factor, R_d. Although one idealization method led to a ductility value above 2.0 the three remaining idealization techniques resulted in values less than 2.0. Wall 2 also displayed a relatively low level of ductility. With the highest displacement ductility value being 2.68, the two idealization techniques which resulted in a value less than 2.0 leave doubt as to the true ductility of this specimen. It would seem that the linear walls, excluding Wall 4, achieved a ductility level which was below the expected level, but still adequate for the current Standards.

Walls 3 performed very well in terms of displacement ductility. The displacement ductility of Wall 3 was bracketed by the values 3.59 and 9.04. When compared to the current force modification factor, the observed ductility is approximately 80 to 350% higher. This leads to the conclusion that perhaps the current value for the force modification factor is not accurate when applied to a flanged section.

Of the four specimens, it can be said that Wall 4 displayed the highest level of ductility. When compared to the results obtained from Wall 2, it is clear that the flexural coupling due to the floor slab provided a significant increase in ductility. Comparing the ductility of two identical Wall 2s with Wall 4, the difference in the design forces used for each of the 3 elements leads to the conclusion that, regardless of the idealization method, taking flexural coupling into consideration results in a much higher R_d value and, therefore, a lower seismic design force. Based on these findings, it appears that the current value of the force modification factor, R_d, may not be suitable when applied to a coupled shear wall. The upper bound values of ductility were 4.80 and 5.70 times the current R_d value and represent design forces which are 10.4% and 8.8% of the elastic design force.

Overall the results obtained from this study provide positive feedback for the use of fully grouted reinforced one third scale concrete block shear wall testing. The observed ductility was below the expected level, however, these results are an indicator that the current R_d value is a lower bound value. Although the relatively brittle steel presented complications and prevented full value from being achieved from the tests, when considered as lower bound results, they provide a positive indication of the resistance of ductile reinforced masonry shear walls subjected to seismic forces.

5.2 Recommendations

Throughout this study, the Author has gained a greater appreciation of experimental testing. The experience gained through this study has provided insight as to improvements and/or recommendations that may be considered in future research within this area.

5.2.1 Reinforcing Steel

As witnessed in the experimental portion of this study, the reinforcing steel and its' behaviour is of paramount importance to the behaviour of the specimen. The reinforcing steel must provide adequate strength and well defined yielding with sufficient ductility. In order to achieve this, it is suggested that the deformed wire reinforcing steel be heat treated. However, additional research is needed to determine which method will provide the desired result.

5.2.2 Strain Gauges

It is the Author's opinion that strain gauging should not be used on the reinforcing steel. If need be, strain gauges should be installed on bars not located at the extreme ends of the wall or at the interface between the reinforced concrete base and the base of the shear wall. In order to install the strain gauge and flag terminal, the ribbed surface of the deformed wire must be ground to a smooth surface. As a result, due to the extremely small diameter of the deformed wire, the amount of material removed during this process is extremely difficult to monitor. In this regard, the reinforcing steel is sensitive to the installation process and removing material impacts the ultimate lateral load capacity and, possibly, the displacement ductility due to the possibility of strain concentrations at the critical wall section.

References

Drysdale, R., and Hamid, A. (2005). *"Masonry structures- behaviour and design."* First Canadian Edition, Canada Masonry Design Centre, Mississauga, ON, Canada.

Drysdale, R., Hamid, A., and Baker, L. (1999). *"Masonry structures: behavior and design."* 2nd Ed., The Masonry Society, Boulder, Colo.

El-Sokkary, H. and Galal, K. (2009). *"A Survey on Masonry Lateral Force Resisting Systems: Codes vs. Research Perspective"* 11th Canadian Masonry Symposium, Toronto, Ontario, Canada.

Hamid, Ahmad A., Abboud, B.D., and Harris, H.G. *"Direct Modeling of Concrete Block Masonry Under Axial Compression"* Masonry: Research, Application, and Problems, STP-871, ASTM, Philadelphia, 1985, pp.151-166.

Hamid, Ahmad A., Abboud, B.D., *"Direct Modeling of Concrete Block Masonry Under Shear and In-Plane Tension"* Journal of Testing and Evaluation, V.14, No. 2, Mar. 1986, pp. 112-121.

Hart, Gary C., Jaw, Jing-Wen, *"A Structural Component Model for Masonry Flexural Walls"* The Masonry Society Journal, August 1993, 25-36.

Hughes, Kevin J. (2010), *"Behaviour of Reduced-Scale Reinforced Concrete Masonry Shear Walls and Components"* M.A.Sc. Thesis, Department of Civil Engineering, McMaster University, Ontario, Canada

Jamison, J. (1997). *"Monotonic and cyclic performance of structurally insulated panel shear walls."* Master Thesis, Department of Civil Engineering, Virginia Polytechnic Institute and State University, Blacksburg, VA, USA.

Long, L. (2006), *"Behaviour of half-scale reinforced concrete masonry shear walls."* M.A.Sc. Thesis, Department of Civil Engineering, McMaster University, Ontario, Canada.

Massone, L. and Wallace, J. *"Load-Deformation Responses of Slender Reinforced Concrete Walls"* ACI Struct. J., Vol. 101, No. 1, pp. 103-113.

Moon, F. (2004), *"Seismic Strengthening of Low-Rise Unreinforced Masonry Structure with Flexible Diaphragms"* Ph.D. Thesis, Department of Civil and Environmental Engineering, Georgia Institute of Technology, USA.

Masonry Standards Joint Committee (MSJC 2005). "Building code requirements for Masonry Structures," ACI 530/ASCE 5 /TMS 402, American Concrete Institute, American Society of Civil Engineers, and The Masonry Society, Detroit, New York, and Boulder.

National Building Code of Canada (NBCC 2005). Institute for Research in Construction, National Research Council of Canada, Ottawa, Canada.

Park, R. and Paulay, R. (1975). *"Reinforced concrete structures."* John Wiley and Sons, New York, N.Y.

Paulay, T. and Priestley, M. (1992). *"Seismic design of reinforced concrete and masonry buildings."* John Wiley and Sons, New York, N.Y.

Paulay, T., and Priestley, M., (1993), "*Stability of ductile structural walls.*" ACI Structural Journal, Vol. 90, No. 4, pp. 385-392.

Pilakoutas, K. and Elnashai, A. (1995), *"Cyclic Behaviour of Reinforced Concrete Cantilever Walls, Part 1: Experimental Results"* ACI Structural Journal, Vol. 92, No. 3, pp. 271-281.

Priestley, M.(1982). *"Ductility of Confined and Unconfined Masonry Shear Walls"* The Masonry Society Journal, (1)2.

Priestley, M. (1986). *"Seismic design of concrete masonry shear walls."* American Concrete Institute Structural Journal, (83)1, 58-68.

Priestley, M., and Park, R. (1987). *"Strength and ductility of concrete bridge columns under seismic loading."* American Concrete Institute Structural Journal, (84)1, 61-76.

Priestley, M., Seible, F., and Calvi, G. (1996). *"Seismic design and retrofit of bridges."* John Wiley and Sons, Inc., 605 Third Avenue, New York, N.Y.

Sasani, M., and Kiureghian (2001). *"Seismic fragility of RC structural walls:Displacement Approach"* J. Struct. Engrg. (127)2, 219-228.

Seible, F., Priestley, M., Kingsley, G., and Kurkchubasche A. (1994), "*Seismic response of full scale five storey reinforced masonry building.*" J. Struct. Eng., (120)3, 925-946.

Shedid, M. (2006). *"Ductility of reinforced concrete masonry shear walls."* M.A.Sc. Thesis, Department of Civil Engineering, McMaster University, Ontario, Canada.

Shedid, M., Drysdale, R., and El-Dakhakhni, W. (2008), *"Behavior of Fully Grouted Reinforced Concrete Masonry Shear Walls Failing in Flexure: Experimental Results"* J. Struct. Engrg. (134)11, 1754-1767

Shedid, M. (2009), *"Ductility of Concrete Block Shear Wall Structures"* Ph.D. Thesis, Department of Civil Engineering, McMaster University, Ontario, Canada,.

Sucuoglu, H. and McNiven, H. (1991). *"Seismic shear capacity of reinforced masonry piers."* J. Struct. Eng., (117)7, 2166-2186.

Thomsen, J., and Wallace, J. (2004). *"Displacement-based design of slender reinforced concrete structural walls- Experimental verification."* J. Struct. Eng., (130)7, 618-630.

Tomazevic, M. (1998). *"Earthquake-Resistant Design of Masonry Buildings"* Imperial College Press, Covent Garden, London, UK.

Vasconcelos, G. and Lourenço, P. B. (2009), *"In-Plane Experimental Behavior of Stone Masonry Walls under Cyclic Loading"* J. Struct. Eng., (135)10, 1269-1277.

Yi, T., Moon, F. Leon, R., Kahn, L. (2006). *"Lateral Load Tests on a Two Storey Unreinforced Masonry Bulding"* J. Struct. Eng., Vol. 132, No. 5, pp. 643-652.

Appendix A

Mortar Cube Test Data

ID No.	Date Created	Date Tested	Age at Test (days)	Load at Failure (kN)	Stress (MPa) Per Batch	Batch Average	Total Batch Average
1-1-1	18-Nov-08	30-Jan-09	73	68.2	26.43		
1-1-2	18-Nov-08	30-Jan-09	73	68.4	26.51	25.92	
1-1-3	18-Nov-08	30-Jan-09	73	64	24.81		
1-2-1	18-Nov-08	30-Jan-09	73	83.7	32.44		
1-2-2	18-Nov-08	30-Jan-09	73	72.7	28.18	30.41	28.65
1-2-3	18-Nov-08	28-Jan-09	71	79	30.62		
1-3-1	18-Nov-08	28-Jan-09	71	75.1	29.11		
1-3-2	18-Nov-08	28-Jan-09	71	78.8	30.54	29.62	
1-3-3	18-Nov-08	28-Jan-09	71	75.4	29.22		
2-1-1	19-Nov-08	28-Jan-09	70	66.4	25.74		
2-1-2	19-Nov-08	28-Jan-09	70	66.2	25.66	26.1	
2-1-3	19-Nov-08	28-Jan-09	70	69.4	26.9		
2-2-1	19-Nov-08	30-Jan-09	72	75.7	29.3		
2-2-2	19-Nov-08	28-Jan-09	70	68.3	26.47	27.94	26.98
2-2-3	19-Nov-08	28-Jan-09	70	72.4	28.06		
2-3-1	19-Nov-08	30-Jan-09	72	73.7	28.57		
2-3-2	19-Nov-08	28-Jan-09	70	62.5	24.22	26.91	
2-3-3	19-Nov-08	28-Jan-09	70	72.1	27.95		
3-1-1	20-Nov-08	20-Jan-09	61	86.3	33.45		
3-1-2	20-Nov-08	28-Jan-09	69	87.3	33.84	34.37	
3-1-3	20-Nov-08	28-Jan-09	69	92.4	35.81		
3-2-1	20-Nov-08	28-Jan-09	69	78.4	30.39		
3-2-2	20-Nov-08	28-Jan-09	69	74.3	28.8	29.9	32.07
3-2-3	20-Nov-08	28-Jan-09	69	78.7	30.5		
3-3-1	20-Nov-08	28-Jan-09	69	82.6	32.02		

ID No.	Date Created	Date Tested	Age at Test (days)	Load at Failure (kN)	Stress (MPa) Per Batch	Batch Average	Total Batch Average
3-3-2	20-Nov-08	28-Jan-09	69	81.2	31.47	31.94	
3-3-3	20-Nov-08	28-Jan-09	69	83.4	32.33		
4-1-1	24-Nov-08	20-Jan-09	57	83.3	32.29		
4-1-2	24-Nov-08	20-Jan-09	57	78.9	30.58	31.33	
4-1-3	24-Nov-08	20-Jan-09	57	80.3	31.12		
4-2-1	24-Nov-08	28-Jan-09	65	70.3	27.25		
4-2-2	24-Nov-08	28-Jan-09	65	54.1	20.97	23.66	29.4
4-2-3	24-Nov-08	28-Jan-09	65	58.7	22.75		
4-3-1	24-Nov-08	28-Jan-09	65	83.7	32.44		
4-3-2	24-Nov-08	28-Jan-09	65	81.6	31.63	31.27	
4-3-3	24-Nov-08	28-Jan-09	65	76.7	29.73		
4-4-1	24-Nov-08	20-Jan-09	57	80.5	31.2		
4-4-2	24-Nov-08	28-Jan-09	65	83.2	32.25	31.32	
4-4-3	24-Nov-08	28-Jan-09	65	78.7	30.5		
5-1-1	25-Nov-08	20-Jan-09	56	79.1	30.66		
5-1-2	25-Nov-08	20-Jan-09	56	79.8	30.93	31.03	
5-1-3	25-Nov-08	20-Jan-09	56	81.3	31.51		
5-2-1	25-Nov-08	20-Jan-09	56	78.3	30.35		
5-2-2	25-Nov-08	20-Jan-09	56	75.3	29.19	30.94	30.43
5-2-3	25-Nov-08	20-Jan-09	56	85.9	33.29		
5-3-1	25-Nov-08	20-Jan-09	56	73.7	28.57		
5-3-2	25-Nov-08	28-Jan-09	64	75.4	29.22	28.67	
5-3-3	25-Nov-08	28-Jan-09	64	72.8	28.22		
5-4-1	25-Nov-08	20-Jan-09	56	79	30.62		
5-4-2	25-Nov-08	20-Jan-09	56	76.7	29.73	31.06	
5-4-3	25-Nov-08	28-Jan-09	64	84.7	32.83		

APPENDIX B

Flexural design

The following equations were used to predict the ultimate flexural strength of the test walls. Units used for all of the following equations are N and mm.

$$P = C_m + C_s - T_s$$

$$C_m = 0.85\, f'_m\, t\, (0.8\, c)$$

$$C_s = \sum A_s f'_s, \text{ where } 0 \le f'_s \le f_y,\ f'_s = \frac{c - d_i}{c}\, 0.0025\, E_s < f_y$$

$$T_s = \sum A_s\, f_s, \text{ where } 0 \le f_s \le f_y,\ f_s = \frac{d_i - c}{c}\, 0.0025\, E_s < f_y$$

$$M_u = C_m \left(\frac{l_w}{2} - 0.4\, c\right) + \sum A_s f_s \left(d_i - \frac{l_w}{2}\right),$$

where:

d_i	=	Distance from the compression fibre to the location of reinforcement;
c	=	Distance from compression fibre to the neutral axis;
t	=	Thickness of wall;
l_w	=	Wall length;
P	=	Applied axial load;
C_m	=	Compression force in cross section of a masonry wall
T_s	=	Tensile force in reinforcement in cross section of a masonry wall
C_s	=	Compression force in reinforcement
f_y	=	Yield strength of vertical reinforcement;
f_s	=	Tensile stress in vertical reinforcement;
f'_s	=	Compressive stress in vertical reinforcement
f'_m	=	Average compressive strengths of masonry;
E_s	=	Modulus of elasticity for steel reinforcement;
M_u	=	Moment resistance at maximum strain in masonry; and
A_s	=	Area of vertical reinforcement in the wall.

The following equations were used to predict the yield flexural strength of the test walls. Units used for all of the following equations are N and mm.

$$P = C_m + C_s - T_s$$

$$C_m = 0.5\, \varepsilon_m\, E_m\, t\, c$$

$$C_s = \sum A_s\, f'_s \text{, where } 0 \leq f'_s \leq f_y$$

$$T_s = \sum A_s\, f_s \text{ , where } 0 \leq f_s \leq f_y$$

$$T_i = A_s \frac{d_i - c}{d_l - c} f_y$$

$$\varepsilon_m = \varepsilon_y\, c \,/\, (d-c)$$

$$M_u = C_m \left(\frac{l_w}{2} - 0.33\, c\right) + \sum A_s\, f_s \left(d_i - \frac{l_w}{2}\right) + \sum A_s\, f'_s \left(\frac{l_w}{2} - d_i\right)$$

where:

ε_m = Compressive strain in the extreme masonry fibre

E_m = Measured modulus of elasticity of masonry

ε_y = Yield strain of the outermost reinforcing bar in tension

APPENDIX C

Displacement prediction

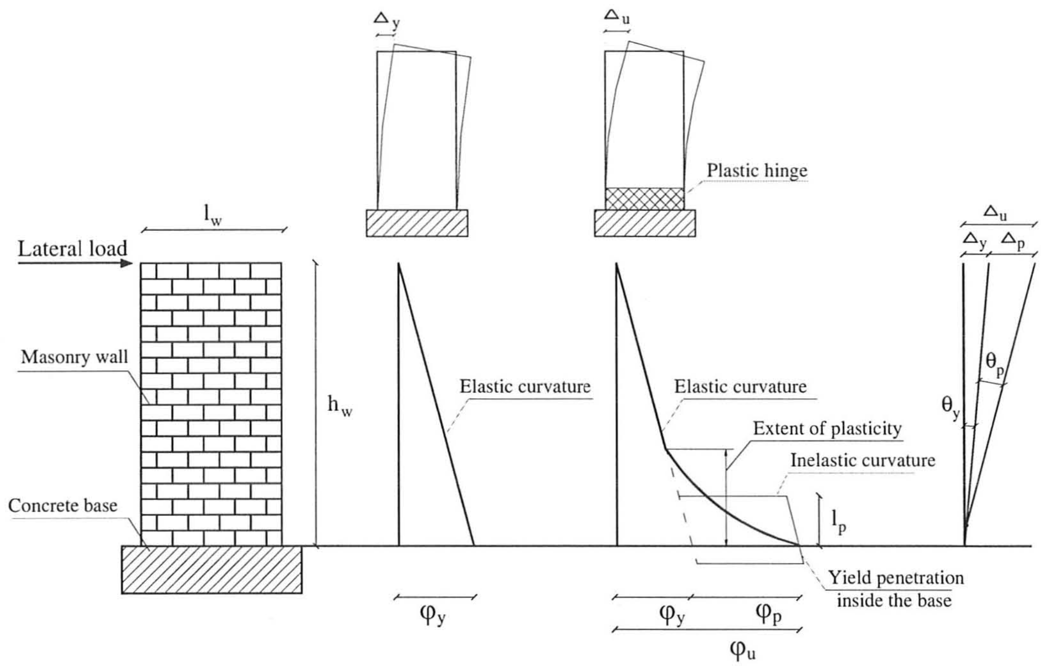

Figure C1: Curvature and Deflection Relationship for a RM Cantilever Shear Wall (from Shedid (2006))

The approach relies on predicting the displacements based on calculating curvatures at the base of the wall at first yield of extreme reinforcing bars and at maximum compressive strain in masonry. The equations used for predictions are presented below:

$$V_y = \frac{M_y}{h_w}$$

$$\varphi_y = \frac{d_1 - c_y}{\varepsilon_y}$$

$$\theta_y = \varphi_y \frac{h_w}{2}$$

$$\Delta_y = \varphi_y \frac{h_w^2}{3} = \theta_y \frac{2}{3} h_w$$

$$V_u = \frac{M_u}{h_w}$$

$\varphi_u \quad = \dfrac{c_u}{\varepsilon_m}$

$\theta_p \quad = \varphi_p \; l_p$, where: $\varphi_p = \varphi_u - \varphi_y$

$\Delta_p \quad = \theta_p \; (h_w - 0.5 \; l_p)$

where, $\Delta_u \quad = \Delta_y + \Delta_p$

$$\mu_\varphi = \frac{\varphi_u}{\varphi_y}$$

$$\mu_\Delta = \frac{\Delta_u}{\Delta_y} = 1 + \frac{\Delta_p}{\Delta_y} = 1 + 3\,(\mu_\varphi - 1)\,\frac{l_p}{h_w}\,(1 - 0.5\,\frac{l_p}{h_w})$$

where:

d_1	=	The distance from extreme compression fibre to the first tension bar;
ε_y	=	yield strain of steel reinforcement;
ε_m	=	Maximum compressive strain in masonry;
c_y	=	Length of compression zone at first yield of reinforcement;
c_u	=	Length of compression zone corresponding to maximum load;
M_y	=	Moment resistance at first yield of reinforcement;
V_y	=	Lateral load resistance at first yield of reinforcement;
M_u	=	Moment resistance at maximum strain in masonry;
V_u	=	Lateral load resistance at maximum strain in masonry;
φ_y	=	Curvature at the base of the wall at first yield of reinforcement;
φ_u	=	Curvature at the base of the wall at maximum strain in masonry
θ_y	=	Rotation of the wall at first yield of reinforcement;
θ_p	=	Plastic rotation of the wall;
Δ_y	=	Lateral displacement of wall at first yield of reinforcement;
Δ_p	=	Plastic displacement of wall;
Δ_u	=	Maximum Lateral displacement of wall;
μ_φ	=	Curvature ductility;
μ_Δ	=	Displacement ductility;
R	=	Force modification factor;
l_w	=	Wall length; and
l_p	=	Equivalent plastic hinge length.